Compact finite difference schemes for shallow-water ocean model

Christine Kazantsev, Eugene Kazantsev, Eric Blayo

INRIA

INSTITUT NATIONAL DE RECHERCHE EN INFORMATIQUE ET EN AUTOMATIQUE

Compact finite difference schemes for shallow-water ocean model.

Christine Kazantsev — Eugène Kazantsev — Eric Blayo

N° 4913

August 2003

THÈME 4

ISSN 0249-6399 ISRN INRIA/RR--4913--FR+ENG

INRIA
RHÔNE-ALPES

Compact finite difference schemes for shallow-water ocean model.

Christine Kazantsev , Eugène Kazantsev , Eric Blayo

Thème 4 — Simulation et optimisation
de systèmes complexes
Projets IDOPT

Rapport de recherche n° 4913 — August 2003 — 66 pages

Abstract: In this paper, we test some high order numerical schemes on simple oceanic models. We first compare fourth-order and sixth-order compact schemes with the classical second-order centered scheme on the system of equations describing the inertia-gravity waves, and then we focus on the performances of the fourth-order compact scheme on oceanic typical processes, such as Munk boundary layer and shallow-water physics. Numerical analysis of the schemes, and many computational results are presented.

Key-words: Oceanic models, shallow-water, numerical schemes, compact schemes, numerical analysis, boundary layer, inertia-gravity waves.

Unité de recherche INRIA Rhône-Alpes
655, avenue de l'Europe, 38334 Montbonnot Saint Ismier (France)
Téléphone : +33 4 76 61 52 00 —Télécopie +33 4 76 61 52 52

Schéma aux différences finies compactes pour un modèle eau peu profonde de l'océan.

Résumé : Dans ce travail, on étudie des schémas numériques d'ordre élevé sur des modèles simples d'océan. Après avoir comparé les schémas compacts d'ordre quatre et six avec le schéma classique centré d'ordre deux sur le système d'équations décrivant les ondes de gravité, on s'intéresse plus particulièrement aux performances du schéma compact d'ordre quatre sur des processus océaniques typiques tels que la couche limite de Munk et la physique induite par l'hypothèse d'eau peu profonde. Des études numériques de ces schémas ainsi que de nombreux résultats de calcul sont présentés.

Mots-clés : Modèles océaniques, eau peu profonde, schémas numériques, schémas compacts, analyse numérique de schémas, couche limite, ondes de gravité.

1 Introduction.

During these past 15 years, numerical models of the oceanic circulation have been very much improved in term of physics, realism of the application and computational techniques. Nevertheless, the basic numerics of these models are almost unchanged since the beginning of ocean modelling, i.e. 40 years. Most ocean general circulation models still use only simple second-order centered finite difference schemes. However, numerous modern schemes exist with interesting properties. For example, the implicit schemes based on Hermitian formulas, which is an old idea [Collatz] are used successfully in aerohydrodynamic problems [Tolstykh-72] [Tolstykh-73], [Tolstykh-73b]. Andrei I. Tolstykh developed and analysed very efficient high accuracy implicit schemes (see [Tolstykh-94] and references inside). In the field of fluid dynamics, these implicit schemes or so-called *compact difference schemes* became popular more recently mostly through the work of Lele [Lele]. In [Tolstykh M.A.], Mikhael A. Tolstykh adapts the schemes proposed by his father to the moisture transport equation in the atmosphere. In the domain of oceanography, Chu and Fan [Chu-Fan] applied a family of these schemes, called *combined compact difference schemes* to the simple stationary Stommel models. Blayo [Blayo] investigates the potential interest of such higher order schemes within the specific context of numerical ocean models. Deriving generic expressions of discrete dispersion relationships for inertia-gravity and Rossby waves, he found that the fourth-order family improves significantly the quality of the approximation of the dispersion properties.

In this paper, we test some of these high order numerical schemes on simple oceanic models. The aim of this work is to continue the studies of the performances of these schemes on oceanic typical processes, such as inertia-gravity waves, Munk boundary layer and shallow-water physics. The paper used the notations introduced in [Blayo] and is organized as follows. In part 2, we study the inertia-gravity wave's equation. We present the model, the discretised equations and numerical results for three space discretisations in this simple case of wave propagation. In the third part, we consider the Munk model of boundary layer. By means of the numerical analysis, we can prove that the main term of the error is due to the derivative of the function at the boundary and to the order of the scheme. Numerical experiments are also presented. In the fourth part, we study a shallow-water model. First of all, we prove the GKS-stability of the equation of continuity with compact schemes on the cell-centered mesh. Then we present numerical results of the shallow-water model for the centered second order schemes and for the fourth order compact schemes. The last part is devoted to the conclusion.

2 Inertia-gravity waves.

Our aim here is to test the accuracy of the compact schemes. To this end, we use a test-case with an exact wave solution. Initial data and boundary values are taken equal to the exact values of the wave, in such a way that the errors are only due to the truncation terms. For details on the following equations and notations, see [Blayo] and references inside.

2.1 The model.

Inertia-gravity waves on an f-plane are described by the linearized shallow-water equations (e.g. [Gill]):

$$\begin{aligned}
\frac{\partial u}{\partial t} - f_0 v + g\frac{\partial h}{\partial x} &= 0, \\
\frac{\partial v}{\partial t} + f_0 u + g\frac{\partial h}{\partial y} &= 0, \\
\frac{\partial h}{\partial t} + H(\frac{\partial u}{\partial x} + \frac{\partial v}{\partial y}) &= 0.
\end{aligned}$$

where f_0 is the Coriolis parameter (assumed constant) and g is the gravity acceleration, H is the mean depth. The unknowns are u, v the horizontal componants of the velocity, and h the depth.

We choose as an initial data a plane wave in u, v and h, given respectively by

$$\begin{aligned}
u(t=0,x,y) &= A_u cos(kx+ly) + B_u sin(kx+ly), \\
v(t=0,x,y) &= A_v cos(kx+ly) + B_v sin(kx+ly), \\
h(t=0,x,y) &= A_h cos(kx+ly) + B_h sin(kx+ly).
\end{aligned}$$

Following [Blayo], we introduce the constants

$$\begin{aligned}
\omega^2 &= gH(k^2+l^2)+f_0^2,\\
\alpha &= gHl^2+f_0^2,\\
\beta &= gHk^2+f_0^2,\\
\gamma &= gHkl\\
B_u &\in \mathbb{R}\\
B_v &\in \mathbb{R}\\
B_h &= H(kB_u+lB_v)\\
A_u &= -\frac{\gamma}{f_0\omega}B_u+\frac{\beta}{f_0\omega}B_v\\
A_v &= \frac{-\alpha}{f_0\omega}B_u+\frac{\gamma}{f_0\omega}B_v\\
A_h &= \frac{-Hl}{f_0}B_u+\frac{Hk}{f_0}B_v
\end{aligned}$$

The exact solutions of this problem are

$$\begin{aligned}
u(t,x,y) &= A_u cos(kx+ly-\omega t)+B_u sin(kx+ly-\omega t),\\
v(t,x,y) &= A_v cos(kx+ly-\omega t)+B_v sin(kx+ly-\omega t),\\
h(t,x,y) &= A_h cos(kx+ly-\omega t)+B_h sin(kx+ly-\omega t),
\end{aligned}$$

2.2 Discretised equations.

In this section, we discretize in space the equations on a Arakawa C grid, in the square domain [0,1]x[0,1]:

$$\begin{aligned}
\frac{\partial u}{\partial t}-f_0\mathcal{S}_0(v)+g\,\mathcal{S}_x^u(h) &= 0,\\
\frac{\partial v}{\partial t}+f_0\mathcal{S}_0(u)+g\,\mathcal{S}_y^v(h) &= 0,\\
\frac{\partial h}{\partial t}+H\,\left[\mathcal{S}_x^h(u)+\mathcal{S}_y^h(v)\right] &= 0.
\end{aligned}$$

where
$\mathcal{S}_0(u)$ denotes the interpolation scheme giving the value of u in a v-point, and symmetrically for $\mathcal{S}_0(v)$, $\mathcal{S}_x^u(h)$ denotes the approximation of $\partial_x h$ in a u-point.

We define by the same way $\mathcal{S}_x^h(u)$, $\mathcal{S}_y^v(h)$, $\mathcal{S}_y^h(v)$. Note that operators $\mathcal{S}_x^u(h)$ and $\mathcal{S}_x^h(u)$ are identical, as for $\mathcal{S}_y^v(h)$ and $\mathcal{S}_y^h(v)$.
With this discretisation, we obtain the following dispersion relationship ([Blayo]):

$$\left(\frac{\omega}{f_0}\right)^2=\mathcal{T}_0^2(k,l)-\lambda^2\,\left[\mathcal{T}_x^u(k,l)^2+\mathcal{T}_y^v(k,l)^2\right]$$

where $\mathcal{S}\left(e^{i(kx+ly)}\right)=\mathcal{T}(k,l)\,e^{i(kx+ly)}$, $\lambda^2=\frac{gH}{f_0^2}$.

Since the operators $\mathcal{S}_0(u)$,$\mathcal{S}_x^u(h)$ etc are very well preesented and studied in ([Blayo]), we are very brief on this subject.

2.3 Numerical experiments.

We consider now different discretisations for the operators S_0 and $S_{1/2}$:

- the usual second order center scheme (E2S),

$$\begin{aligned}
S_0 \quad f_{i+1/2} &= \frac{1}{2}\left(f_i+f_{i+1}\right),\\
S_{1/2} \quad f'_{i+1/2} &= \frac{f_{i+1}-f_i}{d},
\end{aligned}$$

- the fourth-order compact scheme (C4S),

$$\begin{aligned} S_0 \quad & \tfrac{1}{6} f_{i-1/2} + f_{i+1/2} + \tfrac{1}{6} f_{i+3/2} = \tfrac{2}{3} \left(f_i + f_{i+1} \right), \\ S_{1/2} \quad & \tfrac{1}{22} f'_{i-1/2} + f'_{i+1/2} + \tfrac{1}{22}{}' f_{i+3/2} = \tfrac{12}{11} \frac{f_{i+1} - f_i}{d}, \end{aligned}$$

- the sixth-order compact scheme (C6S).

$$\begin{aligned} S_0 \quad & \tfrac{3}{10} f_{i-1/2} + f_{i+1/2} + \tfrac{3}{10} f_{i+3/2} = \tfrac{3}{4} \left(f_i + f_{i+1} \right) + \tfrac{1}{20} \left(f_{i-1} + f_{i+2} \right), \\ S_{1/2} \quad & \tfrac{9}{62} f'_{i-1/2} + f'_{i+1/2} + \tfrac{9}{62}{}' f_{i+3/2} = \tfrac{63}{62} \frac{f_{i+1} - f_i}{d} + \tfrac{17}{62} \frac{f_{i+2} - f_{i-1}}{3d}, \end{aligned}$$

Different time schemes are also tested:

- second-order Runge-Kutta scheme,
- fourth-order Runge-Kutta scheme.

The explicit Euler scheme was also tested, but the time discretisation errors are predominant for long time integration so we do not present these results.
We recall that in this part, the problem is a simple wave-propagation one, the initial data is taken to be exact, and the boundary values are taken to be the values of the exact solutions of the equations.

In the following, we indicate for all cases

- the CPU time,
- the relative error in L^2on h: $\mathrm{err}_2 = \dfrac{\| h_{ex} - h_{nu} \|_2}{\| h_{ex} \|_2}$, where $\| * \|_2^2 = \int (*)^2 dxdy$,
- the relative error in L^∞ on h: $\mathrm{err}_\infty = \dfrac{\| h_{ex} - h_{nu} \|_\infty}{\| h_{ex} \|_\infty} = \dfrac{\max_{x,y} |\text{exact sol.} - \text{num. sol.}|}{\max_{x,y} |\text{exact sol.}|}$.

and plot the solutions with the different schemes.
In all cases, we took

- k=10π, l=2π, $B_u = B_v = 1$
- $H = f_0 = g = 2.5$ (corresponding to dimensional values of $y_0 = 5000km, f_0 = 10^{-4}, g = 10, H = 4000m, \beta = 2.10^{-11}$.), and the time step $\tau = 10^{-3}$ (when different, the exact value is given)

We obtained $\omega = 80.1342$ and $\dfrac{\omega}{f_0} = 32.0537$.

31x31		Runge Kutta 2	Runge-Kutta 4
e2	Time CPU	2.94	6.60
	err_2	3.25	3.42
	err_∞	4.96	5.25
c4	Time CPU	6.30	13.24
	err_2	0.28	0.41
	err_∞	0.54	0.56
c6	Time CPU	6.30	13.42
	err_2	6.99E-02	0.11
	err_∞	0.13	0.12

61x61		Runge Kutta 2	Runge-Kutta 4
e2	Time CPU	12.28	27.37
	err_2	0.97	0.97
	err_∞	0.83	0.79
c4	Time CPU	25.89	54.73
	err_2	9.62E-02	3.65E-02
	err_∞	8.57 E-02	6.62 E-02
c6	Time CPU	26.59	54.62
	err_2	1.30	1.03E-02
	err_∞	1.84	1.68E-02

91x91		Runge Kutta 2 $\tau = 5.10^{-4}$	Runge-Kutta 4
e2	Time CPU	60.66 (4000 it)	76.18
	err_2	0.45	0.47
	err_∞	1.09	1.12
c4	Time CPU	127.95 (4000 it)	145.05
	err_2	2.70E-02	6.35E-03
	err_∞	5.31 E-02	1.13E-02
c6	Time CPU	131.13(4000 it)	146.26
	err_2	3.24E-02	1.37E-03
	err_∞	6.41E-02	2.61E-03

For 2 waves: $u = u_1 + u_2$, (resp. v, h), with

$$u_1(t,x,y) = A_1 \exp i(k_1 x + l_1 y - \omega_1 t) \qquad u_2(t,x,y) = A_2 \exp i(k_2 x + l_2 y - \omega_2 t)$$

and $(k_1 = 10\pi, l_1 = 2\pi)$ $(k_2 = 2\pi, l_2 = 10\pi)$

31x31		Runge Kutta 2	Runge-Kutta 4
e2	Time CPU	3.32	7.27
	err_2	3.35	3.51
	err_∞	5.03	5.17
c4	Time CPU	6.53	13.82
	err_2	0.31	0.442
	err_∞	0.39	0.67
c6	Time CPU	6.63	13.92
	err_2	8.42E-02	0.135
	err_∞	0.101	0.173

61x61		Runge Kutta 2	Runge-Kutta 4
e2	Time CPU	12.88	28.73
	err_2	0.94	0.93
	err_∞	1.67	1.67
c4	Time CPU	26.28	56.35
	err_2	9.55E-02	3.66E-02
	err_∞	0.12	4.46E-02
c6	Time CPU	27.43	55.58
	err_2	0.58	1.05E-02
	err_∞	0.78	1.60 E-02

91x91		Runge Kutta 2 $\tau = 5.10^{-4}$	Runge-Kutta 4
e2	Time CPU	(4000 it)	78.44
	err_2	unstable	0.45
	err_∞		0.82
c4	Time CPU	(4000 it)	147.56
	err_2	unstable	6.23E-03
	err_∞		9.62E-03
c6	Time CPU	(4000 it)	149.55
	err_2	unstable	1.33E-03
	err_∞		1.63E-03

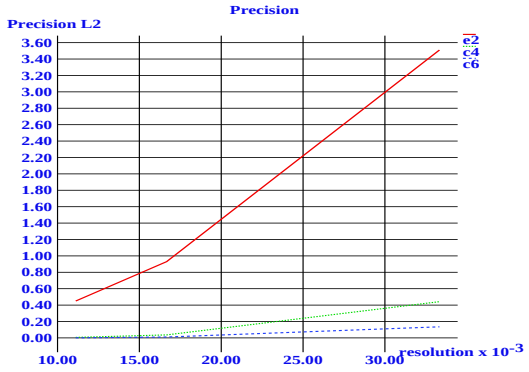

Figure 1A. Precision/resolution for each method, with 4th order Runge-Kutta scheme in time

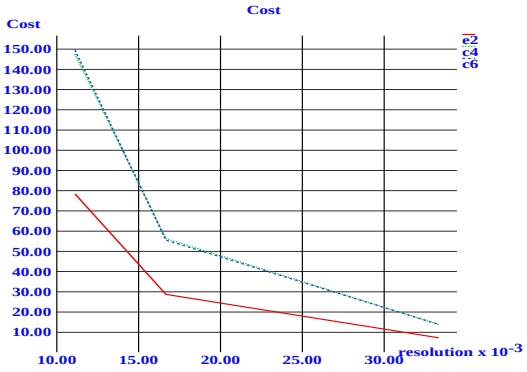

Figure 1B. Cost/resolution for each method, with 4th order Runge-Kutta scheme in time

Figure 2. Precision/Cost for each method, with 4th order Runge-Kutta scheme in time

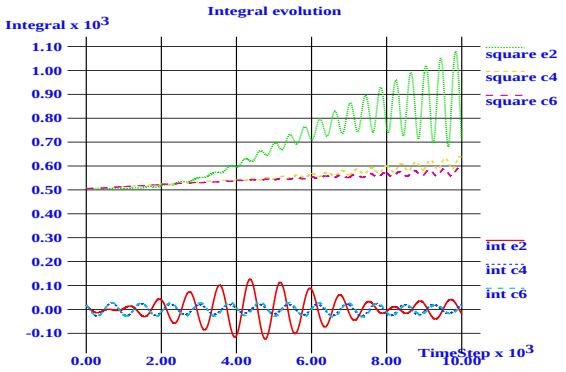

Figure 3A. Evolution of $\int_\Omega u(t,x,y)dxdy$ and $\int_\Omega u(t,x,y)^2 dxdy$ for each schemes with 4th order Runge-Kutta scheme in time and resolution a) $h_x = h_y = 1/30$

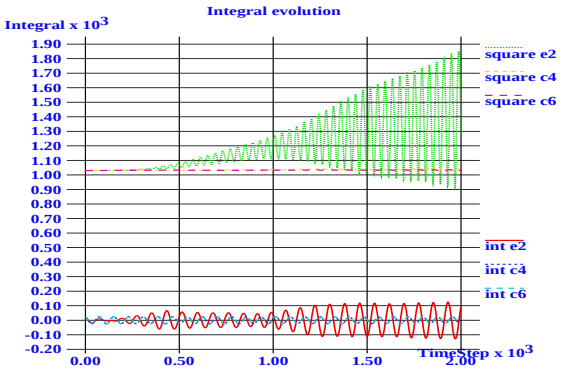

Figure 3B. Evolution of $\int_\Omega u(t,x,y)dxdy$ and $\int_\Omega u(t,x,y)^2 dxdy$ for each schemes with 4th order Runge-Kutta scheme in time and resolution b) $h_x = h_y = 1/60$

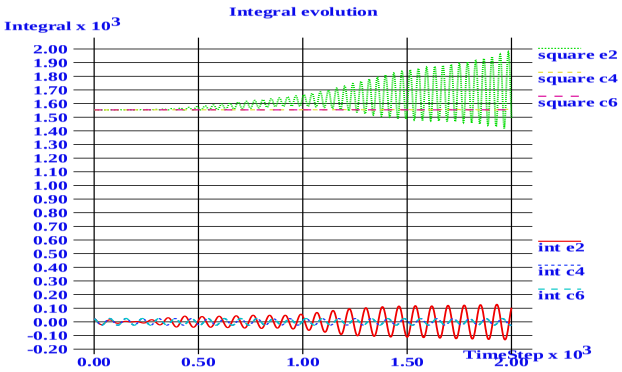

Figure 4. Evolution of $\int_\Omega u(t,x,y)dxdy$ and $\int_\Omega u(t,x,y)^2 dxdy$ for each schemes with 4th order Runge-Kutta scheme in time and resolution $h_x = h_y = 1/90$.

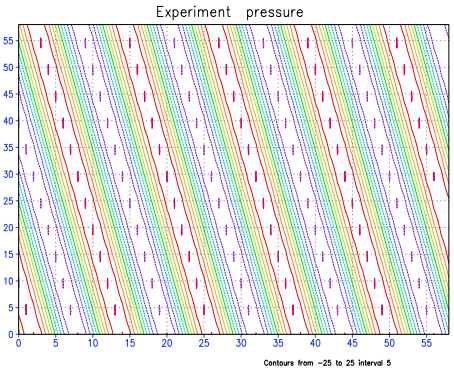

Figure 5. Initial data for h in all experiments.

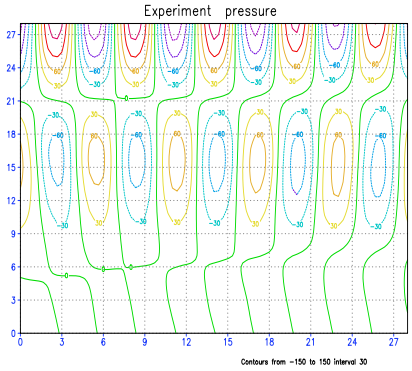

Figure 6A. Solution at T=2, with euler scheme in space, and 4th order Runge-Kutta scheme in time, hx=1/30

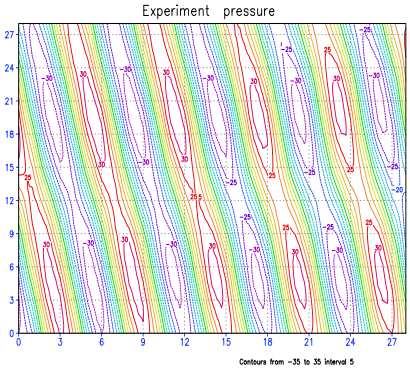

Figure 6B. Solution at T=2, with C4 scheme in space, and 4th order Runge-Kutta scheme in time, hx=1/30

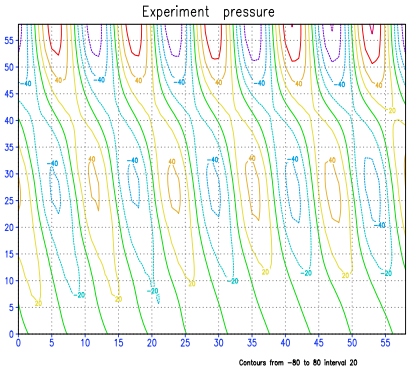

Figure 7A. Solution at T=2, with euler scheme in space, and 4th order Runge-Kutta scheme in time, hx=1/60

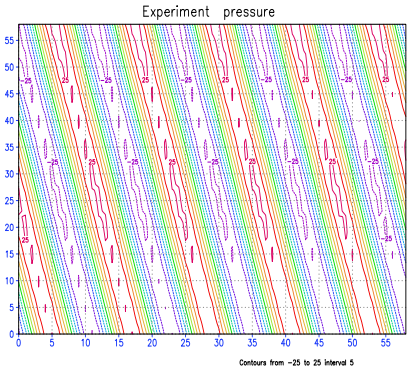

Figure 7B. Solution at T=2, with C4 scheme in space, and 4th order Runge-Kutta scheme in time, hx=1/60

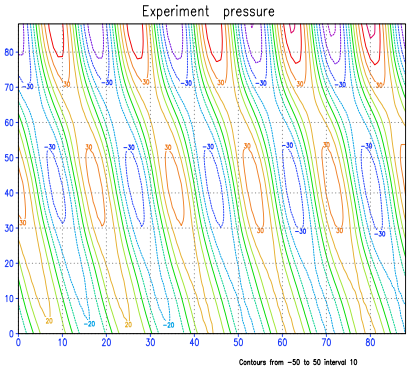

Figure 8A. Solution at T=2, with euler scheme in space, and 4th order Runge-Kutta scheme in time, hx=1/90

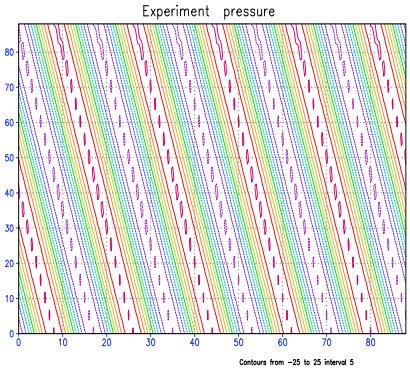

Figure 8B. Solution at T=2, with C4 scheme in space, and 4th order Runge-Kutta scheme in time, hx=1/90

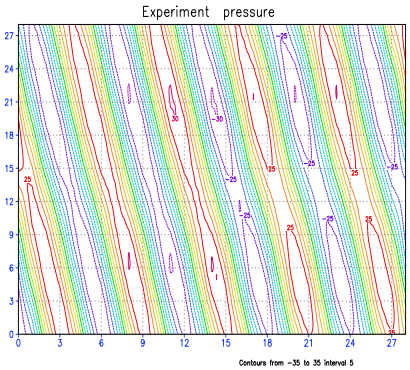

Figure 9A. Solution at T=2, with C6 scheme in space, and 4th order Runge-Kutta scheme in time, hx=1/30

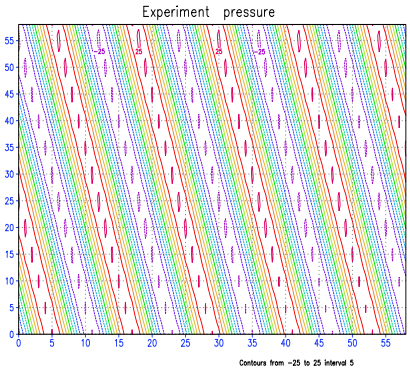

Figure 9B. Solution at T=2, with C6 scheme in space, and 4th order Runge-Kutta scheme in time, hx=1/60

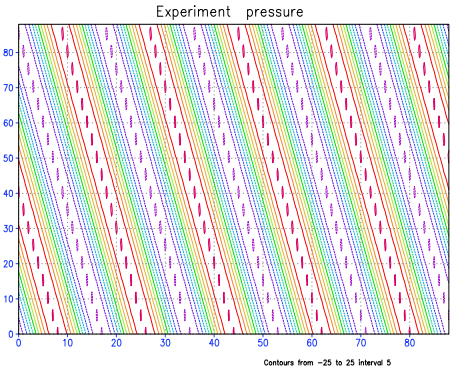

Figure 10. Solution at T=2, with C6 scheme in space,and 4th order Runge-Kutta scheme in time, hx=1/90

2.4 Conclusion of this part.

These numerical results demonstrate the efficiency of compact schemes for this simple wave propagation problem. C4 schemes lead indeed to similar results than E2 schemes for a typically three-times coarser resolution. Even if the C6 schemes are not more expensive than C4 schemes and gives better results in the present case, they are in fact more instable and difficult to tune in practical applications. So we will only focus in the following on the 4th order compact schemes.

3 Munk Model of boundary layer.

In this section, we test scheme on the Munk model of boundary layer. We present in the first subsection a simple analysis. First of all, we show that for unresolved boundary layer, a high order scheme is less suitable than a low order one. Moreover, due to boundary condition, the order of the scheme is different inside the domain, and on the boundary. Due to non-local nature of compact schemes, the error on the boundary propagates inside the domain.

3.1 The Munk Model.

The Munk model is a model of the western boundary layer, obtained by the local equilibrium between the β effect and the lateral dissipation. The equation is

$$\left\{ \begin{array}{l} \dfrac{d^3v(x)}{dx^3} - \dfrac{1}{\delta^3}\, v(x) = 0 \qquad x \geq 0 \\ x(0) = 0 \qquad \text{(no slip boundary condition)} \\ x(+\infty) = 0 \qquad \text{(finite width of the boundary layer)} \end{array} \right. \tag{1}$$

where the parameter $\delta = \left(\dfrac{\nu}{\beta}\right)^{1/3}$ is a characteristic length, ν the viscosity and β the gradient of the Coriolis parameter. The solution of this equation is given by the following expression:

$$v(x) = Ce^{-\frac{x}{2\delta}} \sin \frac{\sqrt{3}x}{2\delta} \tag{2}$$

which is plotted on figure 11 for typical oceanic values of the parameters: $\nu = 100 m^2 s^{-1}$, $\beta = 2. \times 10^{-11} m^{-1} s^{-1}$ and then $\delta = 17$ km. The constant C can be expressed in terms of the maximum value of the velocity

$$V_{\max} = V\left(\frac{2\delta\pi}{3\sqrt{3}}\right) = C\,\frac{\sqrt{3}}{2}\, e^{-\pi/3\sqrt{3}}$$

so

$$v(x) = \frac{2\, e^{\pi/3\sqrt{3}}}{\sqrt{3}}\, V_{\max}\, e^{-\frac{x}{2\delta}} \sin \frac{\sqrt{3}x}{2\delta} \tag{3}$$

The width of the boundary layer is of order $2\pi\delta/\sqrt{3}$.

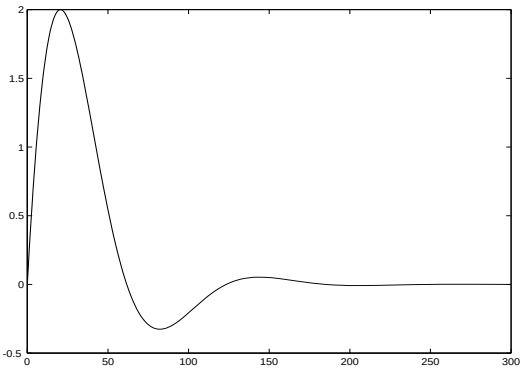

Figure 11. Aspect of the velocity in the Munk boundary layer for typical oceanic values of the parameter ($\delta = 17$ km, abscissas in km, ordinates in m/s)

3.2 Numerical results.

We consider the domain $[0, L]$, with $L = 4\sqrt{3}\pi\delta$ (i.e. 3 periods of the exact solution). We define a regular mesh on $[0, L]$, with space step $d = L/n$: $x_i = id$ $(i = 0, \ldots, n)$. The unknowns will be v_i, v'_i et $v^{(3)}_i$, which are the approximations of v, v' and $v^{(3)}$ at the nodes of the mesh. The equations to be discretised are:

$$\begin{aligned} v^{(3)}(x) &= \frac{d^2 v'(x)}{dx^2} \\ v'(x) &= \frac{dv(x)}{dx} \\ \frac{d^3 v(x)}{dx^3} - \frac{1}{\delta^3} v(x) &= 0 \end{aligned} \tag{4}$$

with the boundary conditions:

$$v(0) = 0 \quad v(L) = 0 \quad v'(0) = \frac{V_{\max}}{\delta} e^{\pi/3\sqrt{3}} \quad v'(L) = 0$$

3.2.1 Standard center schemes

The equations (4) can be discretised as follows

$$\begin{aligned} v^{(3)}_i &= \frac{v'_{i+1} - 2v'_i + v'_{i-1}}{d^2} \qquad (i = 1 \ldots n-1) \\ v'_i &= \frac{v_{i+1} - v_{i-1}}{2d} \qquad (i = 1 \ldots n-1) \\ v^{(3)}_i - \frac{1}{\delta^3} v_i &= 0 \qquad (i = 0 \ldots n) \end{aligned} \tag{5}$$

with the boundaries conditions

$$v_0 = 0 \quad v_n = 0 \quad v'_0 = \frac{V_{\max}}{\delta} e^{\pi/3\sqrt{3}} \quad v'_n = 0$$

These equations result in the system:

$$\begin{cases} -(1 + \frac{2d^3}{\delta^3})v_1 - 2v_2 + v_3 = -2dv'_0 \\ -v_{i-2} + 2v_{i-1} - \frac{2d^3}{\delta^3} v_i - 2v_{i+1} + v_{i+2} = 0 \qquad i = 2, \ldots, n-2 \\ -v_{n-3} + 2v_{n-2} + (1 - \frac{2d^3}{\delta^3})v_{n-1} = 0 \end{cases} \tag{6}$$

The unknowns v'_i et $v^{(3)}_i$ are computed later with the equation (5). We can also compute v".

3.2.2 Compact 4th order schemes

The equations (4) are discretised now as follows

$$\frac{1}{10}v^{(3)}_{i-1} + v^{(3)}_i + \frac{1}{10}v^{(3)}_{i+1} = \frac{6}{5d^2}\left(v'_{i+1} - 2v'_i + v'_{i-1}\right) \qquad (i = 1 \dots n-1) \tag{7}$$

$$\frac{1}{4}v'_{i-1} + v'_i + \frac{1}{4}v'_{i+1} = \frac{3}{4d}(v_{i+1} - v_{i-1}) \qquad (i = 1 \dots n-1) \tag{8}$$

$$v^{(3)}_i - \frac{1}{\delta^3}v_i = 0 \qquad (i = 0 \dots n) \tag{9}$$

with the same boundaries conditions. We can rewrite the system in the following form, with $c = \frac{3}{4d}$ and $c' = \frac{6}{5d}$:

$$\left\{\begin{array}{rcll} v_1 + 2c'v'_1 + \frac{1}{10}v_2 - c'v'_2 &=& c'v'_0 & \\ v'_1 - cv_2 + \frac{1}{4}v'_2 &=& -\frac{1}{4}v'_0 & \\ \frac{1}{10}v_{i-1} - c'v'_{i-1} + v_i + 2c'v'_i + \frac{1}{10}v_{i+1} - c'v'_{i+1} &=& 0 & i = 2, \dots, n-1 \\ cv_{i-1} + \frac{1}{4}v'_{i-1} + v'_i - cv_{i+1} + \frac{1}{4}v'_{i+1} &=& 0 & i = 2, \dots, n-1 \\ \frac{1}{10}v_{n-2} - c'v'_{n-2} + v_{n-1} + 2c'v'_{n-1} &=& 0 & \\ cv_{n-2} + \frac{1}{4}v'_{n-2} + v'_{n-1} &=& 0 & \end{array}\right. \tag{10}$$

The unknowns $v^{(3)}_i$ are computed later with the relationship (7). We compute v" by a scheme similar to (8).

3.2.3 Numerical results.

The two methods previously presented were used to solve the equation (4), with different mesh size d. We compute in each case the error in norm L_2 on v, v' and v" with the exact solution. Note that value of the exact solution on L are $v_{exact}(L) = 0$ and $v'_{exact}(L) = v'_0 \exp(-2\pi\sqrt{3})$ which is approximately $v'_{exact}(L) \sim v'_0 \times 10^{-11} \sim 4.7 \times 10^{-16}$. The results are presented in the following array and on the figure 12.

	E2			C4		
h (km)	$\|v_{app} - v_{ex}\|$ $\times 10^3$	$\|v'_{app} - v'_{ex}\|$ $\times 10^7$	$\|v"_{app} - v"_{ex}\|$ $\times 10^{11}$	$\|v_{app} - v_{ex}\|$ $\times 10^3$	$\|v'_{app} - v'_{ex}\|$ $\times 10^7$	$\|v"_{app} - v"_{ex}\|$ $\times 10^{11}$
74.003	275	66.4	99.8	397	277.3	35.34
52.859	93	313.6	116.3	199	48.8	78.15
37.001	361	320.5	64.2	69.8	60.2	21.24
24.667	269	188.4	78.5	26.2	17.2	8.49
18.501	159	111.6	48.5	8.68	5.63	3.08
12.334	71.9	51.4	21.1	1.77	1.16	0.68
9.250	40.7	29.3	11.8	0.58	0.38	0.41
7.400	25.5	18.4	7.5	0.25	0.16	0.60
6.167	17.9	12.9	5.3	0.14	0.08	0.91
4.625	10.0	7.2	3.1	0.08	0.03	1.73
3.700	6.5	4.7	2.4	0.07	0.02	2.80

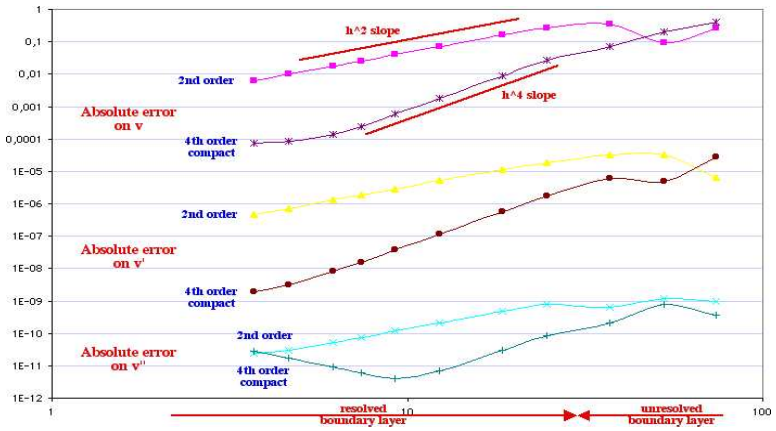

Figure 12. Errors on v, v' and v" function of the mesh size

3.3 Numerical Analysis of the schemes.

We recall the system on a finite domain $[0, L]$ with boundary conditions, namely

$$\frac{\partial^3 v}{\partial x^3} - \frac{1}{\delta^3} v = 0$$

with the boundary conditions:

$$v(0) = 0 \quad v(L) = 0 \quad v'(0) = \frac{V_{\max}}{\delta} e^{\pi/3\sqrt{3}} \quad v'(L) = 0$$

Let us introduce $\xi = \frac{x}{\delta}$, $u(t) = v(x)$, $\Lambda = \frac{L}{\delta}$. We obtain:

$$\frac{\partial^3 u}{\partial \xi^3} - u = 0$$

with the boundary conditions:

$$u(0) = 0 \quad u(\Lambda) = 0 \quad u'(0) = U_{\max} e^{\frac{\pi}{3\sqrt{3}}}; \quad u'(\Lambda) = 0.$$

Let n be the same integer as previously. We introduce $h = \frac{\Lambda}{n} = \frac{d}{\delta}$. We consider the discretised equations presented previously. Whatever the numerical schemes (E2 or C4), they can be rewritten in the form:

$$\begin{aligned} u^{(3)} &= B_2 u' + F \\ u' &= Bu \\ u^{(3)} &= u \end{aligned}$$

Let us denote by $\bar{u}$ the exact solution of the scheme. It verifies, at order p or q in h:

$$\bar{u}^{(3)} = B_2 \bar{u}' + F_1 + c_2 h^p \bar{u}^{(p+3)} \quad (11)$$

$$\bar{u}' = B\bar{u} + c_1 h^q \bar{u}^{(q+1)} \quad (12)$$

$$\bar{u}^{(3)} = \bar{u} \quad (13)$$

where F_i is a vector with the i-th derivative of $\bar{u}$ at the boundaries. Remark that c_1 and c_2 can be matrices as for compact schemes, for example.

3.3.1 Error analysis.

We denote by e (resp. e') the difference between the exact solution and the approximative one, (resp. between their derivatives). We have $e = \bar{u} - u$, and $e' = \bar{u}' - u'$. For e and e' we obtain the system:

$$\begin{aligned} u^{(3)} - \bar{u}^{(3)} &= B_2 e' + c_2 h^p \bar{u}^{(p+3)} \\ e' &= Be + c_1 h^q \bar{u}^{(q+1)} \\ (v^{(3)} - \bar{u}^{(3)}) &= e \end{aligned}$$

so:

$$\begin{aligned} e &= B_2 e' + c_2 h^p \bar{u}^{(p+3)} \\ e' &= Be + c_1 h^q \bar{u}^{(q+1)} \end{aligned}$$

and

$$e = B_2(Be + c_1 h^q \bar{u}^{(q+1)}) + c_2 h^p \bar{u}^{(p+3)}$$

then

$$e = B_2 Be + c_1 h^q B_2 \bar{u}^{(q+1)} + c_2 h^p \bar{u}^{(p+3)}$$

Let us remark that $B_2(\bar{u}^{(q)})' = \bar{u}^{(q+3)} - F_{q+1} - c_2 h^p \bar{u}^{(p+q+3)}$ according to the Taylor expansion or to the first equation of (11). We consequently obtain:

$$e = B_2 Be + c_1 h^q \bar{u}^{(q+3)} - c_1 h^q F_{q+1} + c_2 h^p \bar{u}^{(p+3)}$$

and since $\bar{u}^3 = \bar{u}$, it follows

$$(Id - B_2 B)\, e = c_1 h^q \bar{u}^{(q)} - c_1 h^q F_{q+1} + c_2 h^p \bar{u}^{(p)} \tag{14}$$

Result 1.
Due to the adimensionalisation, for a mesh size d, we obtain that $h = \frac{d}{\delta}$. For unresolved boundary layer, $h > 1$ and then, since the error is a power of h, an accurate scheme of high order in h will give a worse solution that a low order one.

Result 2.
Remark that F_{q+1} is a vector in $\frac{1}{h^2}$ taking into account the derivative of the function at the boundary. If it is not equal to zero, this term is of order $q-2$, which is less than the other terms.

3.3.2 Estimation of $\bar{u}'$ and of $\bar{u}^{(2)}$ and of the norms of D_2, A_4^{-1} and A_{10}^{-1}.

Let us apply the previous result to E2 and C4 schemes.

We introduce the following (n-1)*(n-1) tridiagonal matrices :

$$D = \begin{pmatrix} 0 & 1 & 0 & 0 & \cdots & 0 \\ -1 & 0 & 1 & 0 & \cdots & 0 \\ 0 & -1 & 0 & 1 & \cdots & 0 \\ \vdots & \vdots & \vdots & \vdots & \ddots & \vdots \\ 0 & \cdots & -1 & 0 & 1 & 0 \\ 0 & \cdots & 0 & -1 & 0 & 1 \\ 0 & \cdots & 0 & 0 & -1 & 0 \end{pmatrix} \qquad D_2 = \begin{pmatrix} -2 & 1 & 0 & 0 & \cdots & 0 \\ 1 & -2 & 1 & 0 & \cdots & 0 \\ 0 & 1 & -2 & 1 & \cdots & 0 \\ \vdots & \vdots & \vdots & \vdots & \ddots & \vdots \\ 0 & \cdots & 1 & -2 & 1 & 0 \\ 0 & \cdots & 0 & 1 & -2 & 1 \\ 0 & \cdots & 0 & 0 & 1 & -2 \end{pmatrix}$$

$$A_4 = \begin{pmatrix} 1 & 1/4 & 0 & 0 & \cdots & 0 \\ 1/4 & 1 & 1/4 & 0 & \cdots & 0 \\ 0 & 1/4 & 1 & 1/4 & \cdots & 0 \\ \vdots & \vdots & \vdots & \vdots & \ddots & \vdots \\ 0 & \cdots & 1/4 & 1 & 1/4 & 0 \\ 0 & \cdots & 0 & 1/4 & 1 & 1/4 \\ 0 & \cdots & 0 & 0 & 1/4 & 1 \end{pmatrix} \qquad A_{10} = \begin{pmatrix} 1 & 1/10 & 0 & 0 & \cdots & 0 \\ 1/10 & 1 & 1/10 & 0 & \cdots & 0 \\ 0 & 1/10 & 1 & 1/10 & \cdots & 0 \\ \vdots & \vdots & \vdots & \vdots & \ddots & \vdots \\ 0 & \cdots & 1/10 & 1 & 1/10 & 0 \\ 0 & \cdots & 0 & 1/10 & 1 & 1/10 \\ 0 & \cdots & 0 & 0 & 1/10 & 1 \end{pmatrix}$$

We know the exact solution of the Munk problem for $\Lambda = +\infty$. We suppose that Λ is sufficiently large and that this exact solution for unbounded domain can be considered as the solution for the bounded one. In fact, it verifies the problem with $u'(L) = \epsilon$, ϵ non equal to zero but very small.

We recall that the solution is

$$\bar{u}(x) = C e^{-\frac{x}{2}} sin\left(\frac{\sqrt{3}x}{2}\right)$$

with $C = \frac{2e^{\frac{\pi}{3\sqrt{3}}}}{\sqrt{3}} U_{max}$. Let us compute $\bar{u}'$ et $\bar{u}''$.

$$\bar{u}' = \frac{Ce^{-\frac{x}{2}}}{2}\left(-sin\left(\frac{\sqrt{3}x}{2}\right) + \sqrt{3}cos\left(\frac{\sqrt{3}x}{2}\right)\right),$$

$$\bar{u}'' = \frac{-Ce^{-\frac{x}{2}}}{2}\left(sin\left(\frac{\sqrt{3}x}{2}\right) + \sqrt{3}cos\left(\frac{\sqrt{3}x}{2}\right)\right),$$

We compute the L^2 norm of these solutions and the L^∞ norm on $[0, \Lambda]$ with Λ a multiple of the period of the solution.

$$\| \bar{u}^{(1)} \|_2 = \frac{3C}{4}\sqrt{(1 - e^{-L})},$$

$$\| \bar{u}^{(2)} \|_2 = \frac{3C}{2}\sqrt{(1 - e^{-L})}.$$

$$\| \bar{u}^{(1)} \|_\infty = \frac{C\sqrt{3}}{2},$$

$$\| \bar{u}^{(2)} \|_\infty = \frac{C\sqrt{3}}{2}.$$

We recall that the eigenvalues of D_2 are $\lambda^k = -4\sin^2\left(\frac{k\pi}{2n}\right)$. We then obtain

$$\| D_2 \| \leq 4.$$

Let A_α denote the tridiagonal matrix with value 1 on the diagonal and $\frac{1}{\alpha}$ on the lower and upper sub-diagonals. We are interested by the case $\alpha \geq 4$. Since $\alpha A_\alpha - (\alpha + 2)Id = D_2$, the eigenvectors of D_2 are also eigenvectors of A_α corresponding to the eigenvalues

$$\lambda^k = 1 + \frac{2}{\alpha}cos\left(\frac{k\pi}{n}\right),$$

and this, for $k \in 1, \cdots, n-1$. It follows that the eigenvalues of A_α can be bounded by

$$1 - \frac{2}{\alpha} \leq \lambda_{min} \leq \cdots \leq \lambda_{max} \leq 1 + \frac{2}{\alpha}.$$

Then for $\alpha = 4$ and $\alpha = 10$:

$$\| A_4 \| \leq \frac{3}{2}, \qquad \| A_4^{-1} \| \leq 2$$

$$\| A_{10} \| \leq \frac{6}{5}, \qquad \| A_{10}^{-1} \| \leq \frac{5}{4}.$$

3.3.3 Standard second order centered scheme.

We rewrite the discretised equations (5) in a matricial form:

$$\begin{aligned} u^{(3)} &= \frac{1}{h^2}D_2 u' + F \\ u' &= \frac{1}{2h}Du \\ u^{(3)} &= u \end{aligned}$$

with

$$F = \begin{pmatrix} \frac{1}{h^2}u'_0 \\ 0 \\ 0 \\ \vdots \\ 0 \\ 0 \end{pmatrix}$$

The exact solution $\bar{u}$ verifies, with the second order in h

$$\begin{aligned} \bar{u}^{(3)} &= \frac{1}{h^2} D_2 \bar{u}' + F - \frac{h^2}{12} \bar{u}^{(5)} \\ \bar{u}' &= \frac{1}{2h} D\bar{u} - \frac{h^2}{6} \bar{u}^{(3)} \\ \bar{u}^{(3)} &= \bar{u} \end{aligned}$$

We apply the result of the previous section with:

$$\begin{aligned} p = q &= 2 \\ B_2 &= \frac{1}{h^2} D_2 \\ B &= \frac{1}{2h} D \\ F_1 &= F \\ F_{q+1} &= F_3 = F_0 = 0 \text{ since } u_0 = 0 \\ c_1 &= -\frac{1}{6} \\ c_2 &= -\frac{1}{12} \end{aligned}$$

and obtain, denoting the error by e_2:

$$\left(Id - \frac{1}{2h^3} D_2 D \right) e_2 = -\frac{h^2}{6} \bar{u}^{(2)} - \frac{h^2}{12} \bar{u}^{(2)}$$

i.e.

$$\left(Id - \frac{1}{2h^3} D_2 D \right) e_2 = -\frac{h^2}{4} \bar{u}^{(2)} \tag{15}$$

Taking the norm, we have

$$\boxed{\| e_2 \|_2 \leq \frac{h^2}{4} \| \left(Id - \tfrac{1}{2h^3} D_2 D \right)^{-1} \| \times \| \bar{u}^{(2)} \|,}$$

3.3.4 Compact scheme of 4th order.

We recall the discretised equations (7)-(9) in matricial form:

$$\begin{aligned} u^{(3)} &= \frac{6}{5h^2} A_{10}^{-1} D_2 u' + A_{10}^{-1} G_1 \\ u' &= \frac{3}{4h} A_4^{-1} Du \\ u^{(3)} &= u \end{aligned}$$

with

$$G_1 = \begin{pmatrix} \frac{6}{5h^2} u_0' \\ 0 \\ 0 \\ \vdots \\ 0 \\ 0 \end{pmatrix}$$

Let $\bar{u}$ be the exact solution, as before. It verifies, with the 4th order in h:

$$\begin{aligned} A_{10} \bar{u}^{(3)} &= \frac{6}{5h^2} D_2 \bar{u}' + G + \frac{3h^4}{5.5!} \bar{u}^{(7)} \\ A_4 \bar{u}' &= \frac{3}{4h} D\bar{u} + \frac{h^4}{5!} \bar{u}^{(5)} \\ \bar{u}^{(3)} &= \bar{u} \end{aligned}$$

We apply the result (14) of the first section with:

$$\begin{aligned} p = q &= 4 \\ B_2 &= \frac{6}{5h^2} A_{10}^{-1} D_2 \\ B &= \frac{3}{4h} A_4^{-1} D \\ F_1 &= A_{10}^{-1} G \\ F_{q+1} &= F_5 = A_{10}^{-1} G_5 \\ c_1 &= \frac{1}{5!} A_4^{-1} \\ c_2 &= \frac{3}{5.5!} A_{10}^{-1} \end{aligned}$$

in

$$(Id - B_2 B)\, e = c_1 h^q \bar{u}^{(q)} - c_1 h^q F_{q+1} + c_2 h^p \bar{u}^{(p)}$$

Denoting the error by e_4, we obtain:

$$\left(Id - \frac{9}{10h^3} A_{10}^{-1} D_2 A_4^{-1} D \right) e_4 = \frac{h^4}{5!} A_4^{-1} \bar{u}^{(4)} - \frac{h^4}{5!} A_4^{-1} F_5 + \frac{3}{5.5!} A_{10}^{-1} h^4 \bar{u}^{(4)}.$$

and, due to the fact that $\bar{u}^{(4)} = \bar{u}'$

$$\left(Id - \frac{9}{10h^3} A_{10}^{-1} D_2 A_4^{-1} D \right) e_4 = \frac{h^4}{5!} A_4^{-1} \bar{u}' - \frac{h^4}{5!} A_4^{-1} F_5 + \frac{3}{5.5!} A_{10}^{-1} h^4 \bar{u}'. \tag{16}$$

with $F_5 = A_{10}^{-1} G_5 = A_{10}^{-1} G_2$ and

$$G_2 = \begin{pmatrix} \frac{6}{5h^2} u_0^{(2)} \\ 0 \\ 0 \\ \vdots \\ 0 \\ 0 \end{pmatrix} = \frac{6}{5h^2} u_0^{(2)} \begin{pmatrix} 1 \\ 0 \\ 0 \\ \vdots \\ 0 \\ 0 \end{pmatrix} = \frac{6}{5h^2} u_0^{(2)} T_1$$

so:

$$\left(Id - \frac{9}{10h^3} A_{10}^{-1} D_2 A_4^{-1} D \right) e_4 = \frac{h^4}{5!} A_4^{-1} \bar{u}' + \frac{3}{5.5!} A_{10}^{-1} h^4 \bar{u}' - \frac{6h^2}{5.5!} u_0^{(2)} A_4^{-1} A_{10}^{-1} T_1$$

If we bound the norm of A_{10}^{-1} and A_4^{-1} by the previously obtained estimate, we have

$$\boxed{\| e_4 \|_2 \leq \| \left(Id - \tfrac{9}{10h^3} A_{10}^{-1} D_2 A_4^{-1} D \right)^{-1} \| \left(\frac{3h^2}{5!} u_0^{(2)} + \frac{11h^4}{4.5!} \| \bar{u}' \| \right)}$$

So the error is of order h^2 if $u_0^{(2)} \neq 0$.

3.3.5 Comments.

- This result is independent of the fact that the scheme is compact: it is only due to the order of the scheme. Nevertheless, if the scheme is not compact, the error lies near the boundary of the domain and only there. For compact scheme, the product by the matrices A_4^{-1} and A_{10}^{-1} propagates this error onto the whole domain.
- The norm of the matrices $\| \left(Id - \frac{1}{2h^3} D_2 D \right)^{-1} \|$ and $\| \left(Id - \frac{9}{10h^3} A_{10}^{-1} D_2 A_4^{-1} D \right)^{-1} \|$ are bounded independently of h: this is the classical stability result for the schemes under consideration.

3.4 Conclusion of this part.

This section proves that for unresolved boundary layer, a low-order scheme will be better than a high order one. For a resolved boundary layer, the error is penalized by a term depending on the derivative of the solution at the boundary. Numerically, this term does not weight heavily and high-order scheme gives better solution than low-order one.

4 Shallow-water model.

The shallow-water model is a simple model for fluid motion. The variables are the horizontal velocity u, v and the sea level height h. The equations take into account the Coriolis term, the dissipation and the wind forcing. They represent the equations of motion and the mass conservation. We first present the equations, and in a second part study the GKS-stability of the mass conservation equation on an C-grid when discretised by compact schemes. We then present different numerical results obtained with compact schemes and usual centered schemes. We complete this part by a conclusion.

4.1 Equations.

The equations can be written in different equivalent ways:

$$\frac{\partial u}{\partial t} - (f+\xi)v + \frac{\partial B}{\partial x} = \frac{\tau^{(x)}}{\rho_0 h} - ru + \nu\Delta u \tag{17}$$

$$\frac{\partial v}{\partial t} + (f+\xi)u + \frac{\partial B}{\partial y} = \frac{\tau^{(y)}}{\rho_0 h} - rv + \nu\Delta v \tag{18}$$

$$\frac{\partial h}{\partial t} + \frac{\partial (hu)}{\partial x} + \frac{\partial (hv)}{\partial y} = 0 \tag{19}$$

with

$$f = f_0 + \beta y \tag{20}$$

$$\xi = \frac{\partial v}{\partial x} - \frac{\partial u}{\partial y} \tag{21}$$

$$B = g'h + \frac{1}{2}\left(u^2 + v^2\right) \tag{22}$$

which can be rewritten as:

$$\frac{\partial u}{\partial t} - fv + u\frac{\partial u}{\partial x} + v\frac{\partial u}{\partial y} + \frac{\partial (g'h)}{\partial x} = \frac{\tau^{(x)}}{\rho_0 h} - ru + \nu\Delta u \tag{23}$$

$$\frac{\partial v}{\partial t} + fu + u\frac{\partial v}{\partial x} + v\frac{\partial v}{\partial y} + \frac{\partial (g'h)}{\partial y} = \frac{\tau^{(y)}}{\rho_0 h} - rv + \nu\Delta v \tag{24}$$

$$\frac{\partial h}{\partial t} + \frac{\partial (hu)}{\partial x} + \frac{\partial (hv)}{\partial y} = 0 \tag{25}$$

or

$$\frac{\partial u}{\partial t} - fv + v\frac{\partial u}{\partial y} + \frac{\partial B_u}{\partial x} = \frac{\tau^{(x)}}{\rho_0 h} - ru + \nu\Delta u \tag{26}$$

$$\frac{\partial v}{\partial t} + fu + u\frac{\partial v}{\partial x} + \frac{\partial B_v}{\partial y} = \frac{\tau^{(y)}}{\rho_0 h} - rv + \nu\Delta v \tag{27}$$

$$\frac{\partial h}{\partial t} + \frac{\partial (hu)}{\partial x} + \frac{\partial (hv)}{\partial y} = 0 \tag{28}$$

with

$$f = f_0 + \beta y \tag{29}$$

$$B_u = g'h + \frac{1}{2}\left(u^2\right) \tag{30}$$

$$B_v = g'h + \frac{1}{2}\left(v^2\right) \tag{31}$$

The three formulations are theoretically equivalent. Numerically, they are equivalent when using the center second order scheme (it is easy to prove), but not with compact schemes. For the second order space scheme, we use the first formulation, and for the compact fourth order scheme, the last one.

4.2 GKS-Stability of the conservative divergence operator with compact scheme on cell-centered mesh.

4.2.1 Presentation of the numerical scheme.

We study the following equation:

$$\frac{\partial h}{\partial t} + div(hu) = 0$$

We work on the Arakawa C-grid, and we want to find a compact scheme which preserves the mass conservation law. For simplicity, we consider the one-dimensional problem only.

$$\frac{\partial h}{\partial t} + \frac{\partial (hu)}{\partial x} = 0 \text{ in } (0,1). \tag{32}$$

Due to the impermeability boundary conditions, we have $u(0) = u(1) = 0$.

Let us denote the points in the following way:
the u-points (and every value taken in these points) will be denoted by the index i, i.e. $u(0) = u_0, \ldots, u_i, \ldots, u_N = u(1) = 0$,
the h-points (and every value taken in these points) will be denoted by the index $i + 1/2$. The grid step will be denoted by Δx. The method proposed in [Bleck-Boudra] is used to integrate the equation:

$$\frac{\partial h}{\partial t} + \frac{\partial \left(\overline{h}^x u\right)}{\partial x} = 0 \tag{33}$$

where $\overline{h}^x$ denotes the interpolation of h at the u-points. In the following, for simplicity, we denote by h the unknown $\left(\overline{h}^x u\right)$. We use a compact scheme of 4-th order to discretize the space derivative operator. We denote by prime the space derivatives. For the inner points, the equation is

$$h'_{i-1/2} + 22h'_{i+1/2} + h'_{i+3/2} = \frac{24}{\Delta x}(h_{i+1} - h_i) \tag{34}$$

On the boundary, we need a scheme which ensures first on the left hand side a tridiagonal matrix and also the mass conservation, i.e. $I(h') = \int_0^1 h'(x)dx = h(1) - h(0)$. Let us consider two schemes for the boundary: the first order of accuracy one

$$\begin{array}{rcl} 23h'_{1/2} + h'_{3/2} & = & \frac{24}{\Delta x}(h_1 - h_0). \\ h'_{N-3/2} + 23h'_{N-1/2} & = & \frac{-24}{\Delta x}(h_{N-1} - h_N). \end{array} \tag{35}$$

where $h(1) - h(0) = I(h') = I_2(h') + O(h'^2)$ with

$$I_2(h') = \Delta x \sum_{i=0}^{i=N-1} h'_{i+1/2},$$

and the third order of accuracy one

$$\begin{array}{rcl} h'_{1/2} - h'_{3/2} & = & \frac{1}{\Delta x}(-h_2 + 2h_1 - h_0). \\ -h'_{N-3/2} + h'_{N-1/2} & = & \frac{-1}{\Delta x}(-h_{N-2} + 2h_{N-1} - h_N). \end{array} \tag{36}$$

where $h(1) - h(0) = I(h') = I_4(h') + O(h'^4)$ with

$$I_4(h') = \Delta x \left(\sum_{i=0}^{i=N-1} h'_{i+1/2} + \frac{1}{24}(2h'_{N-1/2} - 3h'_{N-3/2} + h'_{N-5/2} + 2h'_{1/2} - 3h'_{3/2} + h'_{5/2}) \right).$$

Since the system is solved in fact not for h but for hu, we have, due to the impermeability, homogeneous Dirichlet Boundary Conditions.

4.2.2 GKS-stability.

Let us now study the stability of the operator, using the method proposed by Gustafsson, Kreiss and Sundström in [GKS] denoted by GKS-Stability, following the method of line studied in [Strikwerda] [Carpenter-Gottlieb-Abarbanel].

The equations.

The equation is (32), the numerical scheme is (33) . To study the stability of the scheme, we consider that u is a constant.

Since u can be positive or negative, we will study the stability of the two equations:

$$\frac{\partial h}{\partial t} + \frac{\partial \left(\overline{h}^x\right)}{\partial x} = 0 \text{ in } (0,1), \tag{37}$$

$$\frac{\partial h}{\partial t} - \frac{\partial \left(\overline{h}^x\right)}{\partial x} = 0 \text{ in } (0,1) \tag{38}$$

with Dirichlet homogeneous boundary conditions.

We denote by S_0 the interpolation operator, i.e. $\overline{h}^x = S_0 h$. So, the problem can be reduced to the usual GKS-stability for two equations:

$$\begin{aligned} \frac{\partial h}{\partial t} + \frac{\partial (S_0 h)}{\partial x} &= 0 \text{ in } (0,1) \\ \frac{\partial h}{\partial t} - \frac{\partial (S_0 h)}{\partial x} &= 0 \text{ in } (0,1) \end{aligned}$$

with Dirichlet homogeneous boundary conditions.

GKS-stability.

We recall the main theorems concerning this subject [Carpenter-Gottlieb-Abarbanel]. Consider the Initial Boundary Value Problem (IBVP)

$$\begin{aligned} \frac{\partial V}{\partial t} &= MV, x \geq 0 \\ V(t,0) &= 0; \\ V(0,x) &= V_0; \end{aligned} \tag{39}$$

we have:

Theorem 4.1 *GKS Theory (fully discrete [GKS] or semidiscrete [Strikwerda]) asserts that to show stability for the finite domain problem, it is sufficient to show that the inner scheme is Cauchy stable on $(-\infty, +\infty)$ and that each of the two quarter-plane problems is stable with the use of normal mode analysis. Thus, the stability of the finite-domain problem is broken into the summation of three simpler problems.*

Theorem 4.2 *For each quarter-plane problem that arises in the above theorem, a necessary and sufficient condition for stability of the IBVP is that no eigensolution exists. This theorem is true for either the fully-discrete case [GKS] or the semi-discrete case [Strikwerda].*

Theorem 4.3 *Under mild restrictions [Kreiss-Wu], if a semidiscrete approximation is stable in a generalized sense and a Runge-Kutta (R-K) method that is locally stable is used to time-march the semidiscretisation, the totally discrete approximation is stable in the same sense, as long as the stability region of the R-K method encompasses the norm of the semidiscretrization.*

Let us now define the eigensolution of the IBVP [Carpenter-Gottlieb-Abarbanel] [Kreiss] [Strikwerda].

Definition 4.1 *An eigensolution for the IBVP defined by equation (39) is a nontrivial function $V(x,s)$ which satisfies:*

1. $sV = MV, x \geq 0$;
2. $V(0,s) = 0$;
3. $\mathcal{R}e(s) \geq 0$;
4. *for $\mathcal{R}e(s) > 0, V(x,s)$ is bounded as $x \to \infty$,*
5. *for $\mathcal{R}e(s) = 0, V(x,s) = \lim_{\epsilon \to 0^+} V(x, s+\epsilon)$, where $V(x, s+\epsilon)$ satisfied (1) and (4) (with s replaced by $s = \epsilon$).*

Main result.
Let us consider the method-of-lines theory for our equations. Let us introduce some notations:
$H_{1/2}$ is the N-vector defined by $H_{1/2} = (h_{1/2}, h_{3/2}, \ldots, h_{N-3/2}, h_{N-1/2})^T$,
H_1 is the (N+1)-vector defined by $H_1 = (h_0, h_1, \ldots, h_{N-1}, h_N)^T$, we recall that $h_0 = h_N = 0$.
A_x is the matrix corresponding to the numerical scheme for the space derivative. Since we use compact scheme, $A_x = P^{-1}Q$, where P is the tridiagonal matrix defined on the left hand side of the relationships (34) and (35) or (36), and Q is the matrix defined the by right-hand-side of these relationships.

Let us consider first the problem (37). The discrete form of this equation will be:

$$\frac{dH_{1/2}}{dt} + A_x S_0 H_{1/2} = 0, \tag{40}$$

Since we use compact schemes of 6-th order for the interpolation, we will suppose that the interpolation operator S_0 is exact, i.e. $S_0 H_{1/2} = H_1$.

Theorem 4.4 *The IBVP defined by the equation (40) with homogeneous Dirichlet boundary condition, with (35) or (36) as boundary schemes and with S_0 the exact interpolation operator, is stable.*

Using the theorems 4.1 and 4.2, it is sufficient to prove that there is no eigensolution for the previous equation. Let us look for eigensolution. We suppose that we have a solution to:

$$sH_{1/2} = -A_x S_0 H_{1/2} = -A_x H_1 \tag{41}$$

Considering a inner line, we have

$$-s\Delta x(h_{i-1/2} + 22h_{i+1/2} + h_{i+3/2}) = 24(h_{i+1} - h_i).$$

The solution is of the form: $h_i = c_0 y^{2i}$. Introducing this, we have, with $S = s\Delta x$,

$$-S(y^{2i-1} + 22y^{2i+1} + y^{2i+3}) = 24(y^{2i+2} - y^{2i}).$$

We simplify by y^{2i-1} to obtain:

$$-S(1 + 22y^2 + y^4) = 24(y^3 - y),$$

i.e.

$$Sy^4 + 24y^3 + 22Sy^2 - 24y + S = 0. \tag{42}$$

This equation admits four solutions, and all the solutions for h are obtained by linear combinations of these four solutions. It is obvious that if y is a solution, then $\frac{-1}{y}$ is also a solution. So we have two cases. First, at least one of the four solutions has absolute value equal to 1. In this case, the equation can be rewritten for this solution y in the following form, with $y = \exp(i\theta)$:

$$S(y^4 + 1) + 24(y^3 - y) + 22Sy^2 = 0.$$

i.e.

$$\exp(i2\theta)\left(S(\exp(i2\theta) + \exp(-i2\theta) + 22) + 24(\exp(i\theta) - \exp(-i\theta))\right) = 0$$

so

$$S(2cos(2\theta) + 22) = -24(2isin(\theta))$$

and finally

$$S = i\frac{-24sin(\theta)}{cos(2\theta) + 11}$$

then S has a real part equal to 0.

We have then to consider a little perturbation inside the unit circle, that is we have to consider the second case.

Second case: since y and $\frac{-1}{y}$ are solutions, exactly two solutions, say y_1 and y_2, have absolute values less than 1 and the four solutions can be denoted by y_1, y_2, $y_3 = \frac{-1}{y_1}$, $y_4 = \frac{-1}{y_2}$. We know also from (42) that

$$y_1y_2 + y_1y_3 + y_1y_4 + y_2y_3 + y_2y_4 + y_3y_4 = 22$$

i.e.

$$y_1 y_2 + \frac{1}{y_1 y_2} - \frac{y_1^2 + y_2^2}{y_1 y_2} = 24.$$

Moreover, also from (42), we have

$$y_1 + y_2 + y_3 + y_4 = \frac{-24}{S}$$

i.e.

$$y_1 + y_2 - \frac{y_1 + y_2}{y_1 y_2} = \frac{-24}{S}.$$

Let us introduce $z = y_1 + y_2$ and $x = y_1 y_2$, these two equations give us

$$x + \frac{1}{x} - \frac{z^2 - 2x}{x} = 24 \text{ and } z - \frac{z}{x} = \frac{-24}{S},$$

so

$$z^2 = x^2 - 22x + 1 \text{ and } S = \frac{-24x}{z(x-1)}. \tag{43}$$

Since an eigensolution is bounded when $i \to \infty$, every eigensolutions are of the form $v^i = \alpha_1 y_1^i + \alpha_2 y_2^i$. Due to the Dirichlet boundary conditions, $v^0 = 0$ and $\alpha_1 = -\alpha_2$. Norming the eigensolution, we assume that $\alpha_1 = 1$. Then we consider $v^{(i)} = y_1^i - y_2^i$, with y_1 and y_2 solutions of (42).

Let us consider now the first line of the problem (41) with first-order boundary scheme (35). We obtain:

$$-S(23v^{(1)} + v^{(3)}) = 24v^{(2)}$$

i.e.

$$-23S(y_1 - y_2) - S(y_1^3 - y_2^3) = 24(y_1^2 - y_2^2)$$

then

$$-23S(y_1 - y_2) - S(y_1 - y_2)(y_1^2 + y_1 y_2 + y_2^2) = 24(y_1 - y_2)(y_1 + y_2).$$

Since $y_1 = y_2$ implies that $v = 0$ which is not an eigensolution, we can simplify by $(y_1 - y_2)$. It results

$$-23S - S(y_1^2 + y_1 y_2 + y_2^2) - 24(y_1 + y_2) = 0$$

and then

$$-23S - S\left((y_1 + y_2)^2 - y_1 y_2\right) - 24(y_1 + y_2) = 0.$$

Introducing $z = y_1 + y_2$ and $x = y_1 y_2$, we obtain

$$-23S - S(z^2 - x) - 24z = 0.$$

and get

$$S(z^2 - x + 23) = -24z. \tag{44}$$

Introducing (43) in (44), it follows

$$-24x(x^2 - 22x + 1 - x + 23) = -24(x^2 - 22x + 1)(x - 1),$$

then

$$x(-x + 23) = -(x^2 - 22x + 1)$$

and

$$x + 1 = 0.$$

So $x = -1$. But since we have supposed that y_1 and y_2 have an absolute value less than one, it is impossible that the product is equal to -1. So we have no eigensolution, and the scheme is stable.

Consider now the first line of the problem (41) with third-order boundary scheme (36). We obtain

$$v^{(4)} + S(v^{(3)} - v^{(1)}) - 2v^{(2)} = 0$$

i.e.

$$(y_1^4 - y_2^4) + S(y_1^3 - y_2^3) - 2(y_1^2 - y_2^2) - S(y_1 - y_2) = 0$$

then

$$(y_1 - y_2)\left((y_1 + y_2)(y_1^2 + y_2^2) + S(y_1^2 + y_1 y_2 + y_2^2) - 2(y_1 + y_2) - S\right) = 0.$$

Since $y_1 = y_2$ implies that $v = 0$ which is not an eigensolution, we can simplify by $(y_1 - y_2)$. It results

$$(y_1 + y_2)(y_1^2 + y_2^2) + S(y_1^2 + y_1 y_2 + y_2^2) - 2(y_1 + y_2) - S = 0$$

and then

$$(y_1 + y_2)\left((y_1 + y_2)^2 - 2y_1 y_2 - 2\right) + S\left((y_1 + y_2)^2 - y_1 y_2 - 1\right) = 0.$$

In term of $z = y_1 + y_2$ and $x = y_1 y_2$, we obtain

$$z(z^2 - 2x - 2) + S(z^2 - x - 1) = 0. \tag{45}$$

Introducing (43) in (45), it follows

$$(x^2 - 22x + 1)(x - 1)(x^2 - 22x + 1 - 2x - 2) - 24x(x^2 - 22x + 1 - x - 1) = 0,$$

then

$$(x^2 - 22x + 1)(x - 1)(x^2 - 24x - 1) - 24x^2(x - 23) = 0$$

and

$$x^5 - 47x^4 + 550x^3 + 22x^2 + x + 1 = 0.$$

We compute the roots numerically. Three are real, the others two are complexe conjugated. We obtain approximatively

$$x_1 = -0.1308, \qquad x_2 = 22.375 \qquad x_3 = 24.665 \qquad x_4 = 0.0454 - i0.1086, \qquad x_5 = \bar{x}_4.$$

Getting z^2 from (43), we obtain y_1 and y_2 by the equation $y^2 - zy + x = 0$. In all cases, at least one of y_1 or y_2 has an absolute value greater than 1. So, there is no eigenvalues and the scheme is stable.

Notice that if we take the equation (38), the only change is $s \to -s$ and the result is the same.

The schemes are stable for the two problems (37) and (38), with both boundary schemes of first or third order.

4.3 Numerical results.

4.3.1 Discretized Equations.

The discretised first formulation of the shallow-water equations is the following:

$$\frac{\partial u}{\partial t} - \overline{(f+\xi)}^{y}\overline{v}^{xy} + \frac{\partial B}{\partial x} = \frac{\tau^{(x)}}{\rho_0 \overline{h}^{x}} - ru + \nu\Delta u \tag{46}$$

$$\frac{\partial v}{\partial t} + \overline{(f+\xi)}^{x}\overline{u}^{xy} + \frac{\partial B}{\partial y} = \frac{\tau^{(y)}}{\rho_0 \overline{h}^{y}} - rv + \nu\Delta v \tag{47}$$

$$\frac{\partial h}{\partial t} + \frac{\partial\left(\overline{h}^{x}u\right)}{\partial x} + \frac{\partial\left(\overline{h}^{y}v\right)}{\partial y} = 0. \tag{48}$$

with

$$f = f_0 + \beta y \tag{49}$$

$$\xi = \frac{\partial v}{\partial x} - \frac{\partial u}{\partial y} \tag{50}$$

$$B = g'h + \frac{1}{2}\left((\overline{u}^{x})^2 + (\overline{v}^{y})^2\right) \tag{51}$$

The discretised last formulation of the shallow-water equations is:

$$\frac{\partial u}{\partial t} - \overline{\left(f - \frac{\partial u}{\partial y}\right)}^{y}\overline{v}^{xy} + \frac{\partial B_u}{\partial x} = \frac{\tau^{(x)}}{\rho_0 \overline{h}^{x}} - ru + \nu\Delta u \tag{52}$$

$$\frac{\partial v}{\partial t} + \overline{\left(f + \frac{\partial v}{\partial x}\right)}^{x}\overline{u}^{xy} + \frac{\partial B_v}{\partial y} = \frac{\tau^{(y)}}{\rho_0 \overline{h}^{y}} - rv + \nu\Delta v \tag{53}$$

$$\frac{\partial h}{\partial t} + \frac{\partial\left(\overline{h}^{x}u\right)}{\partial x} + \frac{\partial\left(\overline{h}^{y}v\right)}{\partial y} = 0 \tag{54}$$

with

$$f = f_0 + \beta y \tag{55}$$

$$B_u = g'h + \frac{1}{2}\left((\overline{u}^x)^2\right) \tag{56}$$

$$B_v = g'h + \frac{1}{2}\left((\overline{v}^y)^2\right) \tag{57}$$

We recall that the two formulations are equivalent for the second-order center interpolations and discrete measurements of gradients, but not for the fourth-order compact interpolations or measurements of gradients.

4.3.2 Boundary conditions.

The solid boundaries are placed such that north-south sections of coastline fall on v-points, and east-west sections fall on v-points. The solid wall boundary conditions of no normal flow is therefore naturally imposed.

A second boundary conditions is required. We consider two alternatives:

- no-slip where the tangential flow is zero on the boundary, i.e.

$$\overline{v}^x = 0, \text{ (north-south boundary)}, \overline{u}^y = 0, \text{ (east-west boundary)}.$$

- free-slip where the tangential shear vanishes on the boundary but the tangential flow remains finite, i.e.

$$\frac{\partial v}{\partial x} = 0, \text{ (north-south boundary)}, \frac{\partial u}{\partial y} = 0, \text{ (east-west boundary)}.$$

In the solutions with centered second-order schemes, boundary conditions are implemented using "ghost points" lying a half grid point outside the model domain. Along a no-slip boundary, the velocity at the ghost point is set equal and opposite to the interior value, whereas along a free-slip boundary, the ghost velocity is set equal to the interior value. In the solutions with center compact fourth-order schemes, the boundary conditions are implemented using a decentered schemes. For the equation of mass conservation, we use a first-order accuracy scheme. The reason is that this scheme is stable even for small coefficient of viscosity ν, since the third-order accuracy one requires larger coefficient. By the works of Gustafsson [Gustafsson1] [Gustafsson2], we know that the fact that the boundary scheme is only of first order can cause the lost of accuracy even inside the domain, but in numerical experiments, the lost of accuracy does not seem to be so large.

4.3.3 Numerical experiments.

On a basin with thickness 500 m.

The tests are made on an Arakawa C-grid. The coefficients are the following:

- L=2000 km
- nx=ny=82 (with one ghost point)
- hx=hy=25 km
- $\mu = 500\ m^2 s^{-1}$ (viscosity)
- $\sigma = 2.0 \times 10^{-7} s^{-1}$ (bottom friction)
- $\gamma = 0.02$ (Filter of Asselin)
- $f = 7.0 \times 10^{-5} s^{-1}$ (Coriolis)
- $g' = 0.02\ m\ s^{-2}$ (reduced gravity)
- $h_0 = 500\ m$ (initial layer thickness)
- $\beta_0 = 2.0 \times 10^{-11} m^{-1} s^{-1}$ (Coriolis)

- $\rho_0 = 1000\ kg\ m^{-3}$ (reference density)
- $\tau_0 = 0.2\ N\ m^{-2}$ (wind stress coefficient)
- $y_0 = L/2$
- $\tau^{(x)}(y) = \tau_0 * cos(2 * \pi * (y - y_0)/L)$ (wind stress)
- $\tau^{(y)} = 0$

We first present the results with free slip condition on the boundary (14, 15, 13). We present instantaneous view of the thickness for T=200 days, 400 days and 600 days. Then, we present the mean value of the velocity u,v, and the thickness h during the period T=400 to 600 days. Finally, we show the evolution of the mass in the basin, and of the energy. We theoretically have the mass conservation. In fact, with the e2 scheme for the divergence, the mass is exactly conserved (error of order 10^{-15}) but not with c4 or c6 scheme for the divergence. We then present the same results with no slip condition on the boundary (16, 17, 18).

At about 750 days, in both scheme e2 and c4, appears a little domain where $h = 0$. So, since in the equation of u, we divide the external forcing by the thickness h, we have an explosion. Notice that this phenomenon appears at about the same time for both schemes.

We then present result for an ocean basin with thickness equal to 1000 m, for free slip and then no slip boundary conditions.

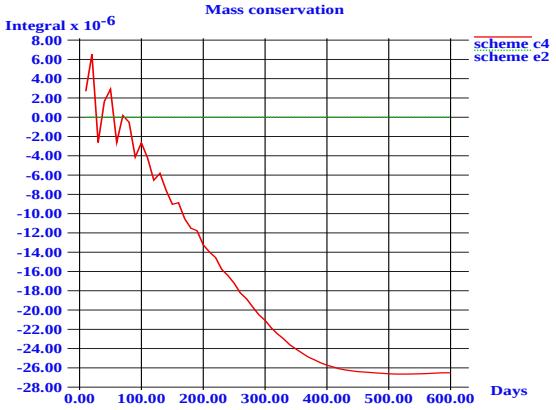

Figure 13A. Mass conservation $\left(\int_\Omega h(t,x,y) - h_0\right)/h_0$ with 4th order Runge-Kutta scheme in time and e2 and c4 in space, free slip conditions on the boundary, dt=1800s.

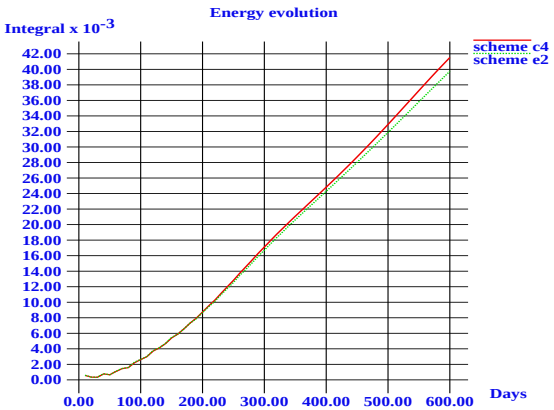

Figure 13B. Evolution of Energy with 4th order Runge-Kutta scheme in time and e2 and c4 in space, free slip conditions on the boundary, dt=1800s.

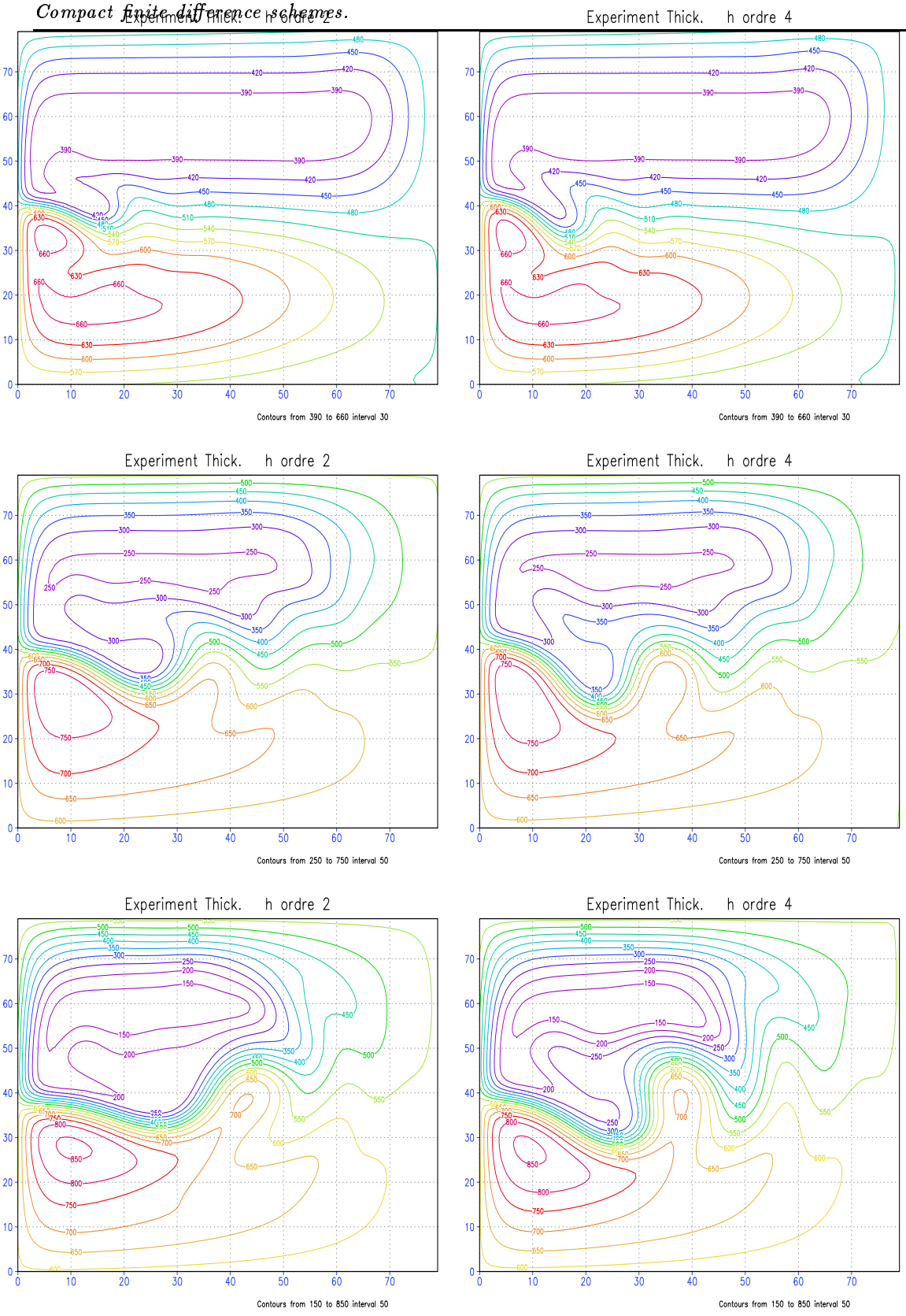

Figure 14. Solution at T=200 (upper), 400 (center), and 600 (bottom) days, for $h(t,x,y)$ with 4th order Runge-Kutta scheme in time and in space e2 (left), c4 (right), free slip conditions on the boundary, dt=1800s, $\tau(y) = \tau_0 * cos(2 * \pi * (y - y_0)/L)$.

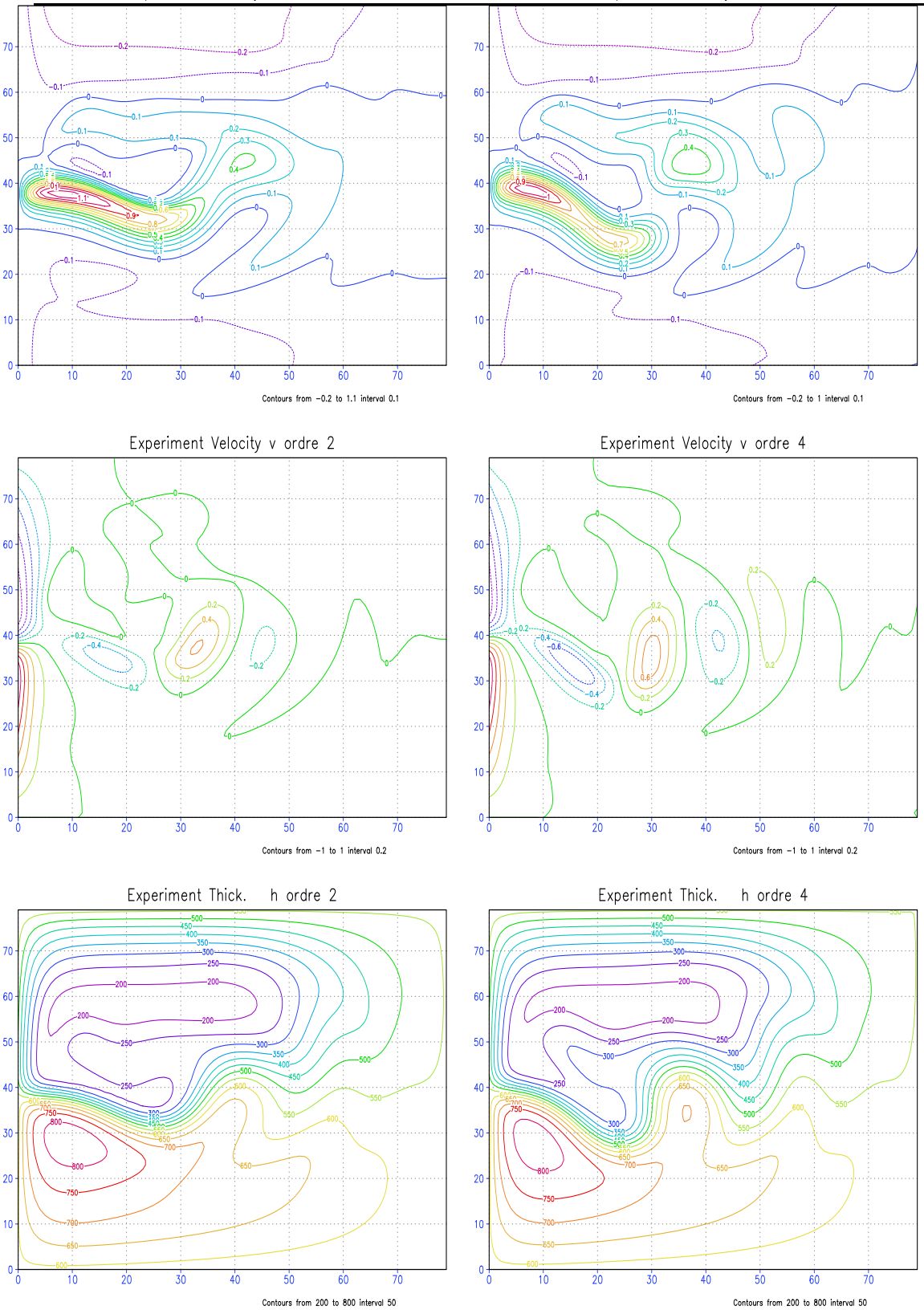

Figure 15. Mean solution between T=400 and T=600 days for $u(t,x,y), v(t,x,y), h(t,x,y)$ with 4th order Runge-Kutta scheme in time and in space e2 (left), c4 (right), free slip conditions on the boundary, dt=1800s.

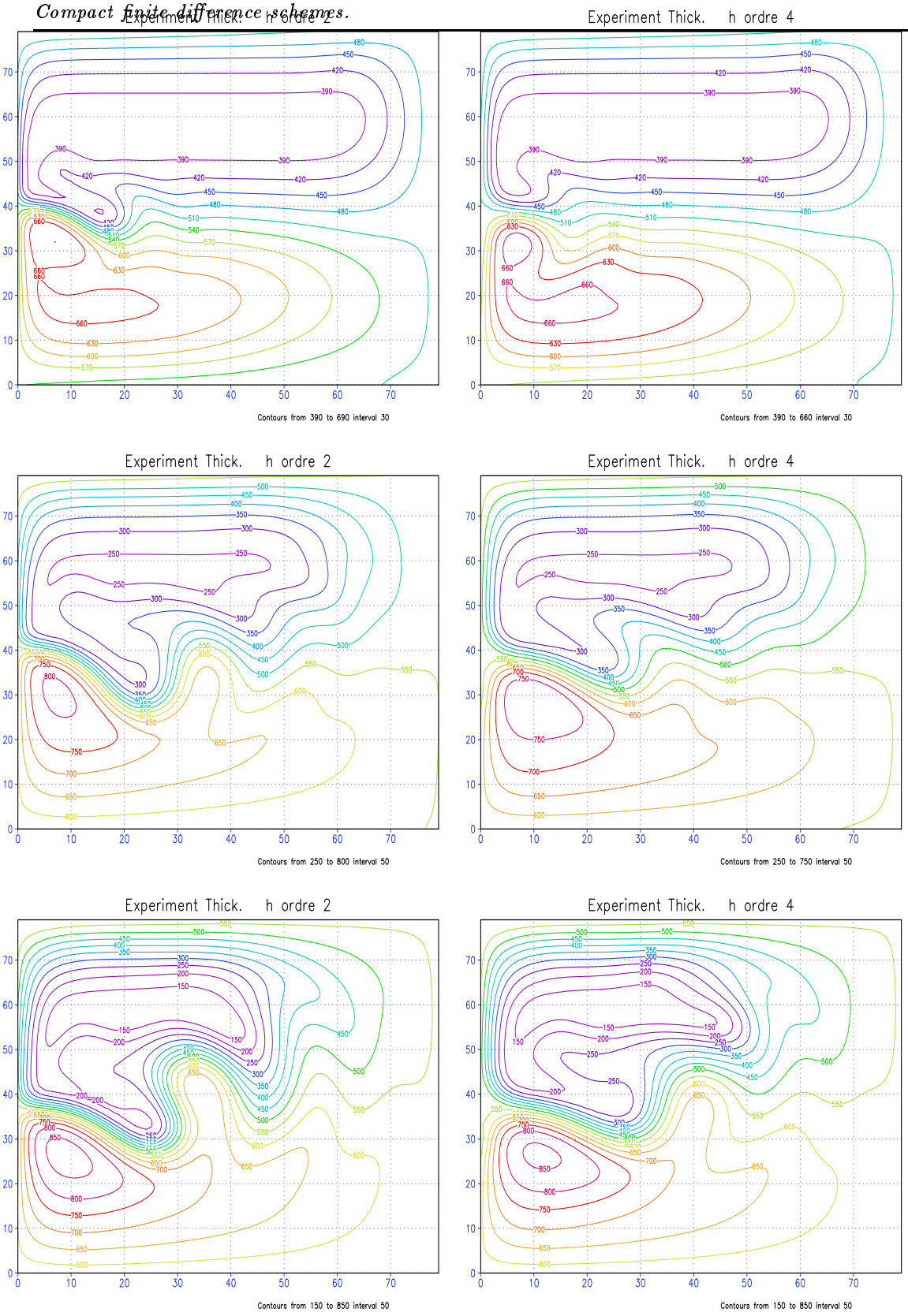

Figure 16. Solution at T=200 (upper), 400 (center), and 600 (bottom) days, for $h(t,x,y)$ with 4th order Runge-Kutta scheme in time and in space e2 (left), c4 (right), no slip conditions on the boundary, dt=1800s,$\tau(y) = \tau_0 * cos(2 * \pi * (y - y_0)/L)$.

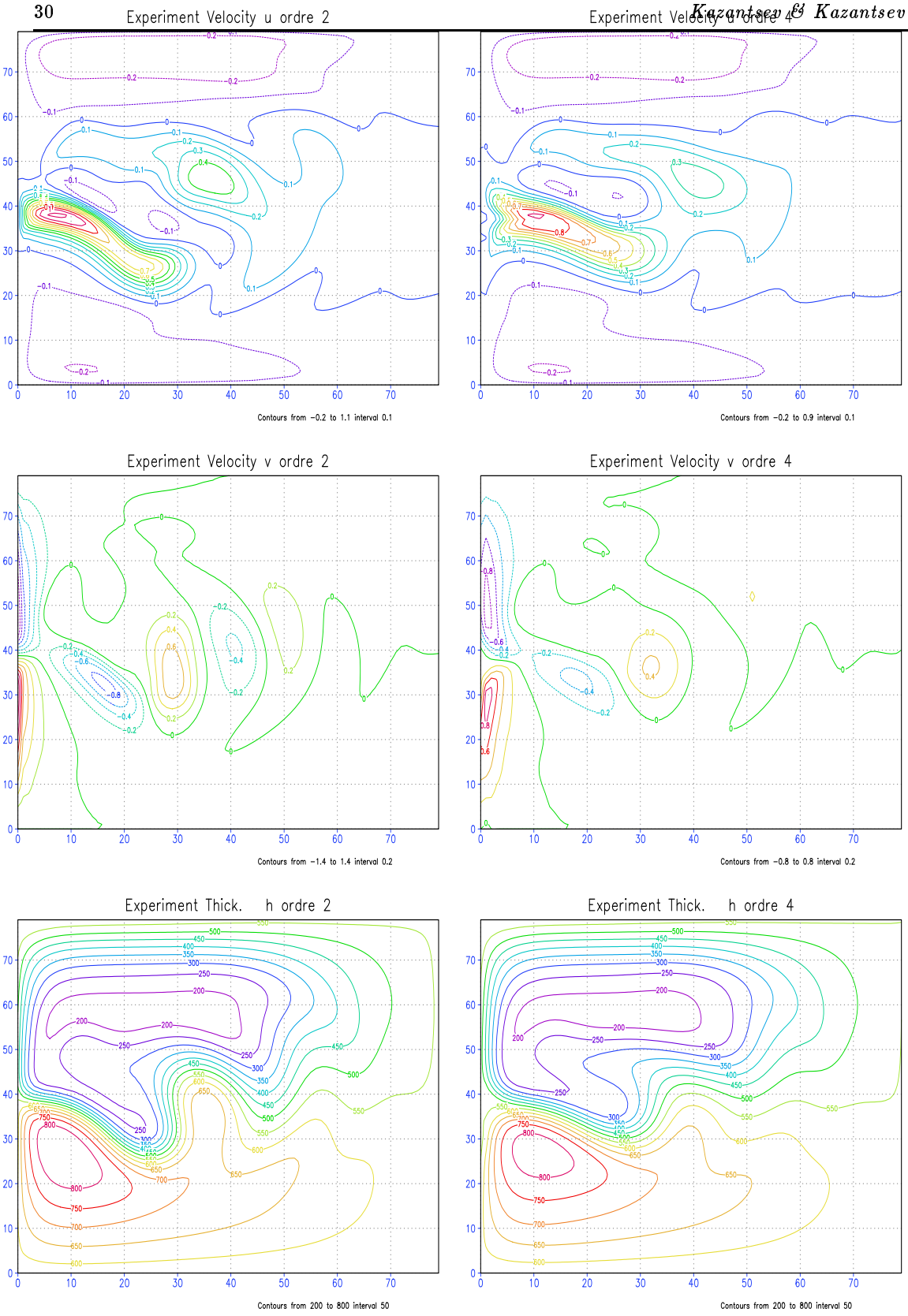

Figure 17. Mean solution between T=400 and T=600 days for $u(t,x,y), v(t,x,y), h(t,x,y)$ with 4th order Runge-Kutta scheme in time and in space e2 (left), c4 (right), no slip conditions on the boundary, dt=1800s.

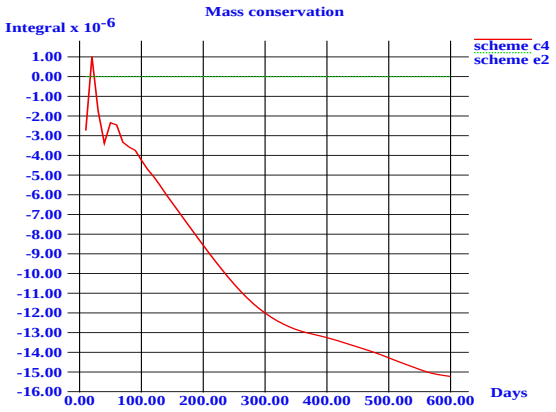

Figure 18A. Mass conservation $\left(\int_\Omega h(t,x,y) - h_0\right)/h_0$ with 4th order Runge-Kutta scheme in time and e2 and c4 in space, no slip conditions on the boundary, dt=1800s.

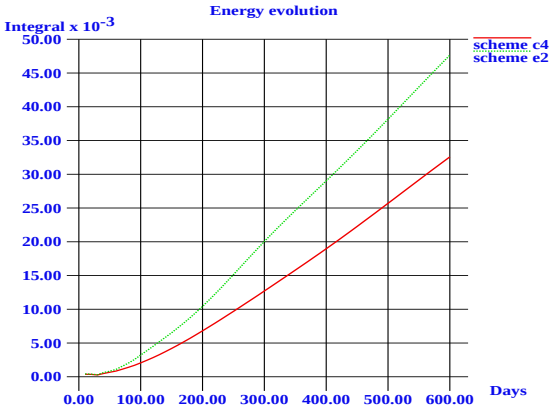

Figure 18B. Evolution of Energy with 4th order Runge-Kutta scheme in time and e2 and c4 in space, no slip conditions on the boundary, dt=1800s.

On a basin with thickness 1000 m.

The tests are made on an Arakawa C-grid. The coefficients are the same as before, except σ and h_0, i.e. are the following:

- L=2000 km
- nx=ny=82 (with one fictive point)
- hx=hy=25 km
- $\mu = 500\ m^2 s^{-1}$ (viscosity)
- $\sigma = 1.0 \times 10^{-7} s^{-1}$ (bottom friction)
- $\gamma = 0.02$ (Filter of Asselin)
- $f = 7.0 \times 10^{-5} s^{-1}$ (Coriolis)
- $g' = 0.02\ m\ s^{-2}$ (reduced gravity)
- $h_0 = 1000\ m$ (initial layer thickness)
- $\beta_0 = 2.0 \times 10^{-11} m^{-1} s^{-1}$ (Coriolis)
- $\rho_0 = 1000\ kg\ m^{-3}$ (reference density)
- $\tau_0 = 0.2\ N\ m^{-2}$ (wind stress coefficient)
- $y_0 = L/2$
- $\tau^{(x)}(y) = \tau_0 * cos(2 * \pi * (y - y_0)/L)$ (wind stress)
- $\tau^{(y)} = 0$

We consider 2 tests, one with free-slip boundary conditions, one with no slip boundary conditions. For each test, we compute 3200 days, by 8 series of 400 days. We save the functions u, v, h each 10 days, and the for each series of 400 days, we compute

- the average of these functions u_{av}, v_{av}, h_{av} (i.e. average between $T_d = 0$ and $T_f = 400$ days, between $T_d = 400$ days and $T_f = 800$ days, etc), defined by

$$f_{av}(x,y) = \frac{1}{T_f - T_d} \int_{t=T_d}^{t=T_f} f(x,y,t)dt,$$

for $f = u, v, h$ respectively,

- the dispersion of these functions u_d, v_d, h_d with

$$f_d(x,y) = \frac{1}{T_f - T_d} \int_{t=T_d}^{t=T_f} \left(f(x,y,t) - f_{av}(x,y,t)\right)^2 dt,$$

  for $f = u, v, h$ respectively,

- the Mean Kinetic Energy $MKE(x,y) = \frac{1}{2}\left(u_{av}^2(x,y) + v_{av}^2(x,y)\right)$
- the Eddy Kinetic Energy $EKE(x,y) = \frac{1}{2}\left(u_d + v_d\right)$
- the Total Kinetic Energy $TKE(x,y) = MKE(x,y) + EKE(x,y)$.

We compute also some other energies along the time. Each 5 days, we save

- the mass conservation error, denoted by

$$"(mass - h_0)"(t) = \frac{1}{h_0}\left(\frac{1}{|\Omega|}\int_\Omega h(x,y,t)dxdy - h_0\right)$$

- the Kinetic Energy, defined by

$$KE(t) = \frac{1}{|\Omega|}\int_\Omega \frac{1}{2}\left(u^2(x,y,t) + v^2(x,y,t)\right) dxdy$$

- the ponderated Kinetic Energy, defined by

$$PKE(t) = \frac{1}{|\Omega|}\int_\Omega \frac{1}{2}h(x,y,t)\left(u^2(x,y,t) + v^2(x,y,t)\right) dxdy$$

- the Potential Energy, defined by

$$PE(t) = \frac{1}{|\Omega|}\int_\Omega \frac{1}{2}g' * h^2(x,y,t)dxdy$$

- the "Relative" Potential Energy, defined by

$$RPE(t) = \frac{1}{|\Omega|}\int_\Omega \frac{1}{2}g' * \left(h(x,y,t) - h_0(x,y)\right)^2 dxdy$$

  Notice that $PE = RPE + \frac{g'}{2}h_0^2(x,y) = RPE + 10^4$ with our parameters.

- the Total Energy defined by $TE(t) = RPE(t) + PKE(t)$ i.e.

$$TE(t) = \frac{1}{|\Omega|}\int_\Omega \frac{1}{2}\left(h(x,y,t) * \left(u^2(x,y,t) + v^2(x,y,t)\right) + g' * h^2(x,y,t)\right) dxdy$$

In fact, (see [Gill] page 111), $\rho_0 * PKE$, $\rho_0 * RPE$ and $\rho_0 * TE$ are respectively the Kinetic Energy, the Potential Energy and the Total Energy.

The difference between solutions with e2 scheme and c4 scheme is very large. So, in the following, we first present the solution h for both schemes at different time, and the mean solution computed between T=800 days and T=1200 days. We then show the different curves of energy $KE(t), PKE(t), RPE$. Finally, we present the pictures of u_{av}, v_{av}, h_{av}, u_d, v_d, h_d, $MKE(x,y), EKE(x,y), TKE(x,y)$ for $T_d = 2800$ and $T_f = 3200$.

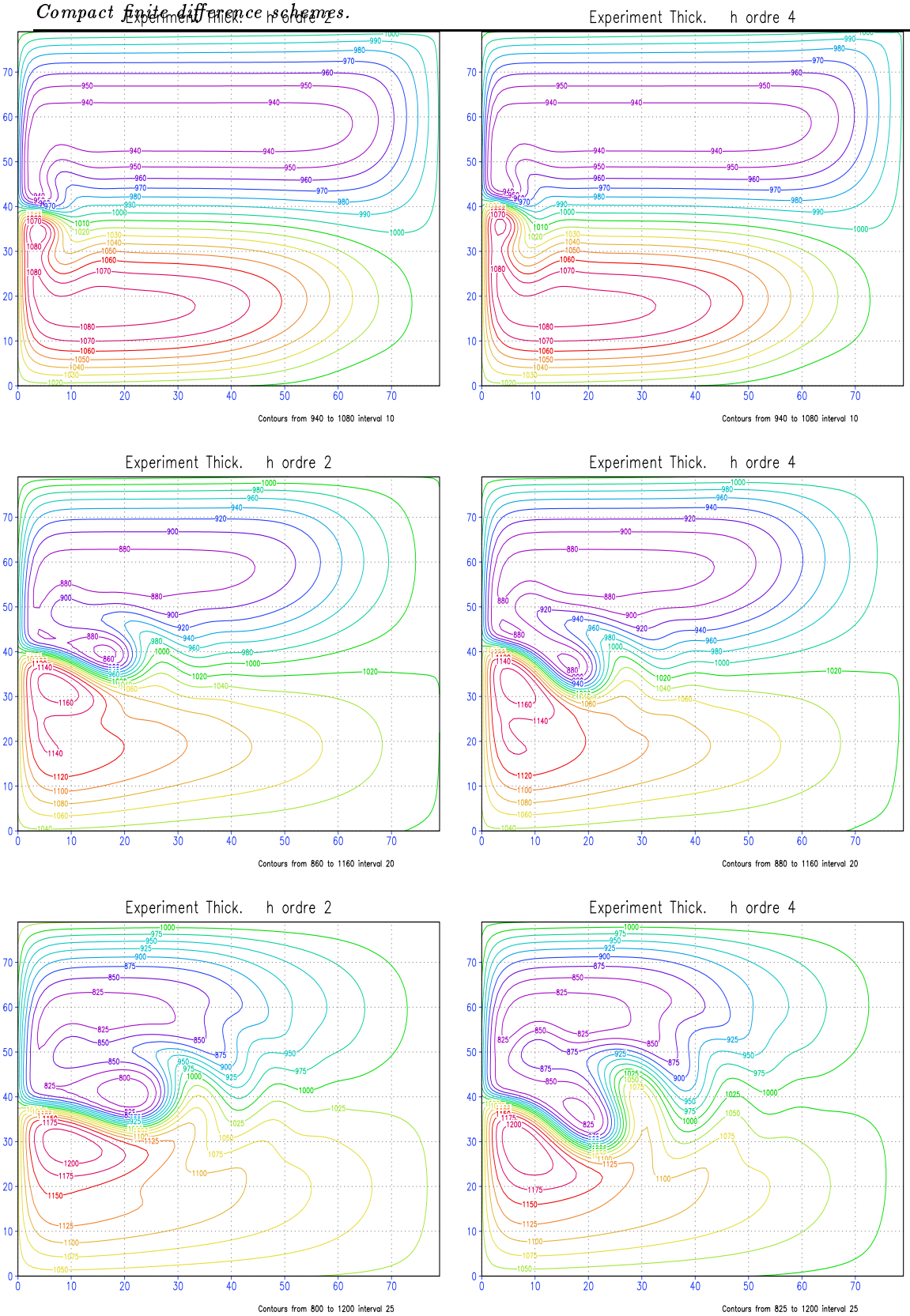

Figure 19. Solution at T=100 (upper), 200 (center), and 300 (bottom) days, for $h(t,x,y)$ with 4th order Runge-Kutta scheme in time and in space e2 (left), c4 (right), free slip conditions on the boundary, dt=1800s, $h_0 = 1000$ m.

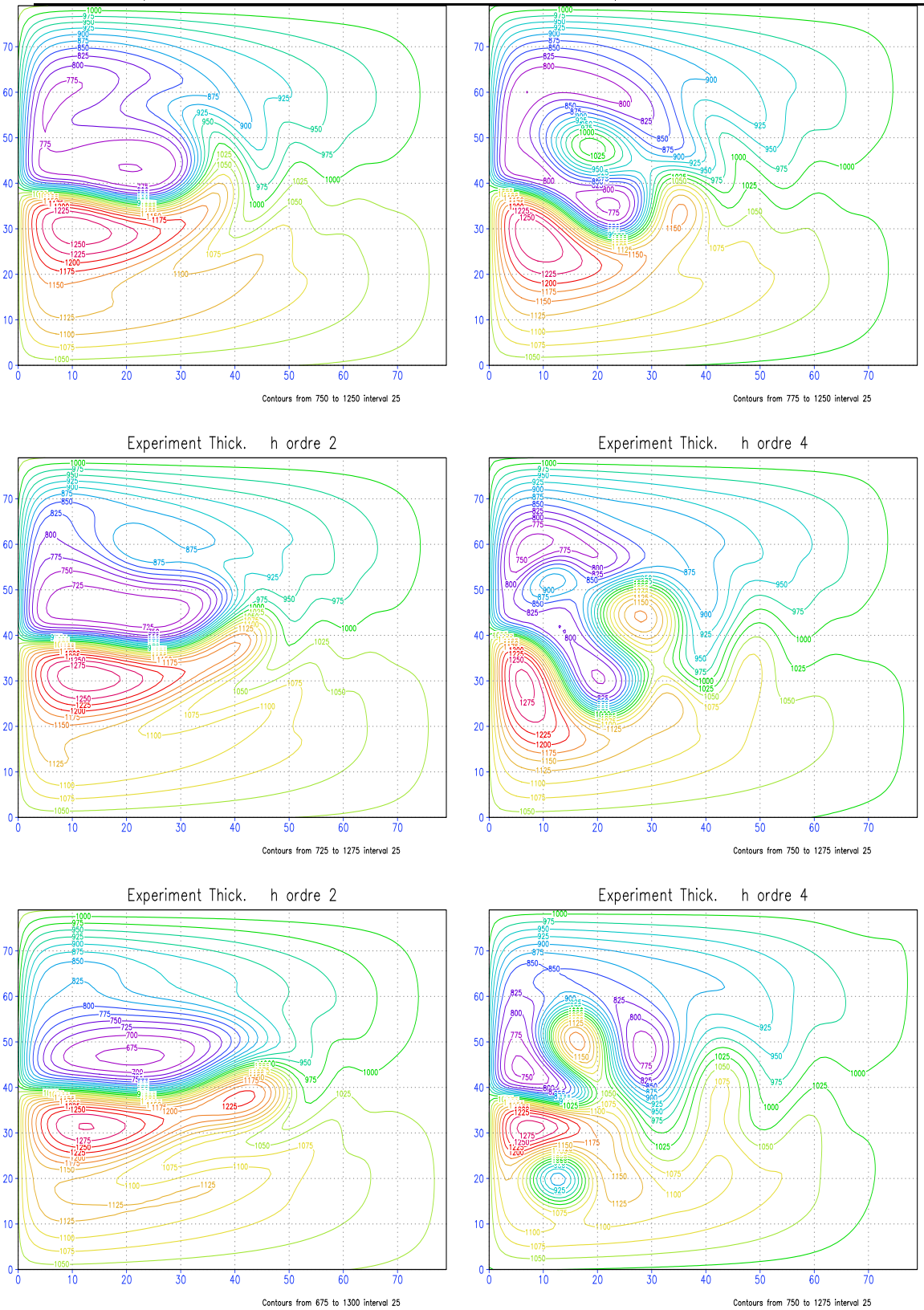

Figure 20. Solution at T=400 (upper), 500 (center), and 600 (bottom) days, for $h(t, x, y)$ with 4th order Runge-Kutta scheme in time and in space e2 (left), c4 (right), free slip conditions on the boundary, dt=1800 s, $h_0 = 1000$ m.

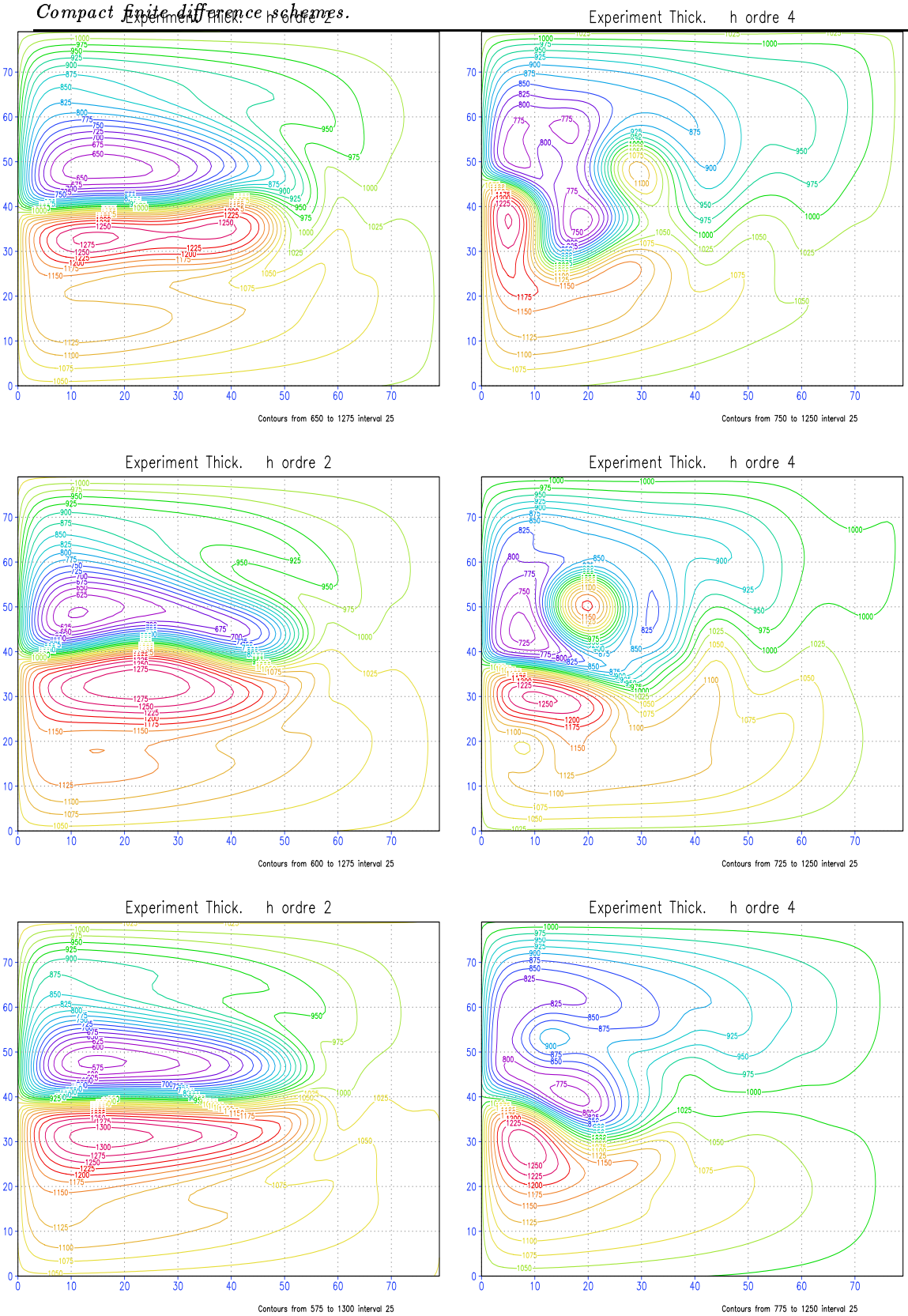

Figure 21. Solution at T=700 d (upper), 800 d(center), and Mean solution between T=800 and T=1200 (bottom) days, for $h(t, x, y)$ with 4th order Runge-Kutta scheme in time and in space e2 (left), c4 (right), free slip conditions on the boundary, dt=1800 s, $h_0 = 1000$ m.

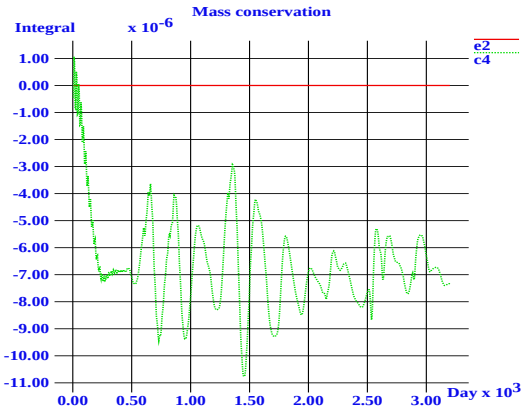

Figure 22A. Mass conservation $\left(\int_\Omega h(t,x,y) - h_0\right)/h_0$ with 4th order Runge-Kutta scheme in time and e2 and c4 in space, free slip conditions on the boundary.

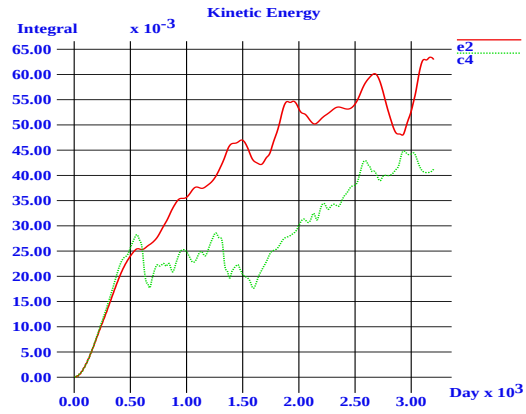

Figure 22B. Evolution of Kinetic Energy with 4th order Runge-Kutta scheme in time and e2 and c4 in space, free slip conditions on the boundary.

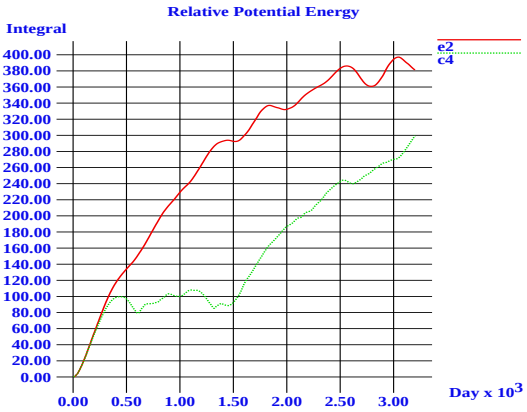

Figure 23A. Evolution of Relative Potential Energy with 4th order Runge-Kutta scheme in time and e2 and c4 in space, free slip conditions on the boundary.

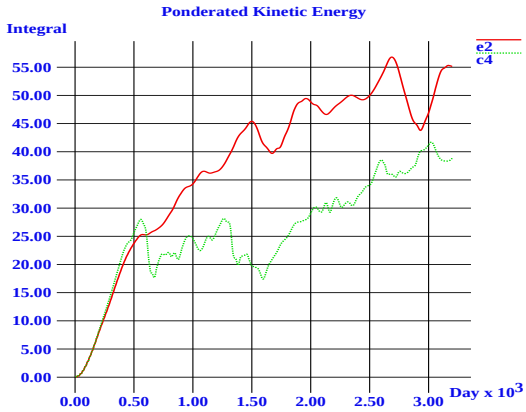

Figure 23B. Evolution of Ponderated Kinetic Energy with 4th order Runge-Kutta scheme in time and e2 and c4 in space, free slip conditions on the boundary.

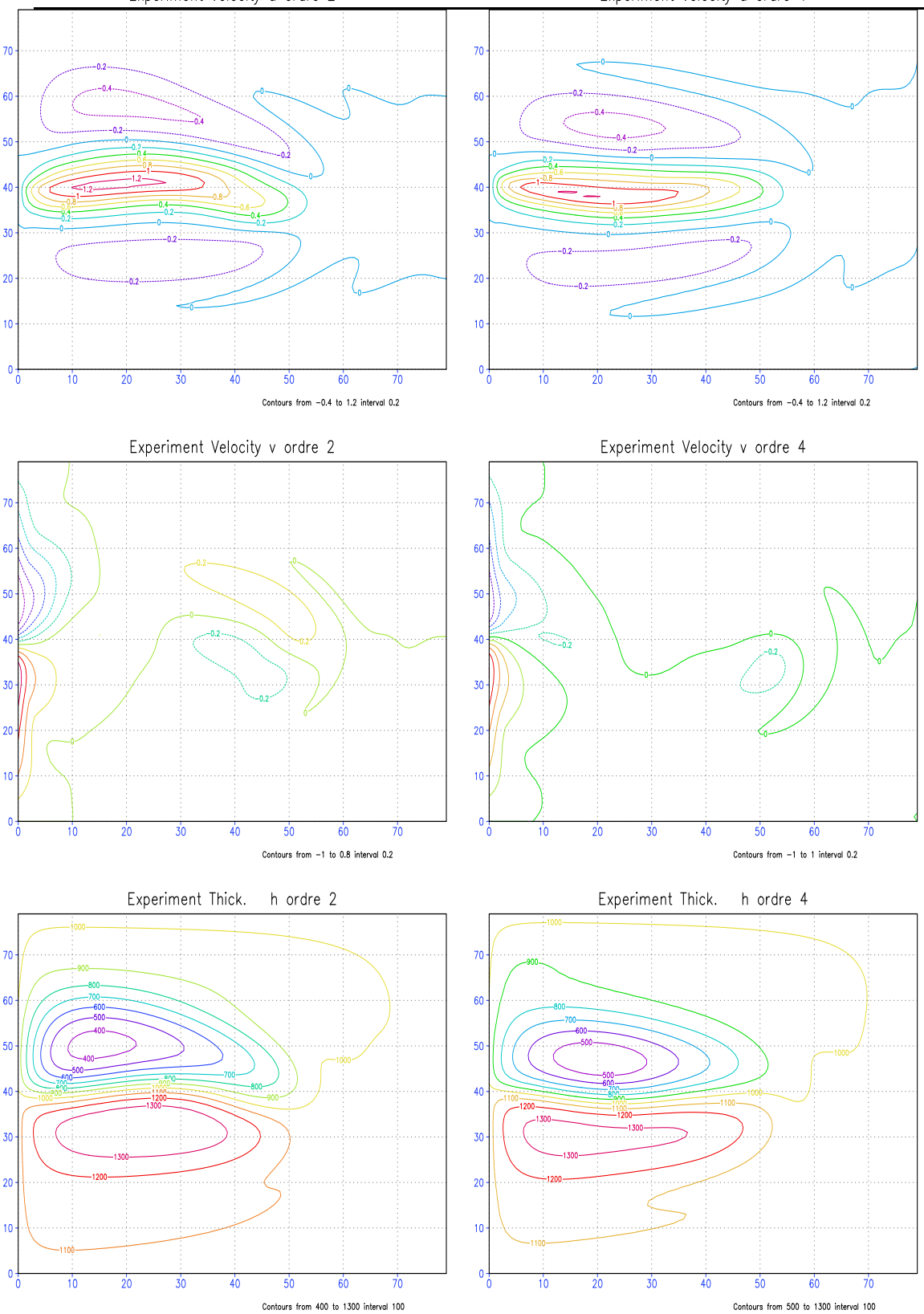

Figure 24. Mean solution between T=2800 and T=3200 days, for u (upper), v (center), and h (bottom) with 4th order Runge-Kutta scheme in time and in space e2 (left), c4 (right), free slip conditions on the boundary, dt=1800 s, $h_0 = 1000$ m.

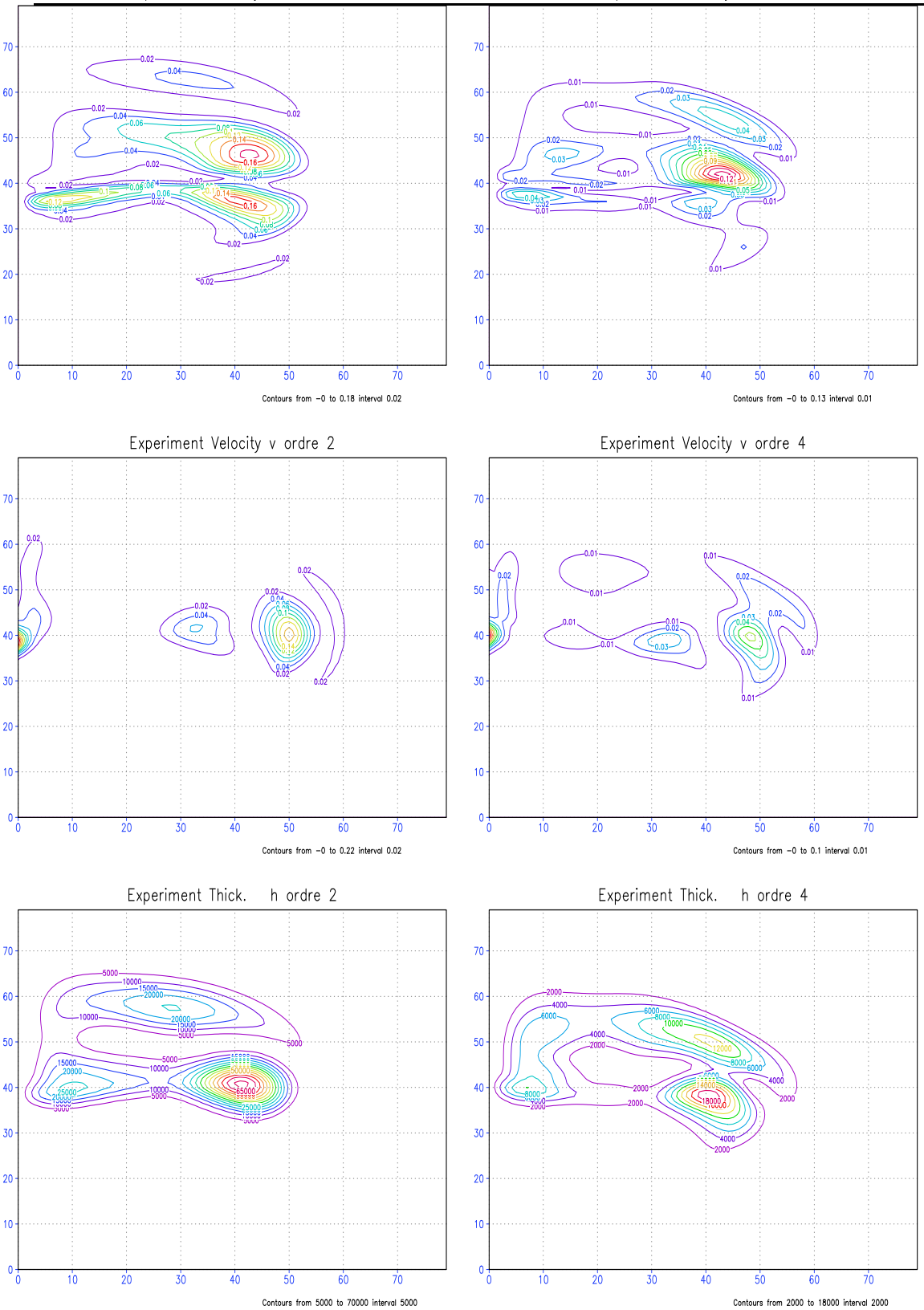

Figure 25. Dispersion between T=2800 and T=3200 days, for u (upper), v (center), and h (bottom) with 4th order Runge-Kutta scheme in time and in space e2 (left), c4 (right), free slip conditions on the boundary, dt=1800 s, h_0 = 1000 m.

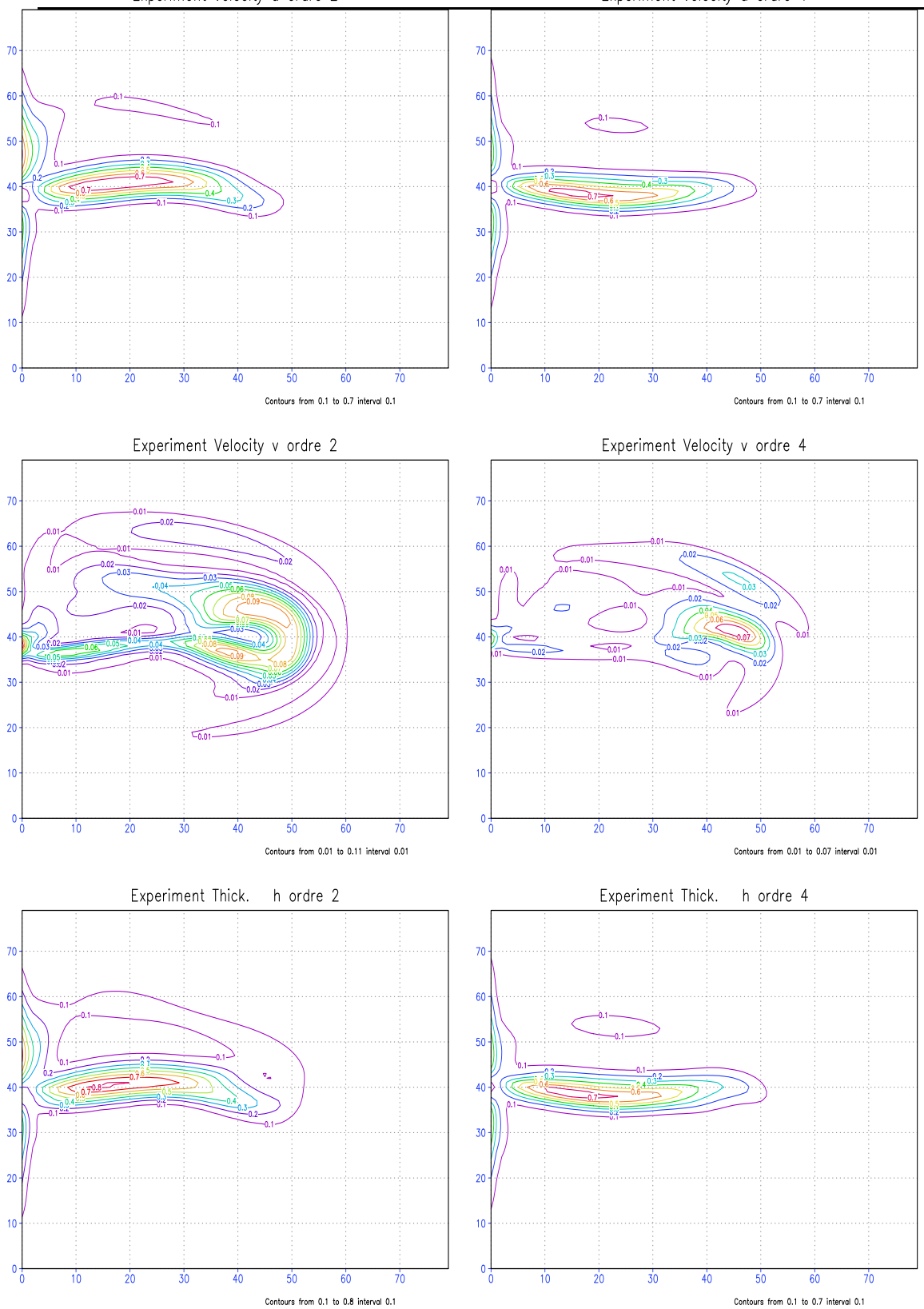

Figure 26. Energy between T=2800 and T=3200 days: MKE (upper), EKE (center), and TKE (bottom) with 4th order Runge-Kutta scheme in time and in space e2 (left), c4 (right), free slip conditions on the boundary, dt=1800 s, $h_0 = 1000$ m.

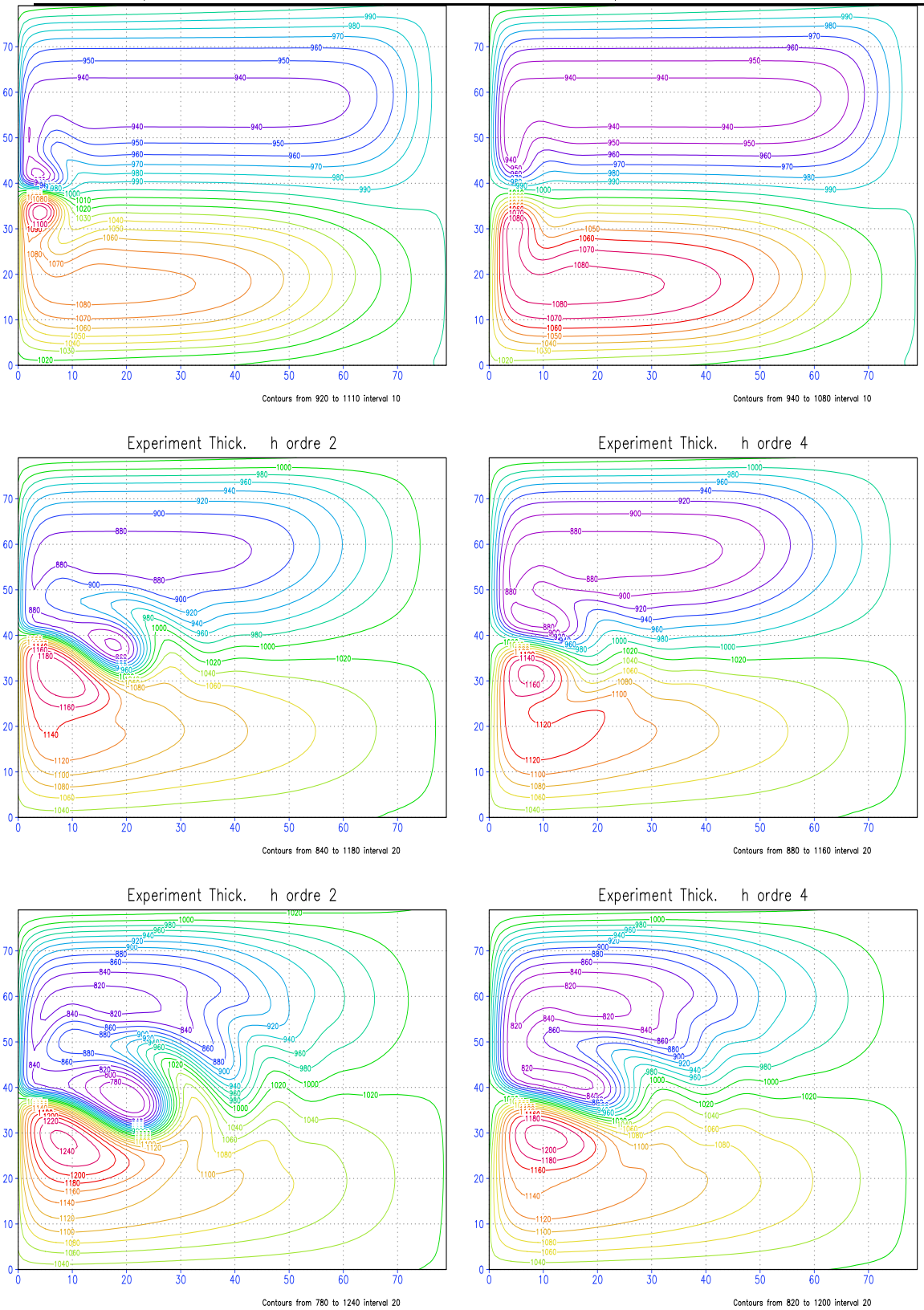

Figure 27. Solution at T=100 (upper), 200 (center), and 300 (bottom) days, for $h(t, x, y)$ with 4th order Runge-Kutta scheme in time and in space e2 (left), c4 (right), no slip conditions on the boundary, dt=1800s, $h_0 = 1000$ m.

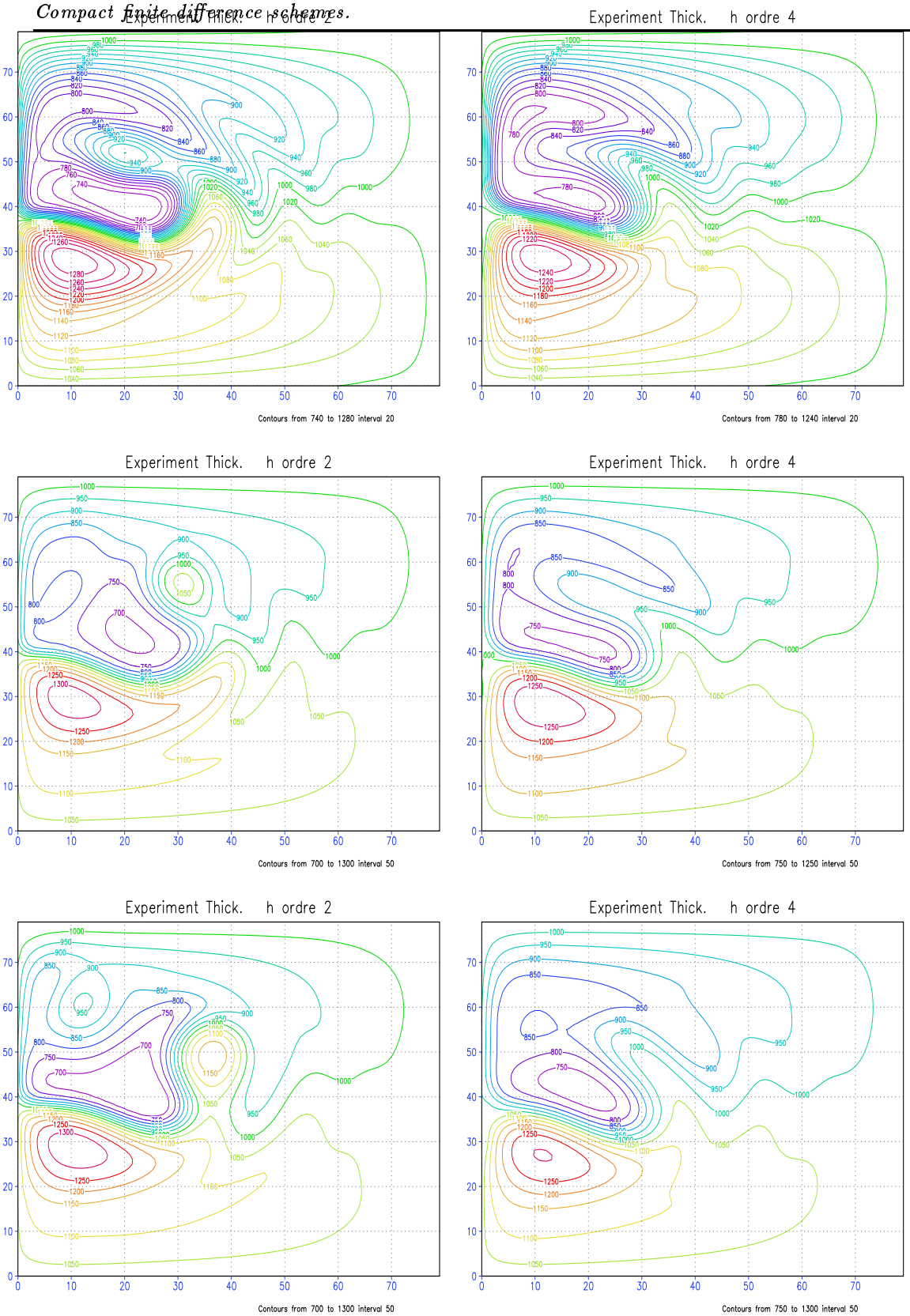

Figure 28. Solution at T=400 (upper), 500 (center), and 600 (bottom) days, for $h(t, x, y)$ with 4th order Runge-Kutta scheme in time and in space e2 (left), c4 (right), no slip conditions on the boundary, dt=1800 s, $h_0 = 1000$ m.

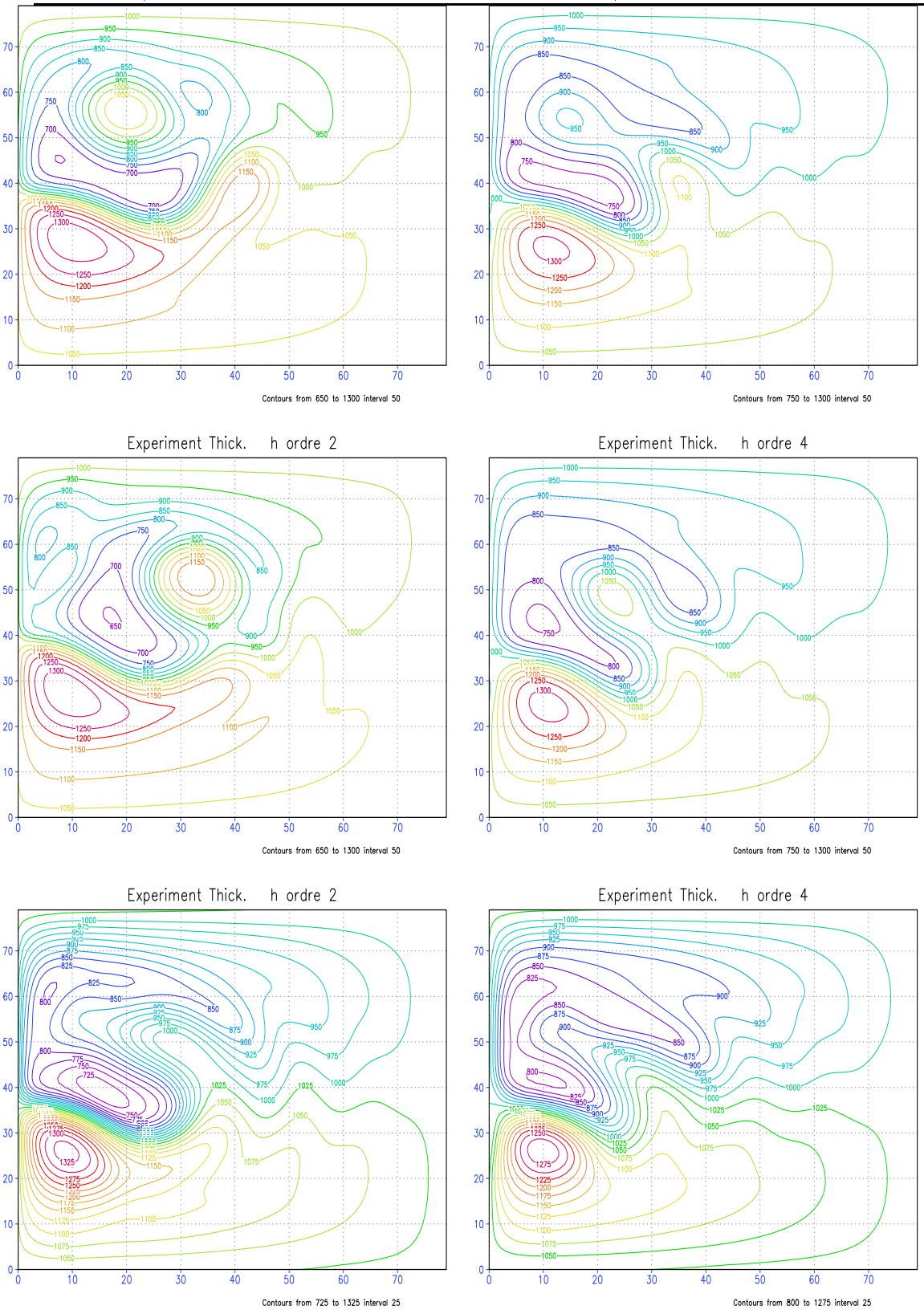

Figure 29. Solution at T=700 d (upper), 800 d(center), and Mean solution between T=800 and T=1200 (bottom) days, for $h(t, x, y)$ with 4th order Runge-Kutta scheme in time and in space e2 (left), c4 (right), no slip conditions on the boundary, dt=1800 s, $h_0 = 1000$ m.

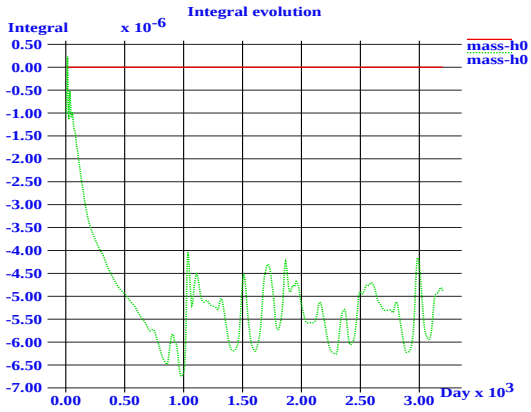

Figure 30A. Mass conservation $\left(\int_\Omega h(t,x,y) - h_0\right)/h_0$ with 4th order Runge-Kutta scheme in time and e2 and c4 in space, no slip conditions on the boundary.

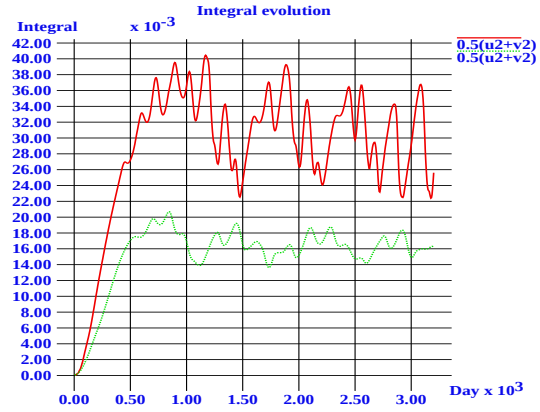

Figure 30B. Evolution of Kinetic Energy with 4th order Runge-Kutta scheme in time and in space e2 and c4, no slip conditions on the boundary.

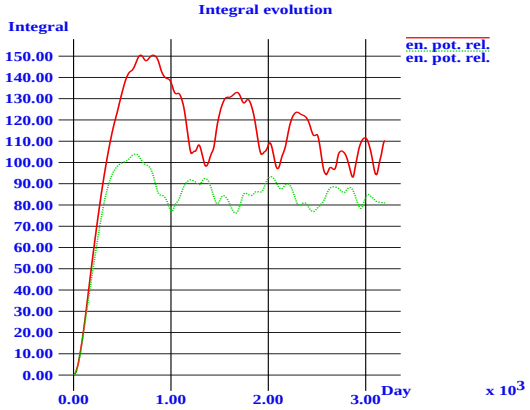

Figure 31A. Evolution of Relative Potential Energy with 4th order Runge-Kutta scheme in time and e2 and c4 in space, no slip conditions on the boundary.

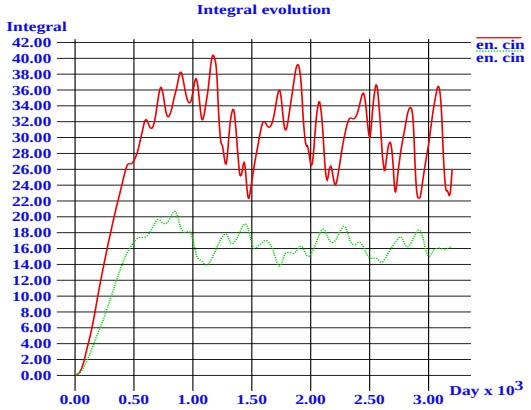

Figure 31B. Evolution of Ponderated Kinetic Energy with 4th order Runge-Kutta scheme in time and in space e2 and c4, no slip conditions on the boundary.

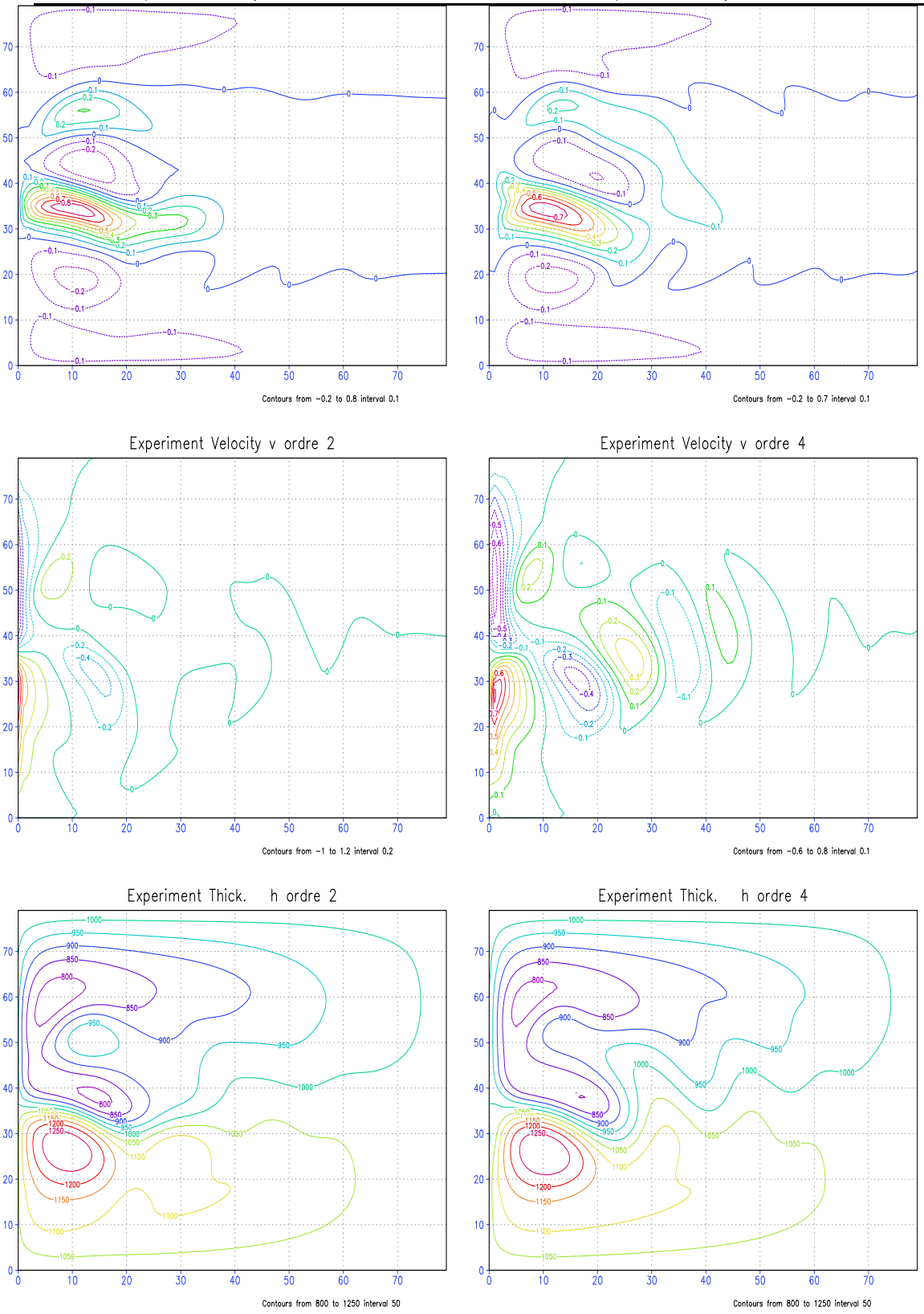

Figure 32. Mean solution between T=2800 and T=3200 days, for u (upper), v (center), and h (bottom) with 4th order Runge-Kutta scheme in time and in space e2 (left), c4 (right), no slip conditions on the boundary, dt=1800 s, $h_0 = 1000$ m.

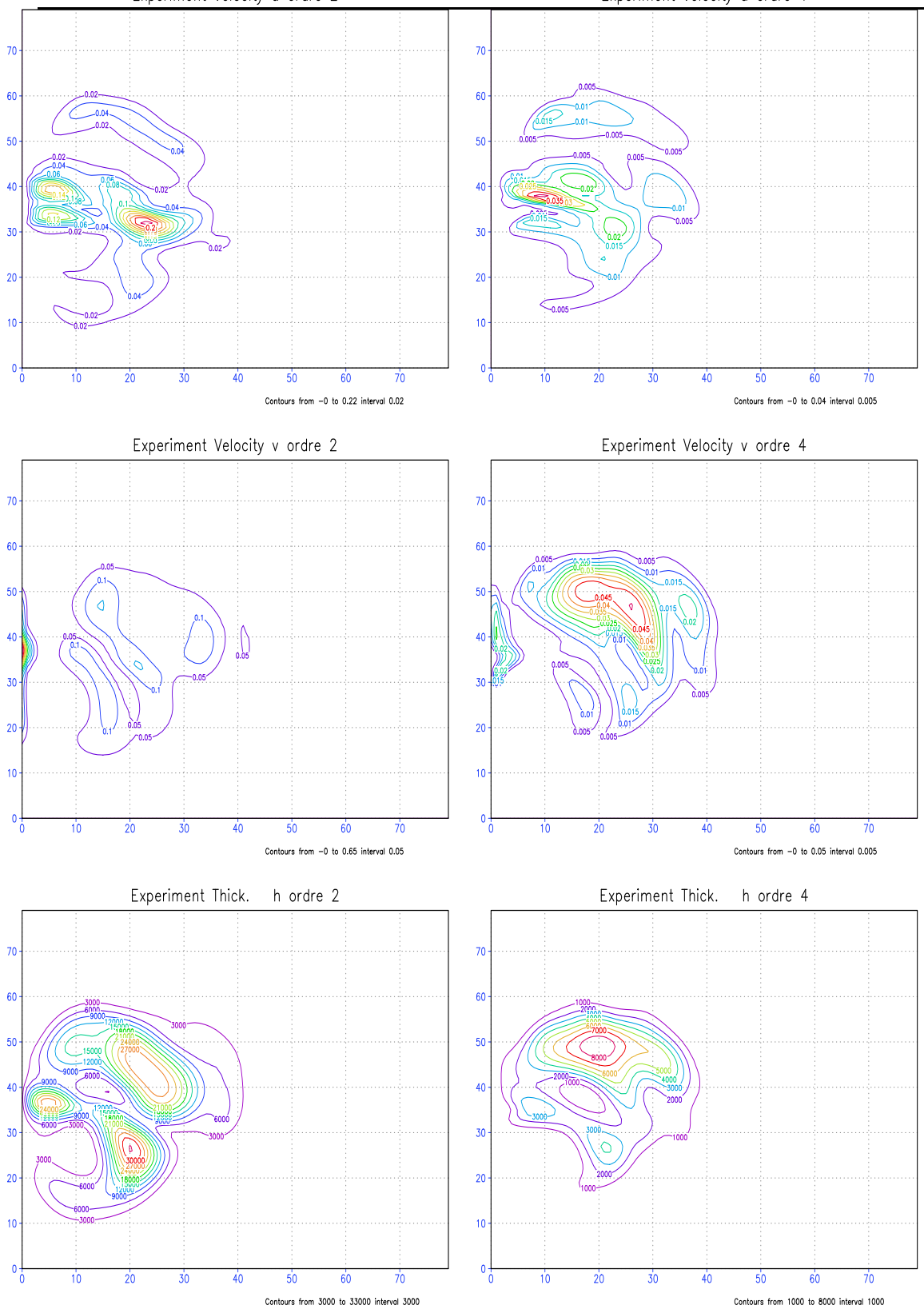

Figure 33. Dispersion between T=2800 and T=3200 days, for u (upper), v (center), and h (bottom) with 4th order Runge-Kutta scheme in time and in space e2 (left), c4 (right), no slip conditions on the boundary, dt=1800 s, $h_0 = 1000$ m.

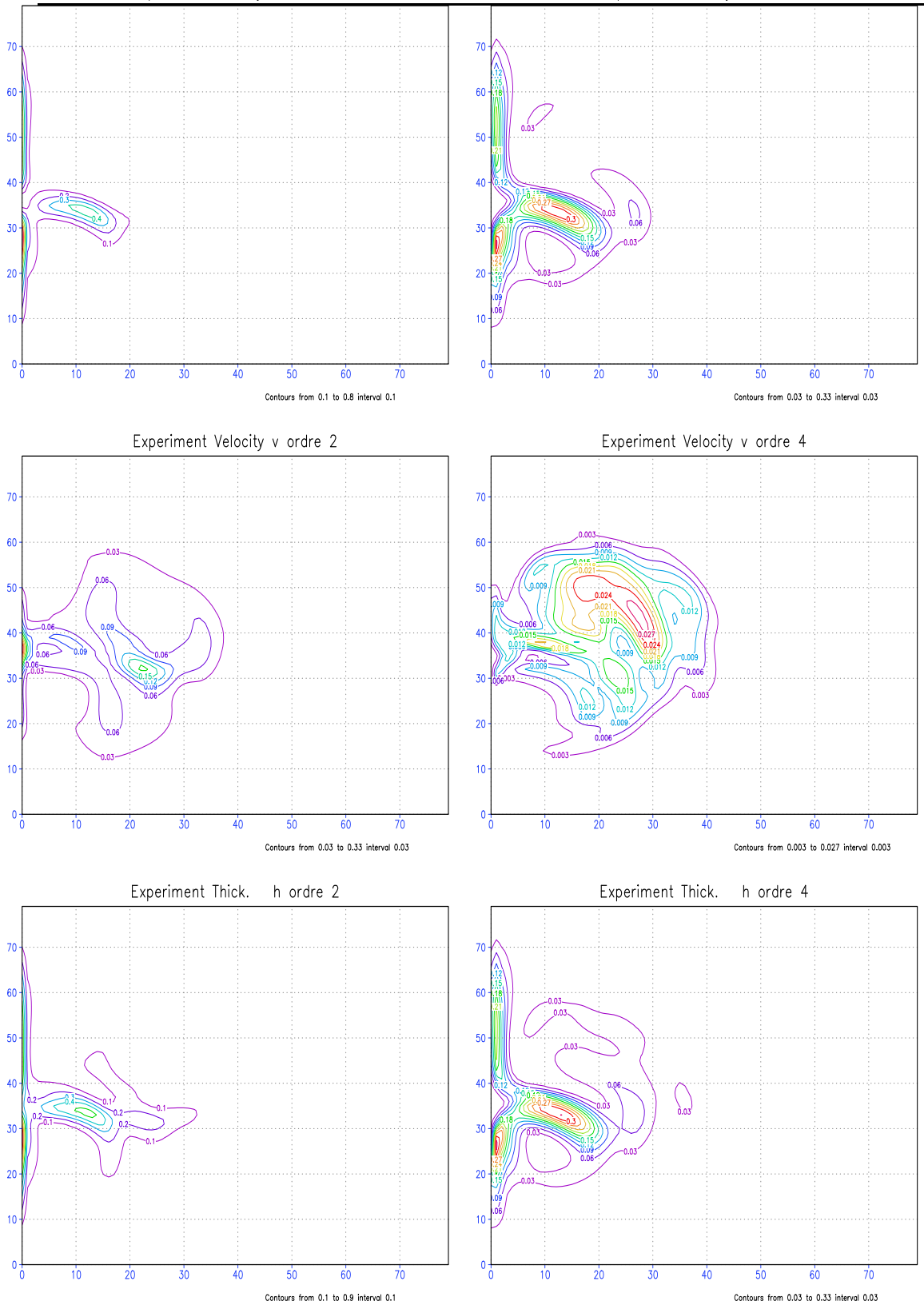

Figure 34. Energy between T=2800 and T=3200 days: MKE (upper), EKE (center), and TKE (bottom) with 4th order Runge-Kutta scheme in time and in space e2 (left), c4 (right), no slip conditions on the boundary, dt=1800 s, $h_0 = 1000$ m.

For a basin of length 2000km, the conclusions are quite difficult since the solutions are very different, and the boundary layer is unresolved. Nevertheless, some remarks must be made.

- in the case of free slip boundary condition (19-26):
  - the solution with the e2 scheme is a little asymmetric, the mean one for h (21) between T=800 and 1200 is symmetric. With the c4 scheme, the solution is very asymmetric. Notice than latter (T=2800 to 3200), then mean solution for each scheme are a little asymmetric, more or less similar, going on the north with e2 scheme, on the south with c4 scheme. MKE, EKE and TKE, (26) confirm that the solution are quite similar with both schemes.
  - the mass conservation is not verified with c4 scheme, but the error does not increase with time. It oscillates around 7. 10^{-6}, with an amplitude of 4. 10^{-6}. This range of error seems to be acceptable from a physical point of view.
  - the c4 scheme is less energetic than the e2 one.
- in the case of no slip boundary condition (27-34):
  - the last picture(34) shows that the energies are quite different, especially on the western boundary. This is due to the fact that the boundary layer is not resolved;
  - concerning the mass conservation and energy, the remark is the same as for free slip boundary condition.

4.3.4 Comparison for different space steps.

In this section, we consider the following parameters:

- L=2000 km
- $\mu = 200\ m^2 s^{-1}$ (viscosity)
- $\sigma = 0.5 \times 10^{-7} s^{-1}$ (bottom friction)
- $\gamma = 0.02$ (Filter of Asselin)
- $f = 7.0 \times 10^{-5} s^{-1}$ (Coriolis)
- $\beta_0 = 2.0 \times 10^{-11} m^{-1} s^{-1}$ (Coriolis)
- $g' = 0.02\ m\ s^{-2}$ (reduced gravity)
- $h_0 = 1000\ m$ (initial layer thickness)
- $\rho_0 = 1000\ kg\ m^{-3}$ (reference density)
- $\tau_0 = 0.15\ N\ m^{-2}$ (wind stress coefficient)
- $y_0 = L/2$
- $\tau^{(x)}(y) = \tau_0 * cos(2 * \pi * (y - y_0)/L)$ (wind stress)
- $\tau^{(y)} = 0$
- no slip boundary condition

We compute the solution with 4th order compact scheme (c4) and usual 2nd order centered scheme (e2) for 4500 days with different space steps: 50km, 25km, 16km. We present the Mean solution u, v, h, and the Mean Kinetic, Eddy Kinetic and Total Kinetic energy for the periods 1500-3000 days, and 3000-4500 days. We present also the curves of the evolution of the kinetic energy and total energy along the 4500 days.

Resolution 41 (50km) Second order.

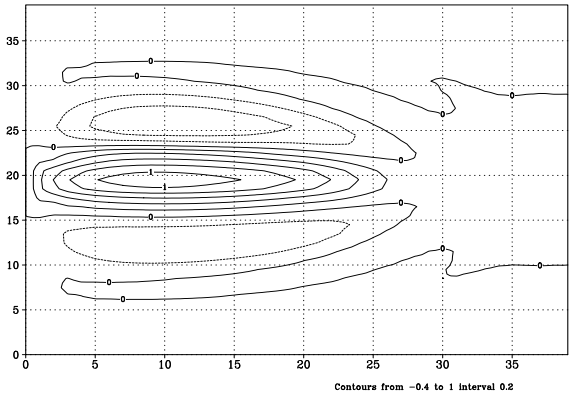

Figure 35A. Mean U velocity on 3000-4500 days

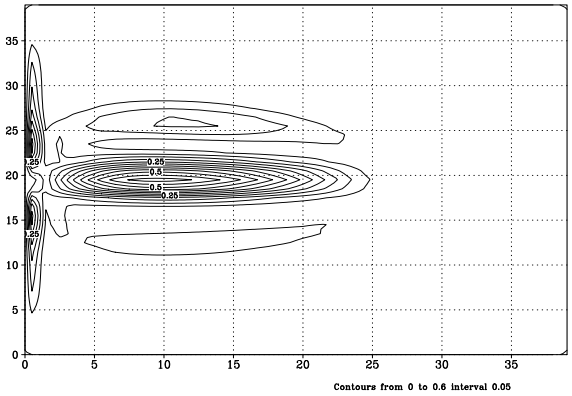

Figure 35B. MKE

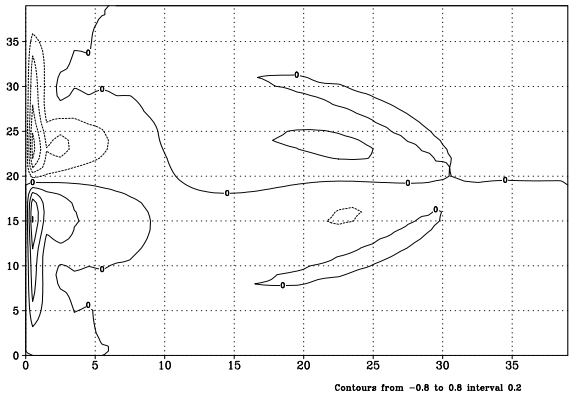

Figure 36A. Mean V velocity on 3000-4500 days

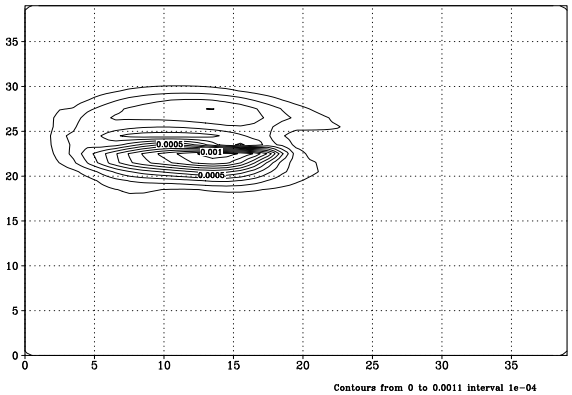

Figure 36B. Mean EKE on 3000-4500 days

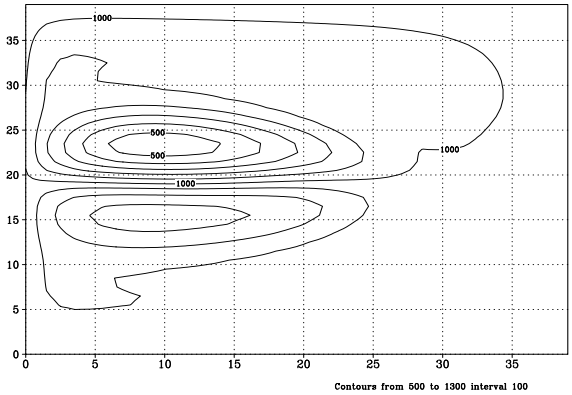

Figure 37A. Mean H height on 3000-4500 days

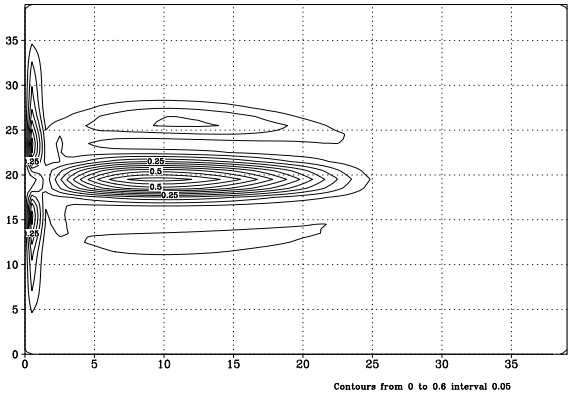

Figure 37B. Mean TKE on 3000-4500 days

Resolution 81 (25km) Second order.

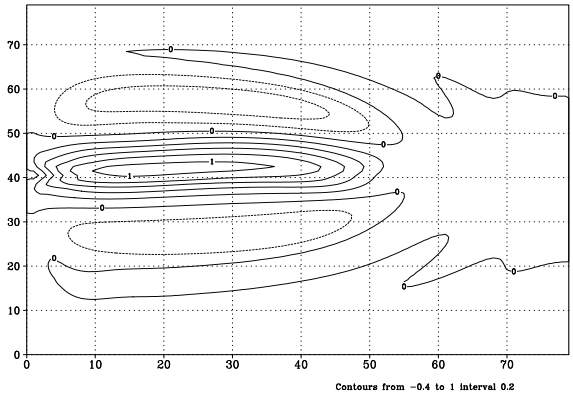

Figure 38A. Mean U velocity on 1500-3000 days

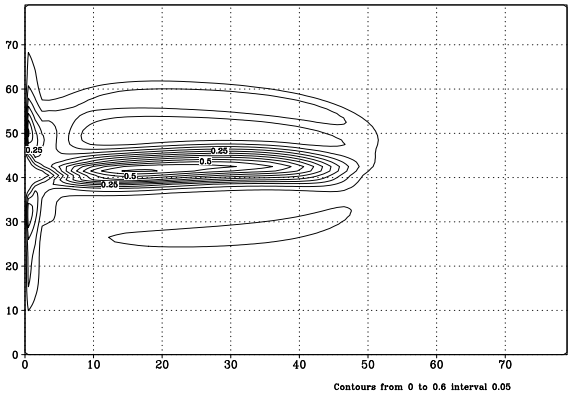

Figure 38B. MKE

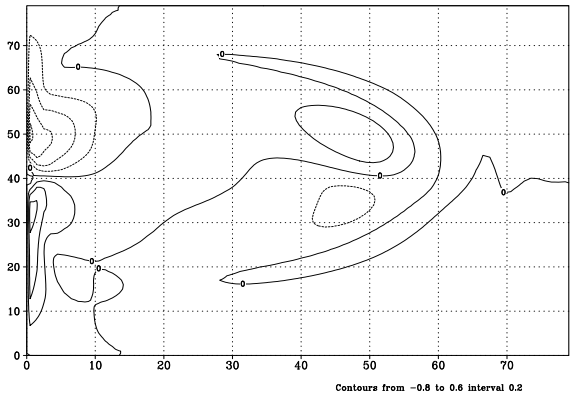

Figure 39A. Mean V velocity on 1500-3000 days

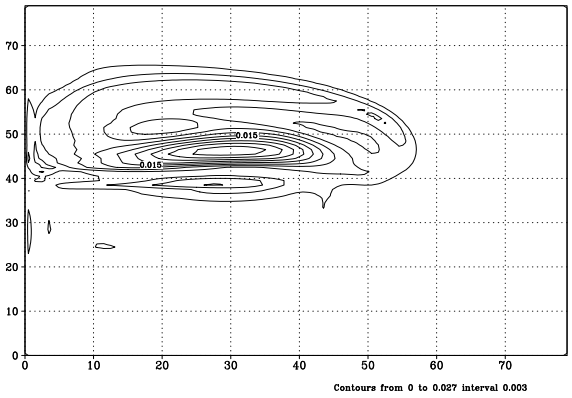

Figure 39B. Mean EKE on 1500-3000 days

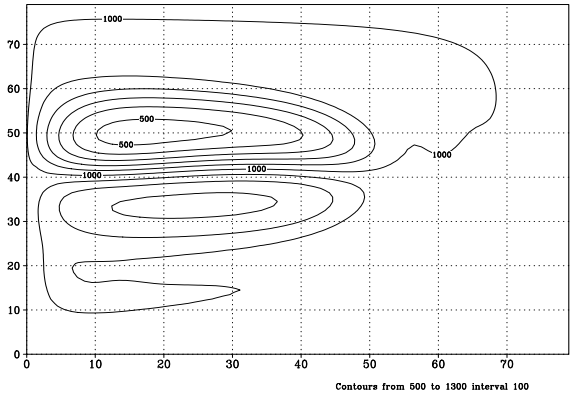

Figure 40A. Mean H height on 1500-3000 days

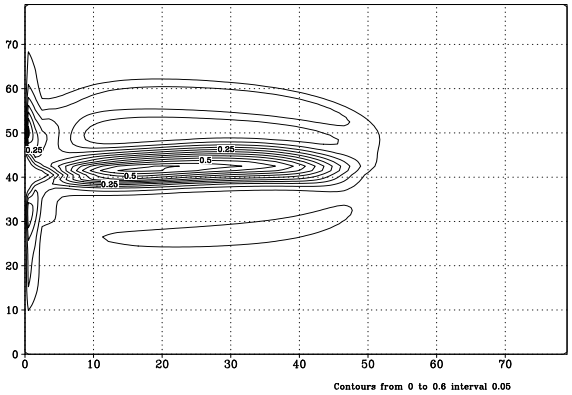

Figure 40B. Mean TKE on 1500-3000 days

Resolution 121 (16km) Second order.

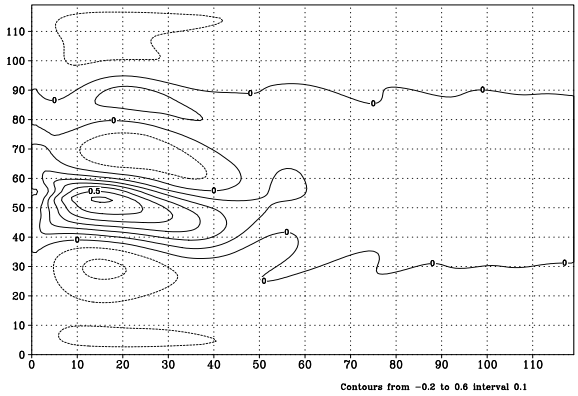

Figure 41A. Mean U velocity on 3000-4500 days

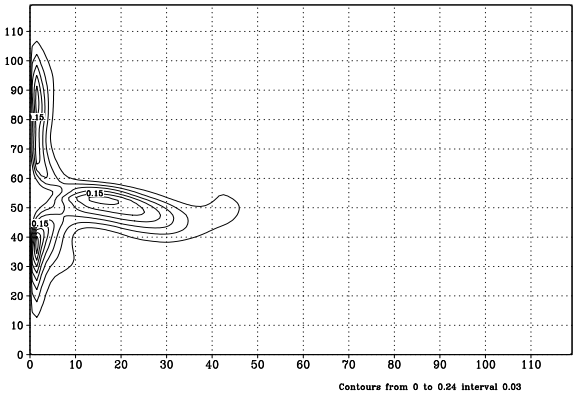

Figure 41B. MKE

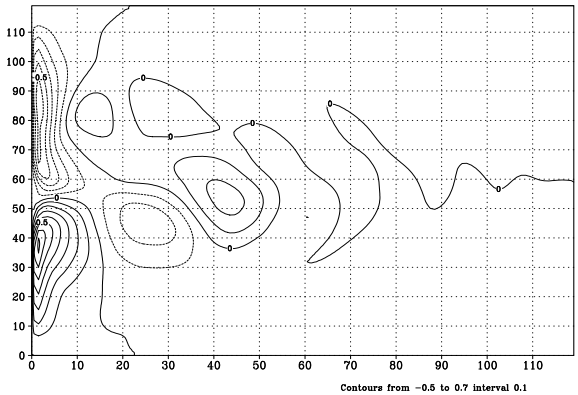

Figure 42A. Mean V velocity on 3000-4500 days

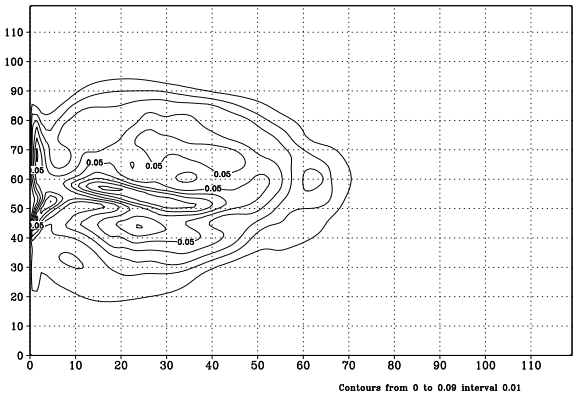

Figure 42B. Mean EKE on 3000-4500 days

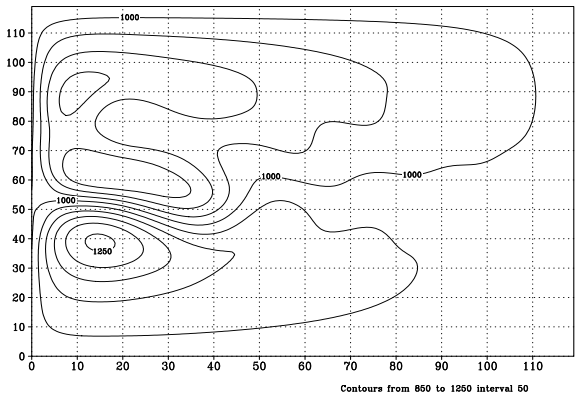

Figure 43A. Mean H height on 3000-4500 days

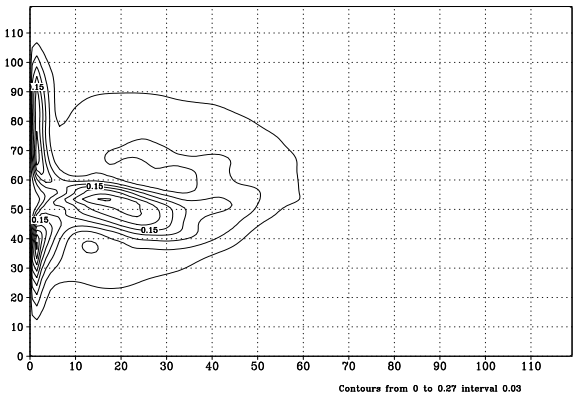

Figure 43B. Mean TKE on 3000-4500 days

Resolution 241 (8km) Second order.

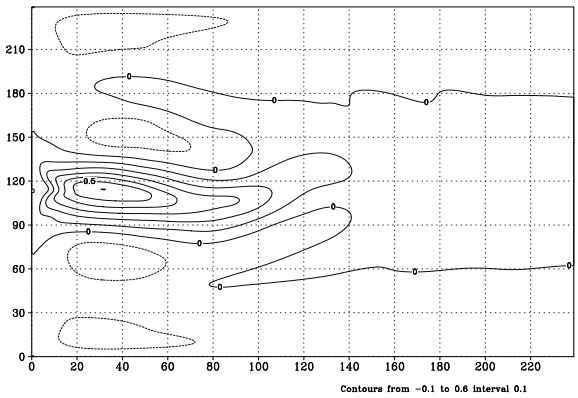

Figure 44A. Mean U velocity on 3000-4500 days

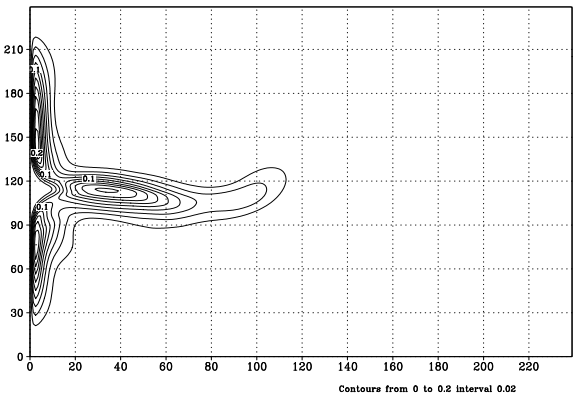

Figure 44B. MKE

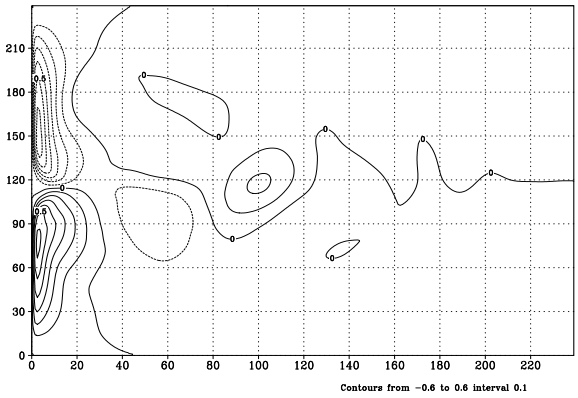

Figure 45A. Mean V velocity on 3000-4500 days

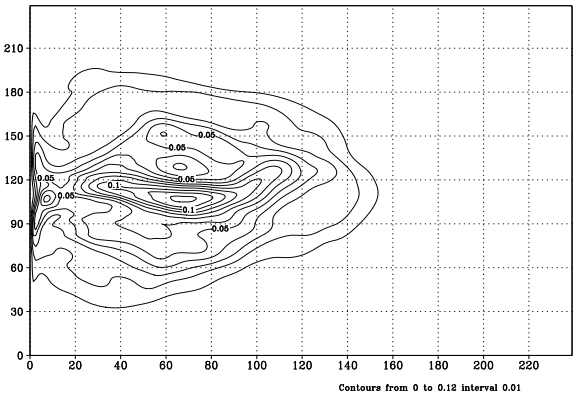

Figure 45B. Mean EKE on 3000-4500 days

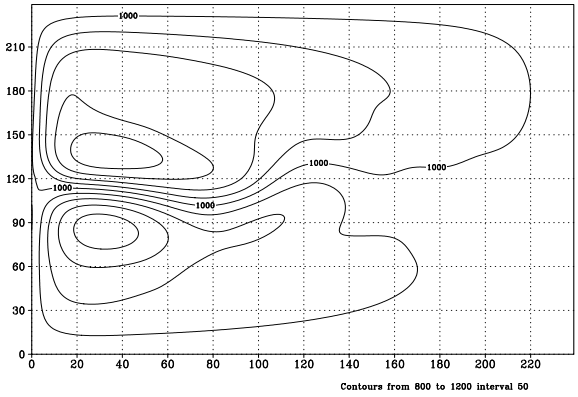

Figure 46A. Mean H height on 3000-4500 days

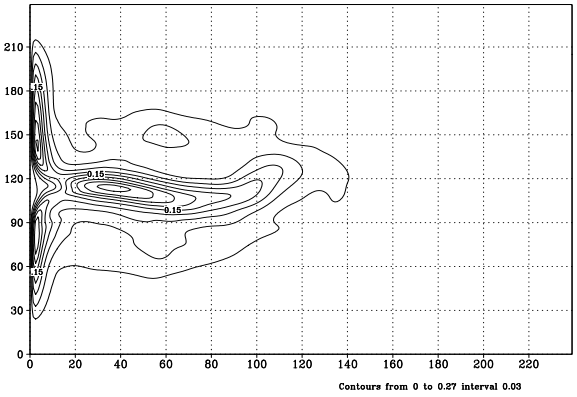

Figure 46B. Mean TKE on 3000-4500 days

Resolution 41 (50km) Fourth order.

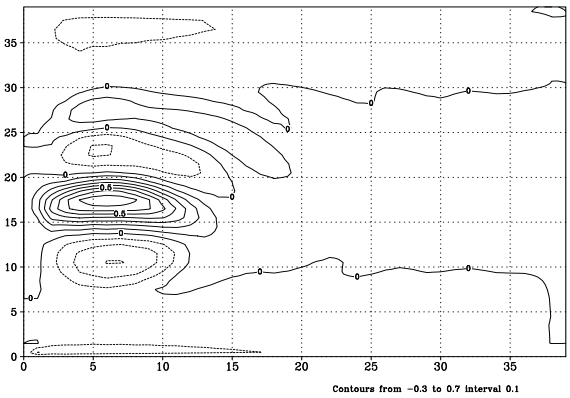

Figure 47A. Mean U velocity on 3000-4500 days

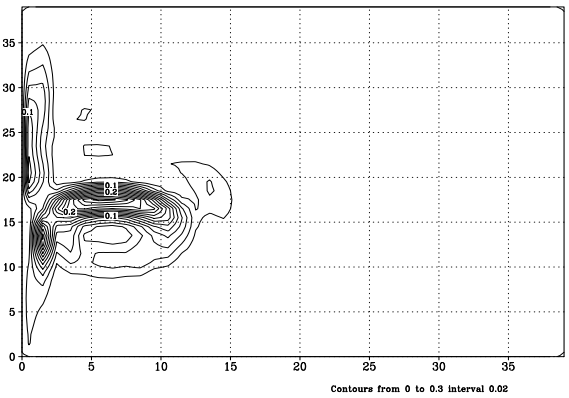

Figure 47B. MKE

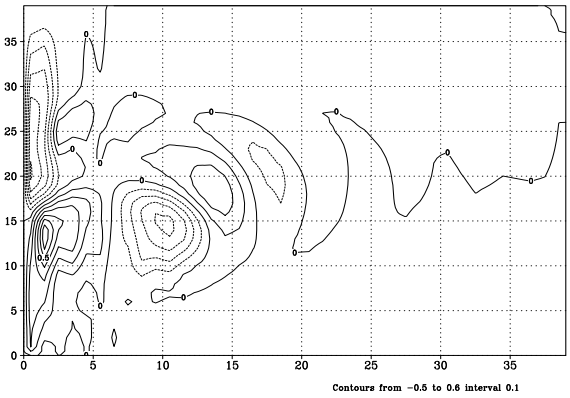

Figure 48A. Mean V velocity on 3000-4500 days

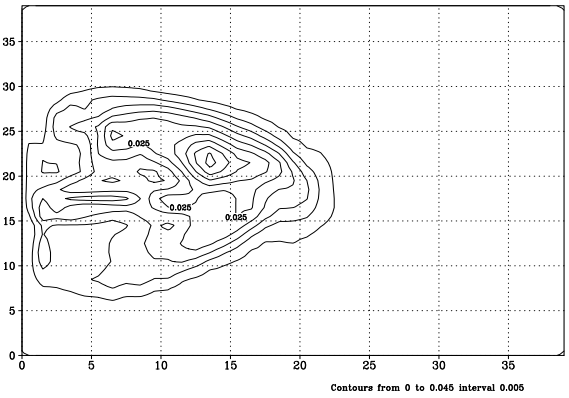

Figure 48B. Mean EKE on 3000-4500 days

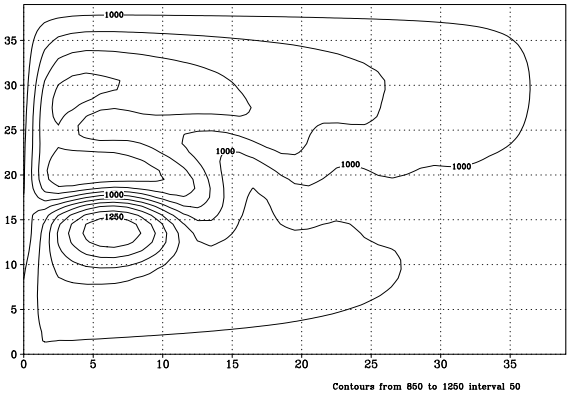

Figure 49A. Mean H height on 3000-4500 days

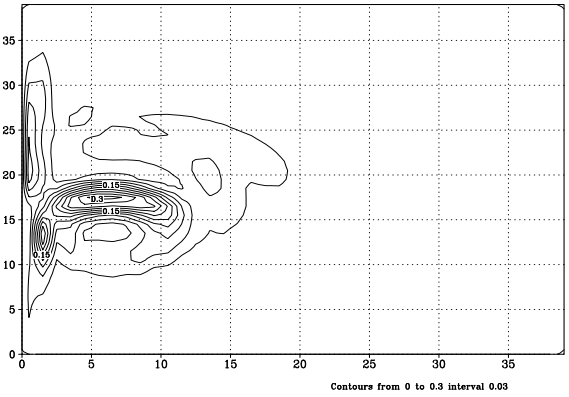

Figure 49B. Mean TKE on 3000-4500 days

Resolution 61 (33km) Fourth order.

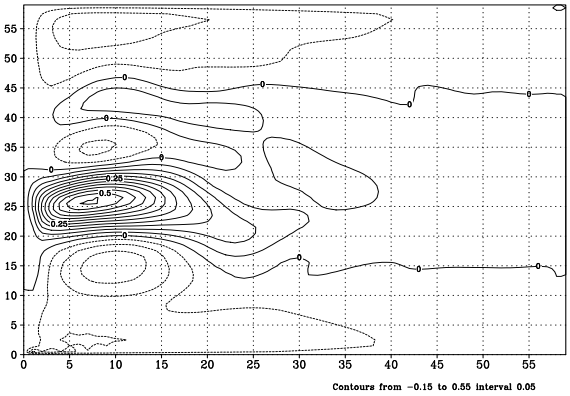

Figure 50A. Mean U velocity on 3000-4500 days

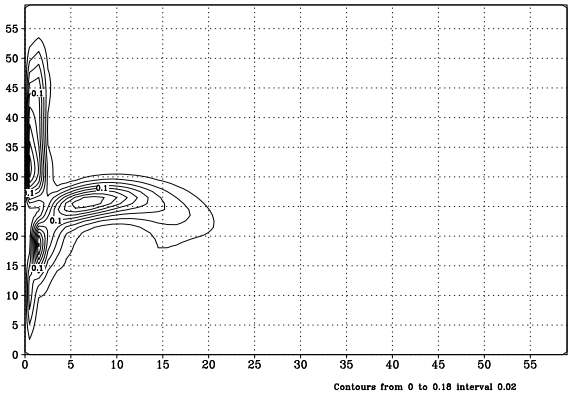

Figure 50B. MKE

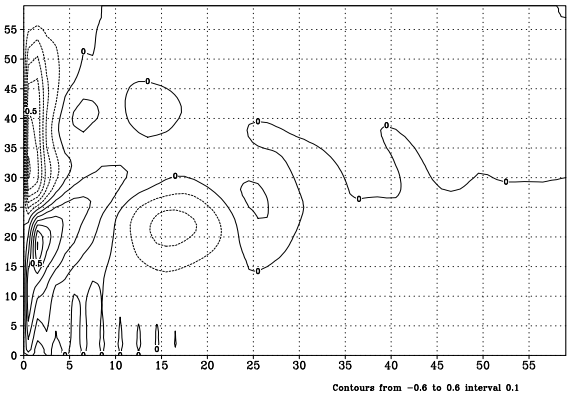

Figure 51A. Mean V velocity on 3000-4500 days

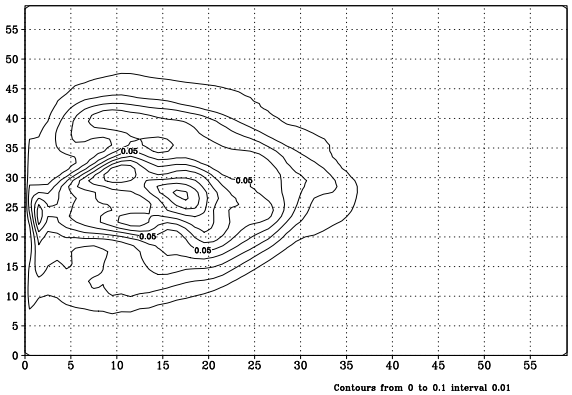

Figure 51B. Mean EKE on 3000-4500 days

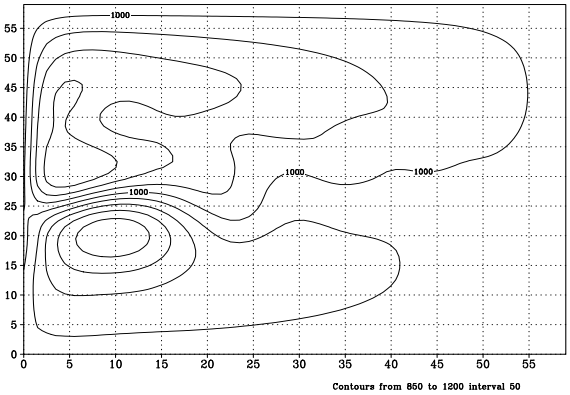

Figure 52A. Mean H height on 3000-4500 days

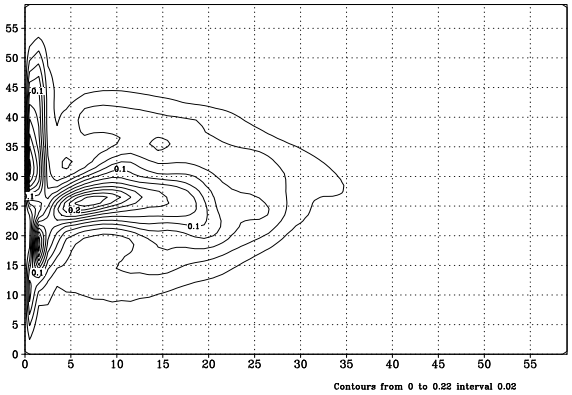

Figure 52B. Mean TKE on 3000-4500 days

Resolution 81 (25km) Fourth order.

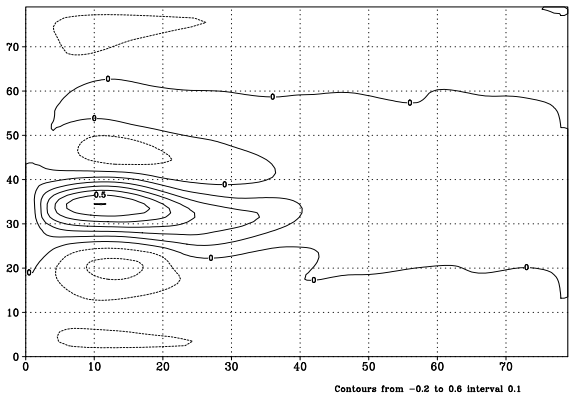

Figure 53A. Mean U velocity on 3000-4500 days

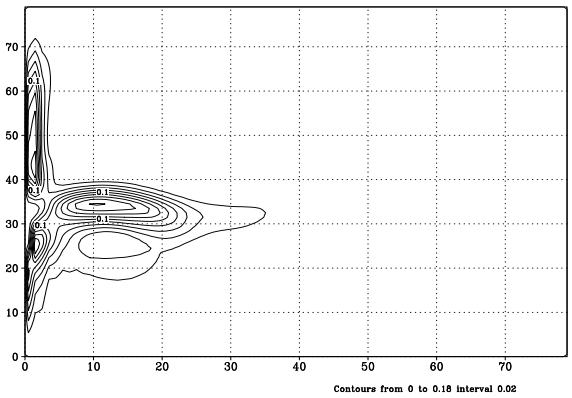

Figure 53B. MKE

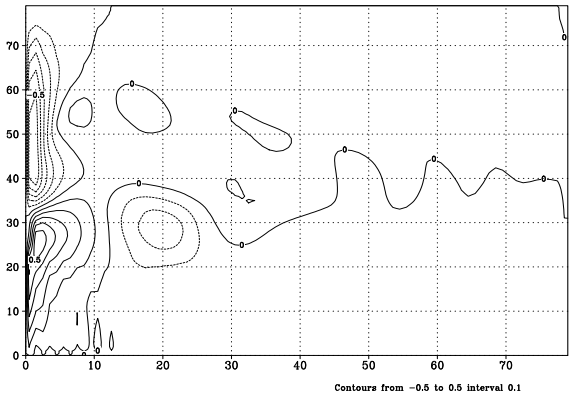

Figure 54A. Mean V velocity on 3000-4500 days

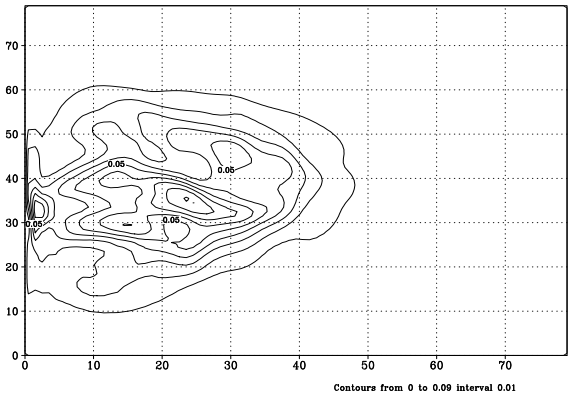

Figure 54B. Mean EKE on 3000-4500 days

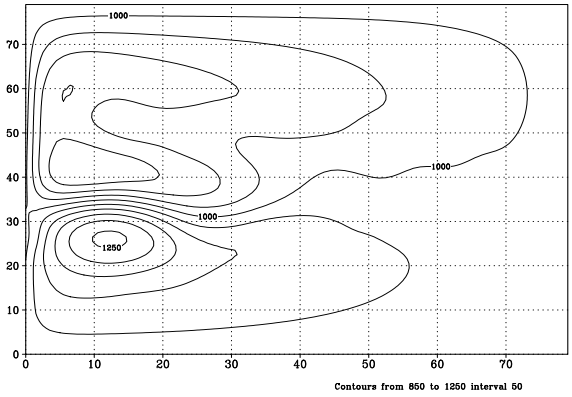

Figure 55A. Mean H height on 3000-4500 days

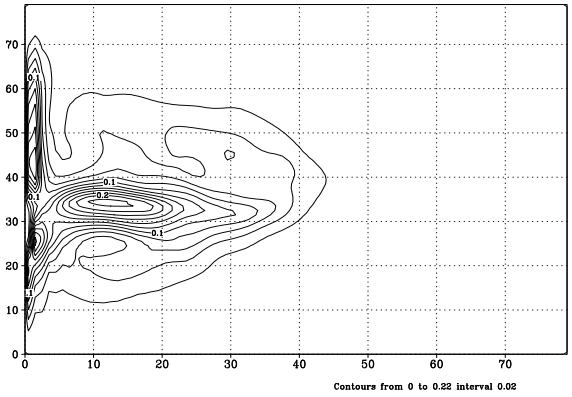

Figure 55B. Mean TKE on 3000-4500 days

Comparing these pictures we see, that when the second order approximation is used the solution exhibits very low variability at low resolutions. The ratio of the MKE to the EKE is extremely low in experiment with 50 km resolution (fig.36B). This ratio increases in the experiment with 25 km resolution (fig.39B), but remains low. The solution in these experiments represents very energetic large stream-jet in the middle of the basin with velocities reaching 1 m/s. In fact, the grid must resolve scales of at least 16 km to get a reasonable variability. One can see in fig.42B a well developed variability with EKE of order 30% to 50% of MKE. In these two reference experiments with high resolution, the solution possesses lower total energy. Pattern of all variables are very similar to each other. The Mean Kinetic Energy (fig.41B and fig.44B) is concentrated in the jet-stream and near the Western boundary. The pattern of the eddy kinetic energy (fig.42B and fig.45B) has a clear maximum in the jet-stream and two maxima to the North and to the South from the jet. The difference between these two reference experiments lies in the proportions of the mean and eddy energies. The mean energy has a tendency to decrease while the eddy energy increases.

When using the compact scheme, we get a developed variability even at 50 km resolution. Of course, at this resolution we can not obtain the solution similar to high resolution reference experiments, but this solution is evidently closer to the reference one than the solution obtained with the second order scheme at the same or even at the double resolution.

However, a little bit higher resolution (33 km) results already at a solution, comparable with reference experiments. As one can see in fig.50 and fig.51, the eddy kinetic energy becomes to be one half of MKE. Similarly to the reference experiments, its pattern possesses a clear maximum in the jet-stream and two maxima to the North and to the South from the jet.

Increasing the resolution up to 25 km we get a solution very similar to the solution of the reference experiment fig.53 — fig.55. The difference lies int the length of the jet in the middle of the basin. In the reference experiment the jet is longer and narrower.

Energy Evolution.

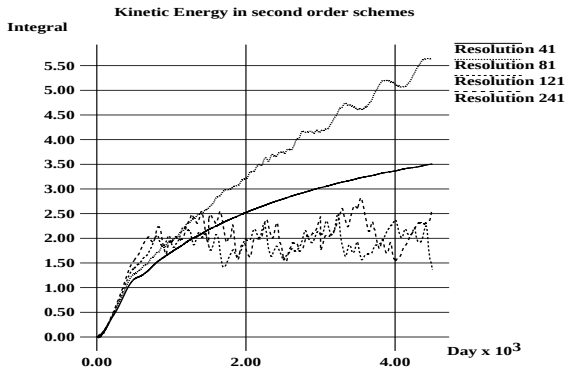

Figure 56A. Kinetic Energy Evolution in second-order schemes.

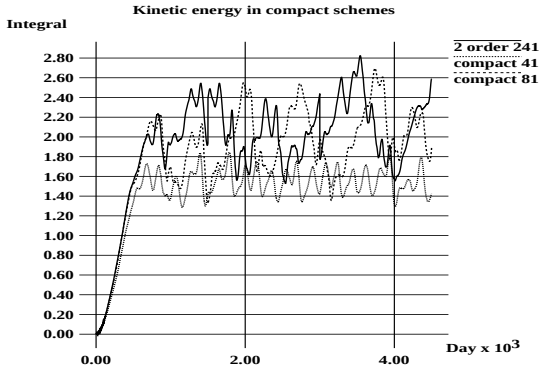

Figure 56B. Kinetic Energy Evolution in compact schemes (dashed lines) comparing to the energy of the reference experiment (solid line).

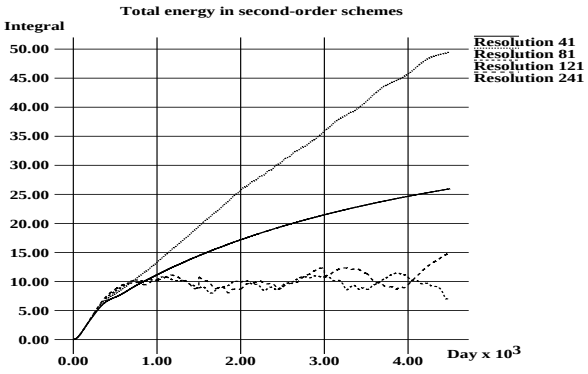

Figure 57A. Total Energy Evolution in second-order schemes.

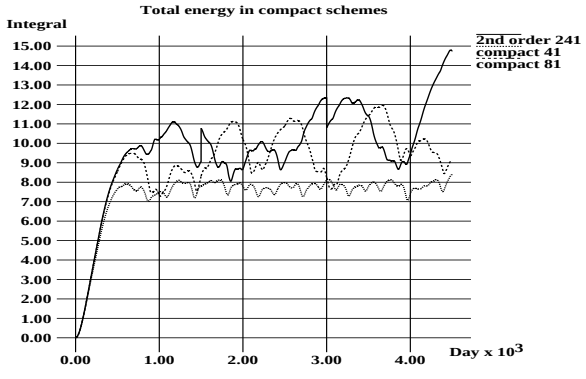

Figure 57B. Total Energy Evolution in compact schemes (dashed lines) comparing to the energy of the reference experiment (solid line).

If we consider the evolution of scalar parameters, we see that in the experiments with second-order schemes low resolution results in an excessive energy of the solution. Thus, the energy of solutions obtained at resolutions of 50 and 25 kilometers is at least two times more than in the high-resolution reference experiment. On the other hand, energies of solutions for resolutions 121 and 241 seem to be similar.

When the model is discretised with a compact scheme, the solution has a correct level of energy even at lowest resolution. However, the energy spectrum is not well reproduced with this low resolution. There is no low-frequency variations with periods about 700 days which are presented in the energy of the reference experiment. It is at the resolution 81 (25km) we get the energy similar to the reference experiment.

CPU Time.

To compare the cost of different schemes, we estimate the CPU time for different resolutions. The source code of the model was compiled with the Intel Fortran Compiler and run on the Intel Pentium 4-1800 MHz processor. Below, we peresent the CPU times spent for 10 000 time steps and for the simulation of 1 year of physical time. Due to use of an explicit leap-frog scheme, we must satisfy the CFL stability condition. So, for the second order scheme we use 24, 48 and 72 time steps per day for resolutions 41, 81 and 121 respectively, for the compact scheme we use 30, 60 and 90 time steps per day for the same resolutions.

Resolution	Second order scheme		Compact fourth order scheme	
	10000 steps	1 year	10000 steps	1 year
41	10.6 sec	9.3 sec	32.6 sec.	35.7 sec
81	55.0 sec	96.4 sec.	149.5 sec	327.4 sec
121	142.0 sec	373.2 sec.		

When compiled with the Compaq Fortran Compiler and run on the DEC DS20 EV6 platform with Alpha 21264 6/500-MHz processor the CPU time for the same 10 000 time steps or 1 year is the following:

Resolution	Second order scheme		Compact fourth order scheme	
	10000 steps	1 year	10000 steps	1 year
41	6.5 sec	5.7 sec.	35.5 sec.	38.9 sec.
81	27.0 sec	47.3 sec.	146.4 sec	320.6 sec.
121	72.0 sec	189.2 sec.		

The comparison of the CPU time shows that high-order compact schemes are more expensive than classical second-order ones. This is an evident conclusion, but the difference in CPU times for compact schemes seem to be greater than supposed on the DEC platform. In fact, one can suppose this ratio to be approximately 3, because two operations per node are necessary for a second-order operator, while 6 operation must be made for the fourth order scheme. This ratio is equal to 3 on the Intel processor, but become close to 5 on the DEC platform.

This fact can be explained easily by different optimization capabilities of the Fortran compiler for different processors. The code of e2 procedure is better optimized by the Compaq compiler thanks to easy optimization. In the same time, the c4 code can hardly be optimized due to the presence of dependencies in the procedure of the tridiagonal solver. Analyzing the CPU time spent in each subroutine, we see that the tridiagonal solver on the DEC platform become the major consumer of the CPU time with about 70% of the total consumption.

It should be noted here, that implementation of the compact code on massively parallel computers would rise additional difficulties and additional decrease of performance of compact schemes. Parallel version of the classical second order code can be obtained by straightforward application of the domain decomposition method. In the same time, compact schemes with their tridiagonal solver would require some other method for parallelization.

4.3.5 Small basin.

In this section, we work on a basin of length 1000 km, where the boundary layer can be solved. We solve the equation with different space step resolution, and compare the results in term of Mean Kinetic Energy and Eddy Kinetic Energy. The parameters are the following.

- L=1000 km
- $\mu = 150\ m^2 s^{-1}$ (viscosity)
- $\sigma = 0.5 \times 10^{-7} s^{-1}$ (bottom friction)
- $\gamma = 0.07$ (Filter of Asselin)
- $f = 7.0 \times 10^{-5} s^{-1}$ (Coriolis)
- $\beta_0 = 2.0 \times 10^{-11} m^{-1} s^{-1}$ (Coriolis)
- $g' = 0.02\ m\ s^{-2}$ (reduced gravity)
- $h_0 = 1000\ m$ (initial layer thickness)
- $\rho_0 = 1000\ kg\ m^{-3}$ (reference density)
- $\tau_0 = 0.15\ N\ m^{-2}$ (wind stress coefficient)
- $y_0 = L/2$
- $\tau^{(x)}(y) = \tau_0 * cos(2 * \pi * (y - y_0)/L)$ (wind stress)
- $\tau^{(y)} = 0$
- no slip boundary condition

Energy Evolution.

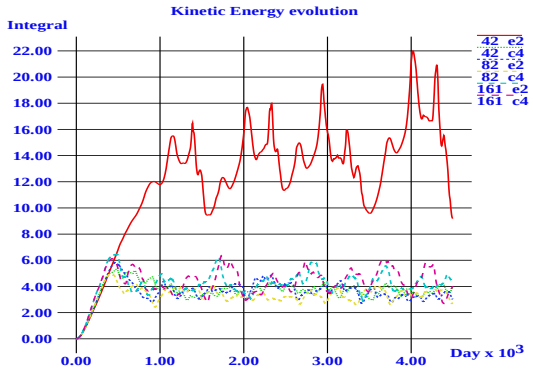

Figure 58A. Kinetic Energy Evolution

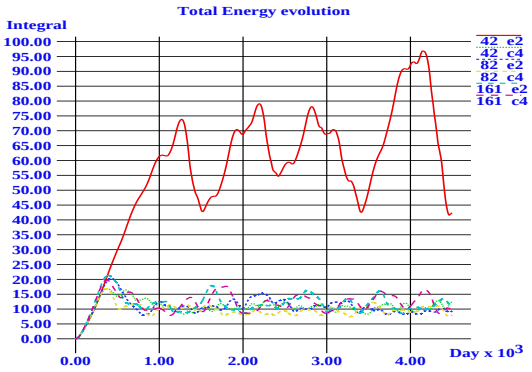

Figure 58B. Total Energy Evolution

Resolution 41 (25km) Second order.
Evolution between 3000 and 4500 days

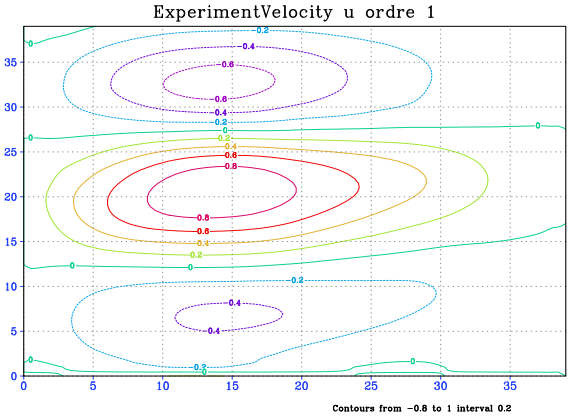

Figure 59A. Mean U velocity on 3000-4500 days

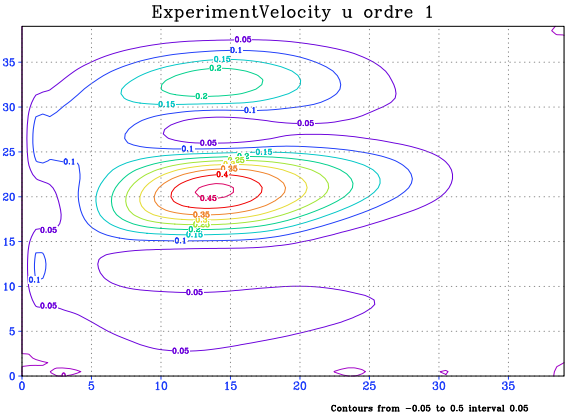

Figure 59B. MKE

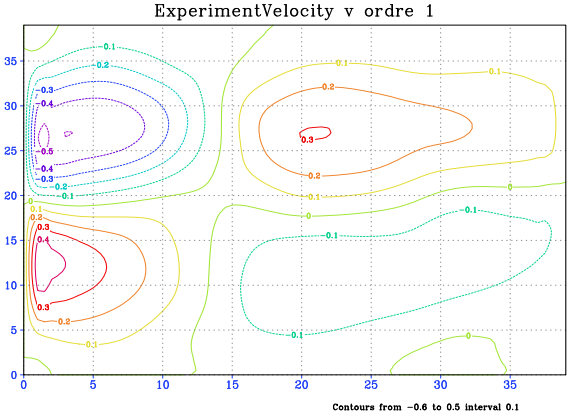

Figure 60A. Mean V velocity on 3000-4500 days

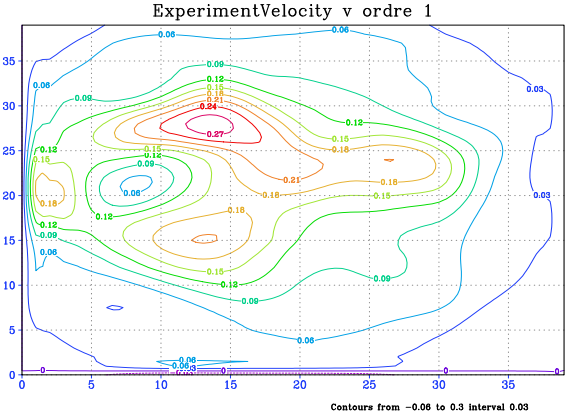

Figure 60B. Mean EKE on 3000-4500 days

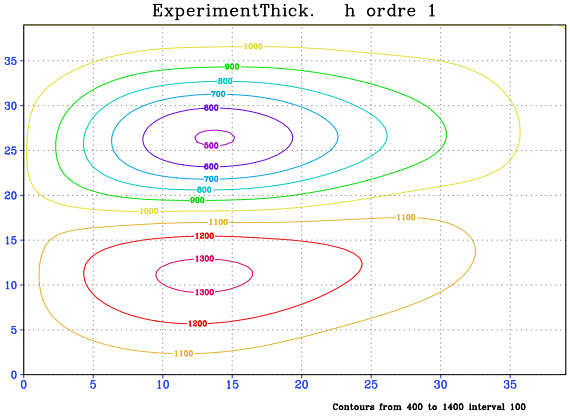

Figure 61A. Mean H height on 3000-4500 days

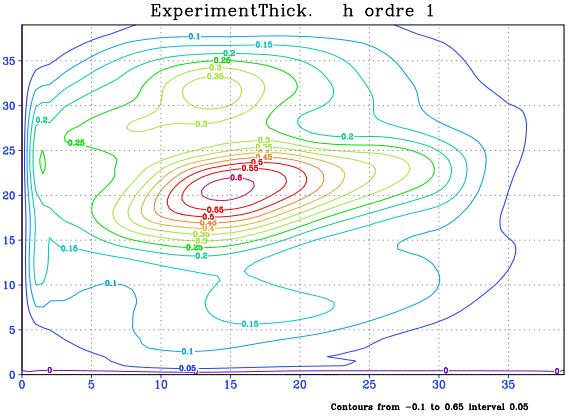

Figure 61B. Mean TKE on 3000-4500 days

Resolution 81 (12,5km) Second order.
Evolution between 3000 and 4500 days

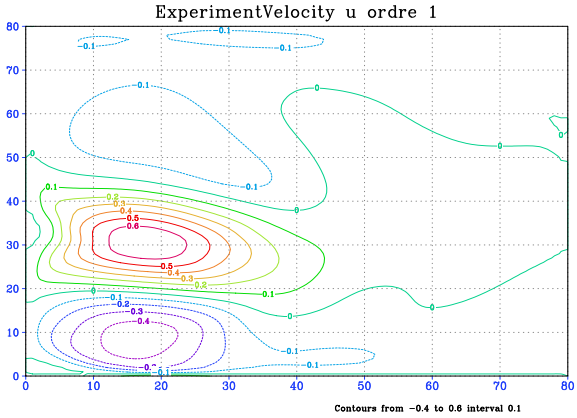

Figure 62A. Mean U velocity on 3000-4500 days

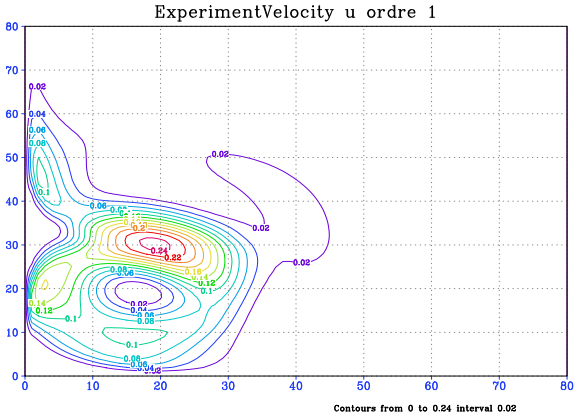

Figure 62B. MKE

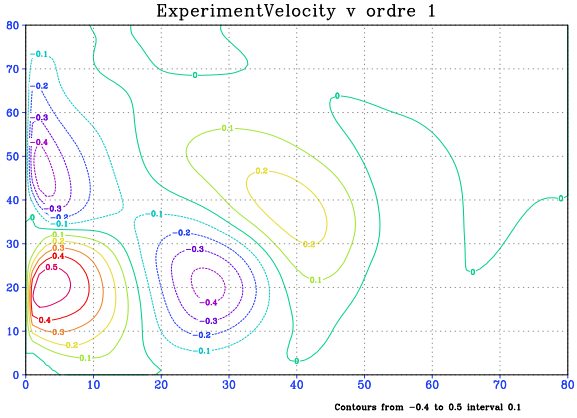

Figure 63A. Mean V velocity on 3000-4500 days

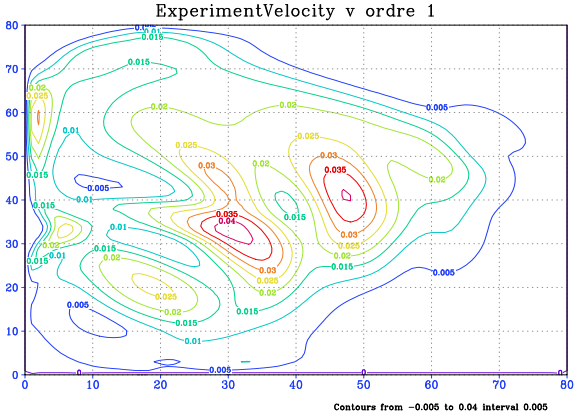

Figure 63B. Mean EKE on 3000-4500 days

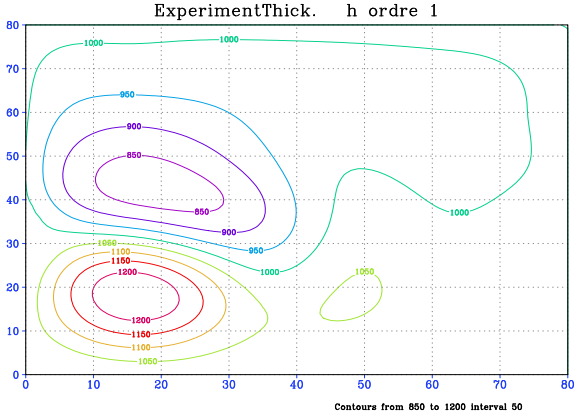

Figure 64A. Mean H height on 3000-4500 days

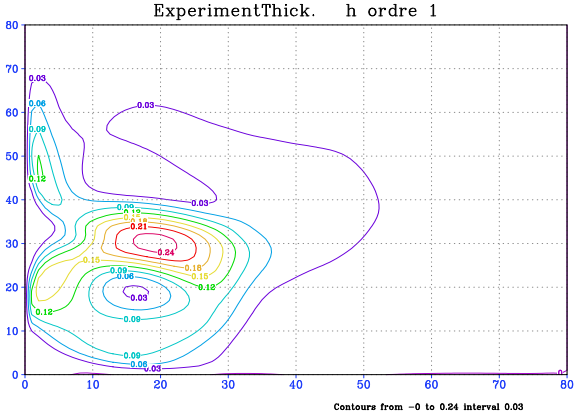

Figure 64B. Mean TKE on 3000-4500 days

Resolution 161 (6,25km) Second order.
Evolution between 3000 and 4500 days

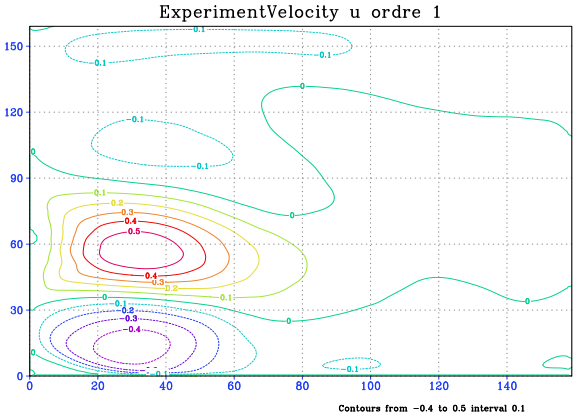

Figure 65A. Mean U velocity on 3000-4500 days

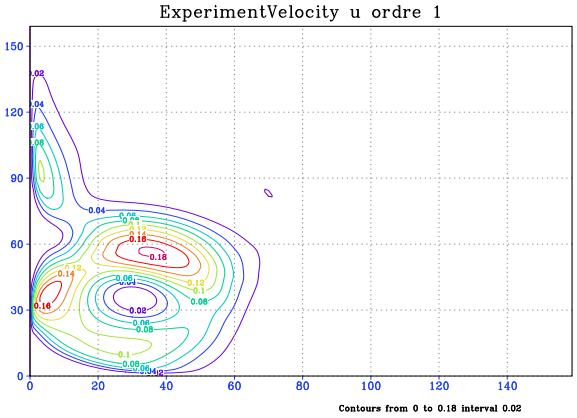

Figure 65B. MKE

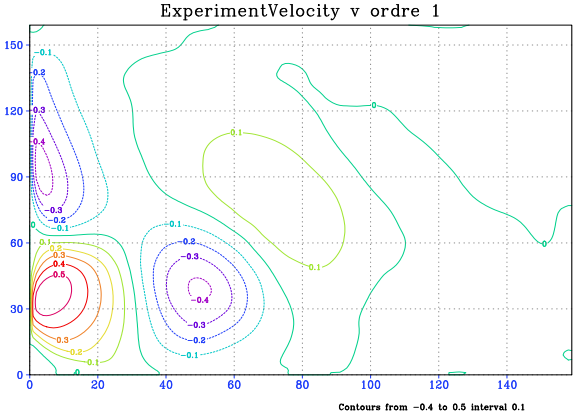

Figure 66A. Mean V velocity on 3000-4500 days

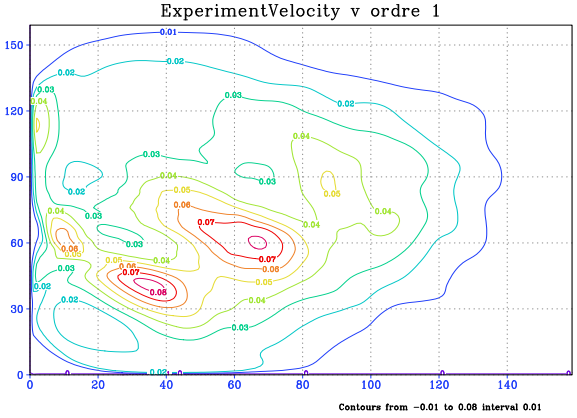

Figure 66B. Mean EKE on 3000-4500 days

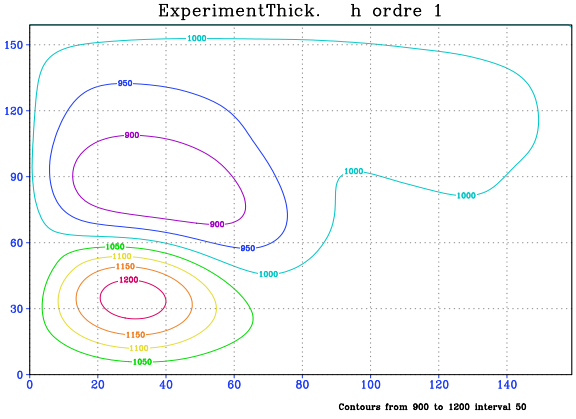

Figure 67A. Mean H height on 3000-4500 days

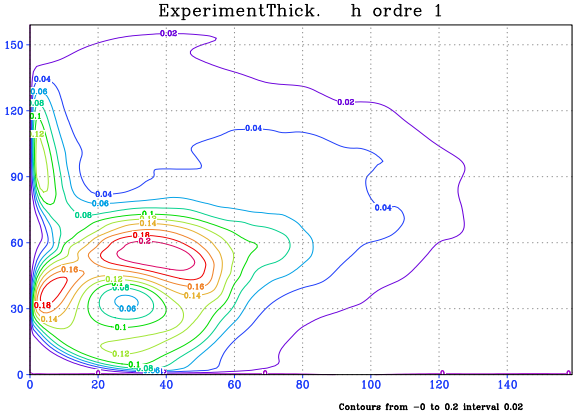

Figure 67B. Mean TKE on 3000-4500 days

Resolution 41 (25km) Fourth order.
Evolution between 3000 and 4500 days

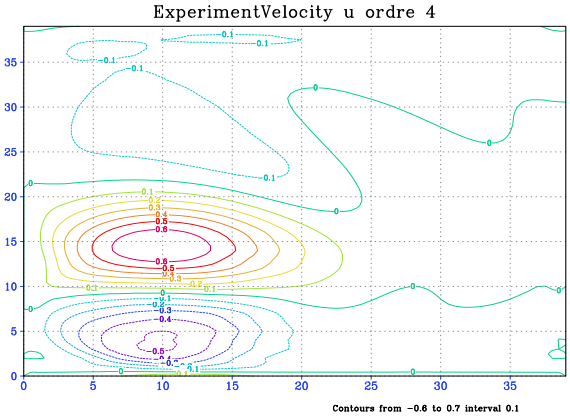

Figure 68A. Mean U velocity on 3000-4500 days

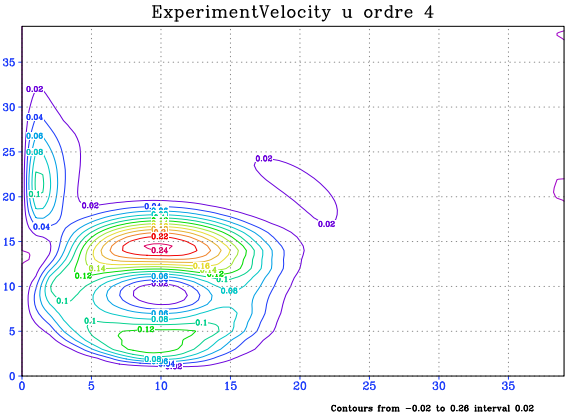

Figure 68B. MKE

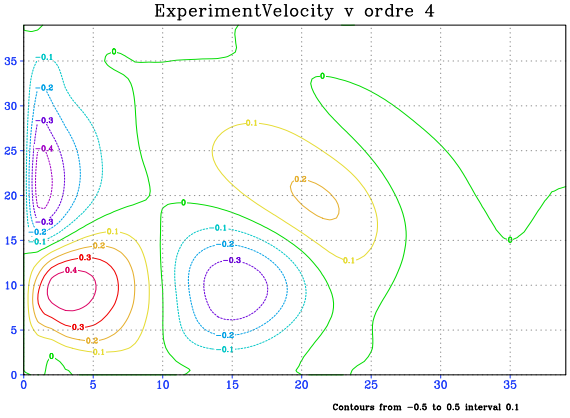

Figure 69A. Mean V velocity on 3000-4500 days

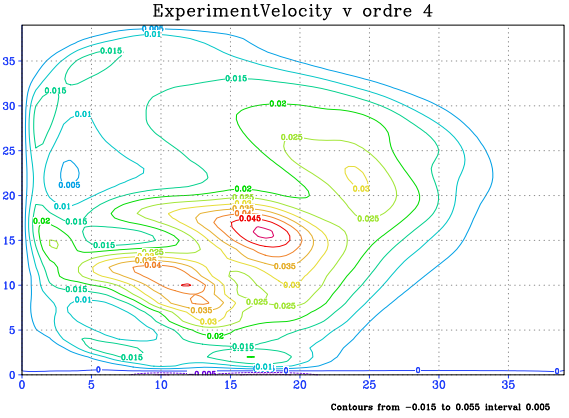

Figure 69B. Mean EKE on 3000-4500 days

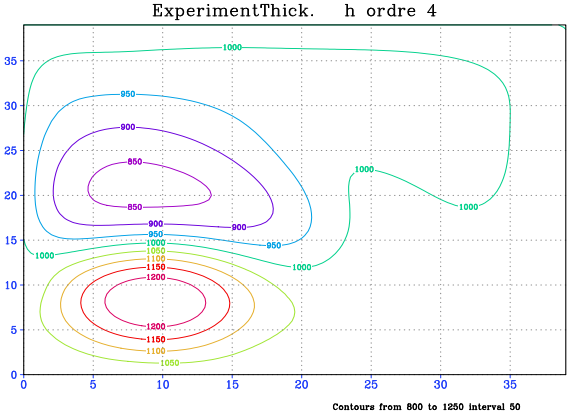

Figure 70A. Mean H height on 3000-4500 days

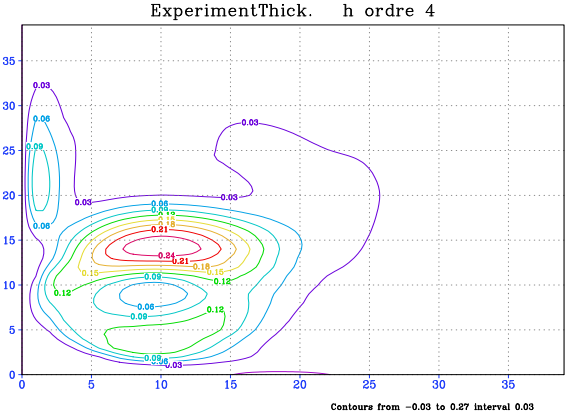

Figure 70B. Mean TKE on 3000-4500 days

Resolution 81 (12,5km) Fourth order.
Evolution between 3000 and 4500 days

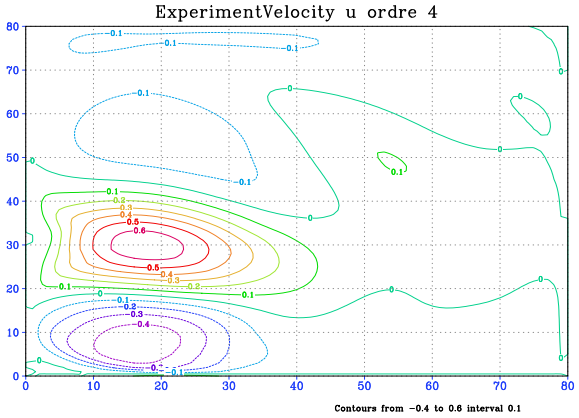

Figure 71A. Mean U velocity on 3000-4500 days

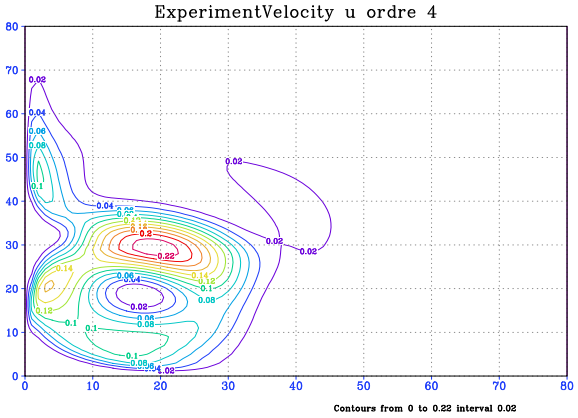

Figure 71B. MKE

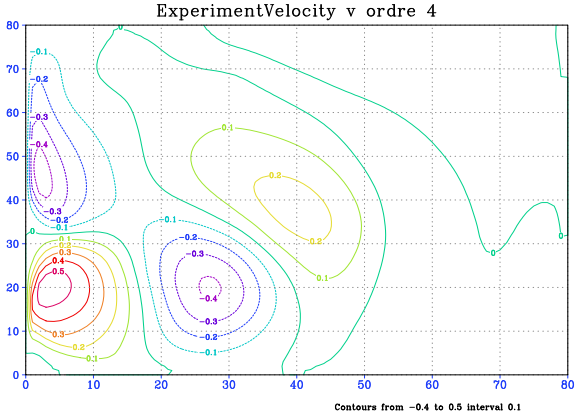

Figure 72A. Mean V velocity on 3000-4500 days

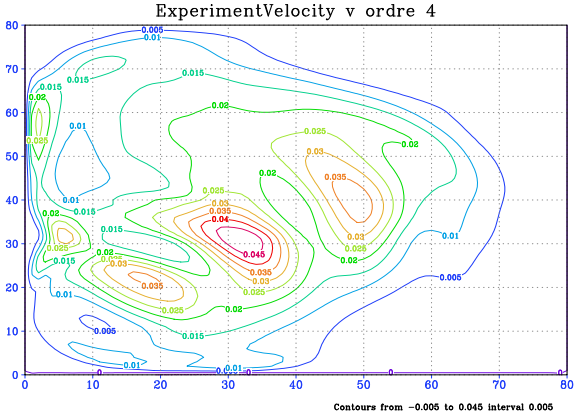

Figure 72B. Mean EKE on 3000-4500 days

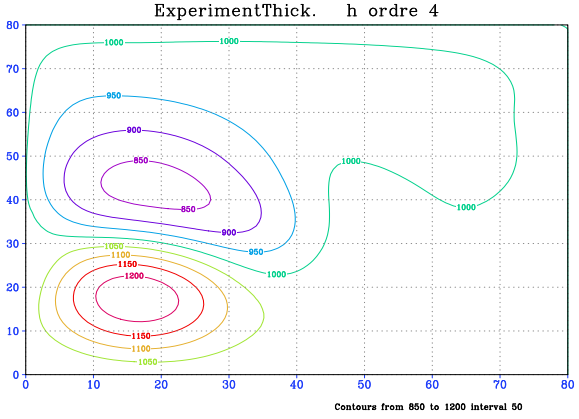

Figure 73A. Mean H height on 3000-4500 days

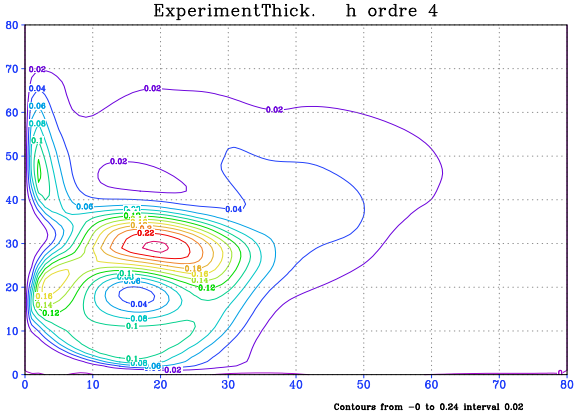

Figure 73B. Mean TKE on 3000-4500 days

Resolution 161 (6,25km) Fourth order.
Evolution between 3000 and 4500 days

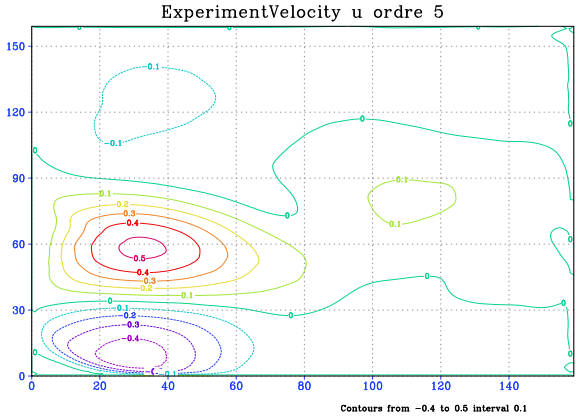

Figure 74A. Mean U velocity on 3000-4500 days

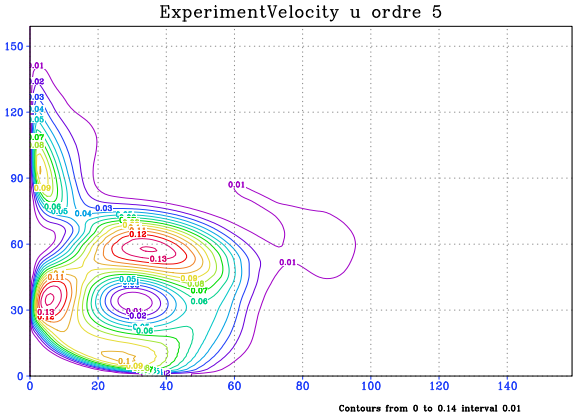

Figure 74B. MKE

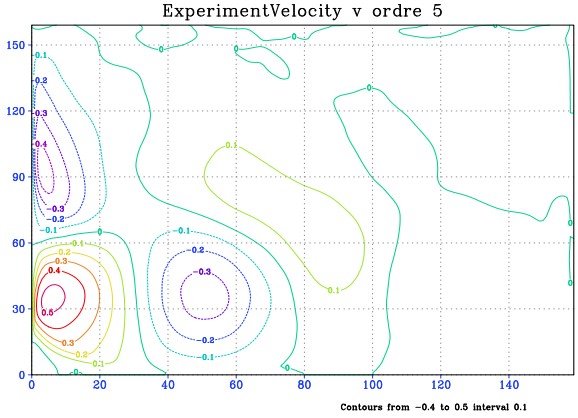

Figure 75A. Mean V velocity on 3000-4500 days

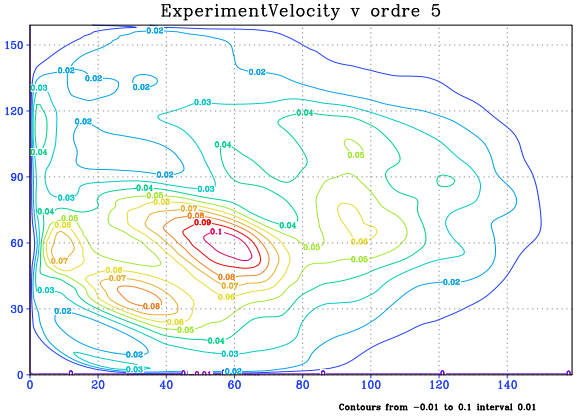

Figure 75B. Mean EKE on 3000-4500 days

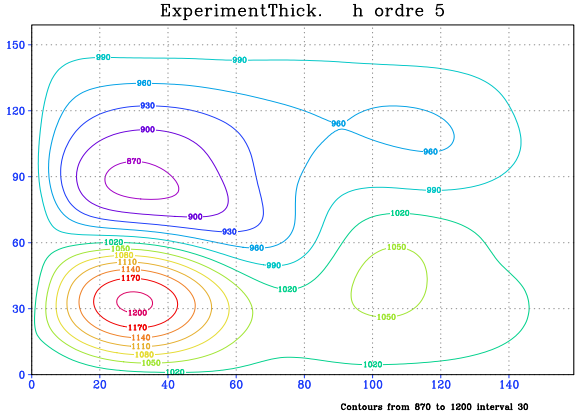

Figure 76A. Mean H height on 3000-4500 days

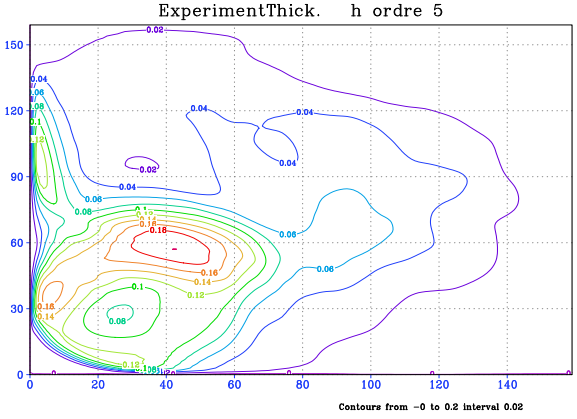

Figure 76B. Mean TKE on 3000-4500 days

As in the previous section, we can see that the behaviour of the model with the second order scheme at low resolution differs a lot from the solution obtained at high resolution. In the same time, there is almost no difference between solutions obtained at high resolution grids. Either at 12 km resolution (fig.62,fig.63,fig.64), or at 6 km (fig.65,fig.66,fig.67), the pictures are similar to each other.

When the compact scheme is used, the solution similar to the reference experiment can be obtained even at low resolution of 25 km (fig.68,fig.69,fig.70).

5 Conclusion.

Compact schemes are very competitive in many problems like wave propagation, Munk model or shallow-water equations in a domain with simple geometries. The resolution of the boundary layer is crucial in these last two models, and this is confirmed by the numerical results. When this layer is resolved, the c4 scheme is more efficient than the usual e2 one.

But, the implementation of compact scheme on the shallow-water model shows us that it will be very expensive in term of computer memory when the domain will be realistic. Moreover, the parallelization of the code will be almost impossible in this case. So, even if compact scheme seems to be more efficient in many cases than usual one, due to practical implementation and code optimization, no compact scheme may be preferable in realistic models.

It should be noted also, that stability and conservativity properties are more difficult to ensure in high-order schemes, especially in bounded domains. In these experiments with simple geometry, we can see a slight deformation of the solution obtained with the compact schemes. Thus, in figures fig.47 — fig.55 one can see numerical noise in the lower left corner, especially for the v velocity pattern.

6 Acknowledgments.

The authors thank M. Tolstykh from the Russian Hydrometeorological Center for his helpfull discussions. This study has been granted by the french MERCATOR project for operational oceanography www.mercator.com.fr

References

[Blayo] Blayo E. *Compact finite difference for ocean models. Part 1: ocean waves.* J. of Comp. Ph., vol 164, pp 241-257, 2000.

[Bleck-Boudra] Bleck R., Boudra D. *Wind-Driven Spin-Up in Eddy-Resolving Ocean Models Formulated in Isopycnic and Isobaric Coordinates.* J. of Geophys. Res., vol 91, No C6, pp 7611-7621, 1986.

[Carpenter-Gottlieb-Abarbanel] Carpenter M., Gottlieb D., Abarbanel S. *Stable and accurate boundary treatments for compact, high-order finite-difference schemes.* Applied Num. Math., No12, pp 55-87, 1993.

[Chu-Fan] Chu P.C., Fan C. *A Three-ponit combined compact difference scheme.* J. of Comp. Ph., vol 140, pp 370-399, 1998.

[Collatz] Collatz L. *The Numerical Treatment of Differential Equations.* Springer-Verlag, New-York, 1966.

[Gill] Gill A. *Amtmosphere and Ocean dynamics* Academic Press, 1982.

[Gustafsson1] Gustafsson B. *The convergence Rate for Difference Approximations to Mixed Initial Boundary Value Problems.* Math. of Comput., Vol 29, No 130, pp 396-406, 1975.

[Gustafsson2] Gustafsson B. *The Convergence Rate for Difference Approximations to General Mixed Initial Boundary Value Problems.* SIAM J. Numer. Anal., Vol 18, No 2, pp 179-190, 1981

[GKS] Gustafsson B., Kreiss H-O., Sundström A., *Stability Theory of Difference Approximations for Mixed Initial Boundary Value Problems II*, Math. of comput., Vol 26, No 119, pp 649-686, 1972.

[Kreiss] Kreiss H-O, *Initial Boundary Value Problems for Hyperbolic systems.* Com. Pure Appl. Math, Vol 23, pp 277-298, 1970.

[Kreiss-Wu] Kreiss H-O., Wu L. *On the stability definition of difference approximations for the Initial Boundary Value Problem.* Appl. Numer. Math, vol 12, No 1-3, pp213-227, 1993.

[Lele] Lele S.K. *Compact finite difference scheme with spectral-like resolution* J. of Comp. Ph., vol 103, 16, 1992.

[Strikwerda] Strikwerda J. *Initial Boundary Value Problems for the Method of Lines* J. Comput. Physics, Vol 34, pp 94-107, 1980.

[Tolstykh-72] Tolstykh A.I. *On a method of numerical solution of the Navier-Stokes equations of compressible gas.*, Uchen. Zap. TsAGI, Vol 3, pp 78-87, 1972, in russian.

[Tolstykh-73] Tolstykh A.I. *On a method for the numerical solution of the compressible Navier-Stokes equations over a wide range of Reynolds numbers.*, Dokl. Akad. Nauk. SSSR, Vol 210, pp 48-51, 1973, Engl. transl. Sov. Phys. Dokl., Vol 18, pp 74-77, 1973.

[Tolstykh-73b] Tolstykh A.I. *On high accuracy schemes for numerical solution of some aerohydrodynamics problems.* Uchen. Zap. TsAGI, Vol 4, 36-44, 1973, in Russian.

[Tolstykh-94] Tolstykh A.I. *High Accuracy Non-Centered Compact Difference Schemes For Fluid Dynamics Application.*, Series on Advances in Mathematics for Applied Sciences, Vol 21, World Scientific Pub, 1994.

[Tolstykh M.A.] Tolstykh M.A. *Application of Fifth-Order Compact Upwind Differencing to Moisture Transport Equation in Atmosphere.*, J. Comput. Physics, Vol 112, pp 394-403, 1994.

Contents

Unité de recherche INRIA Rhône-Alpes
655, avenue de l'Europe - 38334 Montbonnot Saint-Ismier (France)

Unité de recherche INRIA Futurs : Parc Club Orsay Université - ZAC des Vignes
4, rue Jacques Monod - 91893 ORSAY Cedex (France)
Unité de recherche INRIA Lorraine : LORIA, Technopôle de Nancy-Brabois - Campus scientifique
615, rue du Jardin Botanique - BP 101 - 54602 Villers-lès-Nancy Cedex (France)
Unité de recherche INRIA Rennes : IRISA, Campus universitaire de Beaulieu - 35042 Rennes Cedex (France)
Unité de recherche INRIA Rocquencourt : Domaine de Voluceau - Rocquencourt - BP 105 - 78153 Le Chesnay Cedex (France)
Unité de recherche INRIA Sophia Antipolis : 2004, route des Lucioles - BP 93 - 06902 Sophia Antipolis Cedex (France)

Éditeur
INRIA - Domaine de Voluceau - Rocquencourt, BP 105 - 78153 Le Chesnay Cedex (France)
http://www.inria.fr
ISSN 0249-6399